Report No. 174 / UILU ENG-97-4002

# An Analytical Model Which Combines Roughness and Plasticity Induced Fatigue Crack Closure

by

Nong Chen

B.S., Southwest Jiaotong University, 1989
M.S., University of Illinois at Urbana-Champaign, 1992

THESIS

Submitted in partial fulfillment of the requirements
for the degree of Doctor of Philosophy in Civil Engineering
in the Graduate College of the
University of Illinois at Urbana-Champaign, 1997

Urbana, Illinois

UNIVERSITY OF ILLINOIS AT URBANA-CHAMPAIGN

THE GRADUATE COLLEGE

January, 1997

WE HEREBY RECOMMEND THAT THE THESIS BY

NONG CHEN

ENTITLED AN ANALYTICAL MODEL WHICH COMBINES ROUGHNESS AND PLASTICITY INDUCED FATIGUE CRACK CLOSURE

BE ACCEPTED IN PARTIAL FULFILLMENT OF THE REQUIREMENTS FOR THE DEGREE OF DOCTOR OF PHILOSOPHY

Director of Thesis Research

Head of Department

Committee on Final Examination†

Chairperson

† Required for doctor's degree but not for master's.

0-517

# AN ANALYTICAL MODEL WHICH COMBINES ROUGHNESS AND PLASTICITY INDUCED FATIGUE CRACK CLOSURE

**Nong Chen, Ph. D**
**Department of Civil Engineering**
**University of Illinois at Urbana-Champaign, 1997**
**Frederick V. Lawrence, Jr., Advisor**

## ABSTRACT

In this study an analytical PICC-RICC Model was developed to describe better the near-threshold fatigue behavior. The PICC-RICC Model was built upon a strip-yield type PICC model originally proposed by Newman and later modified by Hou and Lawrence. A zigzag crack growth path was introduced to simulate surface roughness. The two opposing crack surfaces were considered to be translated and thus mismatched by the mixed-mode displacements occurring near the deflected crack tip. The model is powerful and unique in that it combines the effects of RICC and PICC. Thus, the gradual transition from RICC to PICC dominated crack closure is handled naturally by this model.

The influences of the geometrical features of the surface roughness, R-ratio and the cyclic load range on RICC were examined using the PICC-RICC Model. Near-threshold fatigue behavior of various materials was predicted. The effect of microstructure on the RICC level was studied. The predicted results compared favorably with experimental data.

The fatigue notch size effect was investigated using the PICC-RICC model. The initial crack length ($a_i$) for propagation was estimated. The predicted notch fatigue strength compared favorably with the Initiation-Propagation (I-P) Model prediction and test data. The existence of a "worst case notch" previously postulated using the I-P Model was confirmed.

*In memory of*

*my maternal Grandmother, Mrs. J.-F. Chen*

# ACKNOWLEDGEMENTS

I would like to express my profound gratefulness to my advisor, Professor F. V. Lawrence, Jr. for his guidance and encouragement. He has helped me greatly and constantly in both my professional and personal development with his wisdom, experience, intuition and patience.

I would like to sincerely thank Professor R. H. Dodds, Professor H. Sehitoglu and Professor D. F. Socie for their encouragement and advice and for serving on the dissertation committee of both my preliminary exam and final defense.

This research was funded mainly by the Conoco, Inc, in Ponca City, Oklahoma. I would like to deeply thank Dr. M. Salama from Conoco for his invaluable suggestions and support. The research had also been funded by the Fracture Control Program (FCP) at the University of Illinois at Urbana-Champaign, which has provided me with invaluable opportunity to keep in touch with the applications of fatigue research.

I wish to express my deep appreciation to members of our fatigue group: Dr. G. Banas, Dr. C.-Y. Hou, Dr. G. Fry, Dr. H.-Y. Hsieh, Mr. S. Dimitrakis, Ms. W. Liu and Mr. J. Withee for creating a most supportive group environment. I would especially like to thank Dr. C.-Y. Hou for his help during my "freshman" year.

To my parents, Mr. Q.-Y. Chen and Mrs. G.-H. Liu, whose only request of me was that I be a good human being, I wish I could find enough words to describe my gratitude towards them for being so loved and cared for.

To my husband, Ji-min, who has accompanied me through ups and downs with love, faith and a forever upbeat spirit, I am so happy and grateful, everyday, for having you.

# TABLE OF CONTENTS

# LIST OF TABLES

# FIGURE CAPTIONS

# LIST OF SYMBOLS

| | |
|---|---|
| $a$ | Crack length |
| $a_p$ | Peterson's constant |
| $a_i$ | Initial crack length for crack propagation |
| $a_f$ | Crack length at failure |
| $\alpha$ | Constraint factor of Newman |
| $b$ | Fatigue strength exponent |
| $c$ | Fatigue ductility exponent |
| $C$, $C'$, $m$ | Paris law and modified Paris law material constants |
| $d$ | Grain size |
| $D$ | Notch depth |
| $\varepsilon'_f$ | Fatigue ductility coefficient |
| $E$ | Young's modulus |
| $\psi$ | Inclination angle of the slip plane |
| $G$ | Shear modulus |
| $g(x, a)$ | Weight function of a crack of length a |
| $K$ | Strength coefficient |
| $K'$ | Cyclic strength coefficient |
| $K_{cl}$, $K_{open}$ | Crack-closure and Crack-opening stress-intensity factor |
| $K_{cont}$ | Stress intensity factor due to contact stress $\sigma_c(x)$ |
| $K_f$ | Fatigue notch factor |
| $k_1$, $k_2$ | Local Mode-I and Mode-II stress intensity factors at the deflected crack tip |
| $K_I$, $K_{II}$ | Mode-I and Mode-II stress intensity factors |
| $K_{max}$, $K_{min}$ | Applied maximum and minimum stress-intensity factor |
| $K_t$ | Stress concentration factor |

| | |
|---|---|
| $L, h, \theta$ | Branch length, branch amplitude and tilt angle of the assumed zigzag crack growth path |
| $l_t$ | Transition crack length |
| $\lambda(x)$ | Deviation of crack from a straight path |
| $\nu$ | Possion's Ratio |
| $n$ | Strain hardening exponent |
| $n'$ | Cyclic strain hardening exponent |
| $N_F$ | Total crack propagation life |
| $N_I$ | Crack initiation life |
| $N_N$ | Crack nucleation life |
| $N_{P1}$ | Short crack propagation life |
| $N_{P2}$ | Long crack propagation life |
| $N_T$ | Total fatigue life |
| $q$ | Notch sensitivity factor |
| $r$ | Notch radius |
| $R$ | Stress ratio |
| $\rho_N$ | Neuber's constant |
| $\rho_c$ | Crack-tip plastic zone size |
| $\rho_n$ | Notch plastic zone size |
| $S_{cl}, S_{open}$ | Crack-closure and crack-opening stresses, respectively |
| $S_e$ | Fatigue strength |
| $S_e^{unnotched}, S_e^{notched}$ | Fatigue strength of unnotched and notched specimen |
| $S_{max}, S_{min}$ | Applied maximum and minimum stress |
| $\sigma(x), \tau(x)$ | Unflawed tensile and shear stress distribution |
| $\sigma_c(x)$ | Distribution of contact stress along crack wake at $S_{min}$ |
| $\sigma'_f$ | Fatigue strength coefficient |
| $\sigma_m$ | Mean stress |

| | |
|---|---|
| $\sigma_y$, $\sigma_u$ | Yield and ultimate strength of material |
| $\sigma_0$ | Flow stress |
| t | Plate thickness |
| $T_n(x)$, $T_s(x)$ | Distribution of normal and shear stress along the deflected crack path |
| $\tau_c$ | Critical stress to initiate slip |
| u | Crack-face displacement |
| U | Effective stress-intensity factor ratio |
| w | Plate width |
| $w_c$ | Specific fracture energy per area |
| x | Coordinate system located at notch root |
| $\Delta K$, $\Delta K_{eff}$ | Stress-intensity range and effective stress-intensity range |
| $\Delta S$ | Applied stress range |
| $\Delta\tau_\psi$ | Range of resolved cyclic shear stress along the slip plane |

# LIST OF ABBREVIATIONS

| | |
|---|---|
| CTPS | Crack-Tip Plastic Stretches |
| FEA | Finite Element Analysis |
| FDM | Finite Difference Method |
| I-P | Initiation-Propagation |
| LEFM | Linear Elastic Fracture Mechanics |
| NPS | Notch Plastic Stretches |
| OICC | Oxide-Induced Crack Closure |
| PICC | Plasticity-Induced Crack Closure |
| RICC | Roughness-Induced Crack Closure |
| SYMNC | Strip-Yield Model for Notched Components |
| TPS | Total Plastic Stretches |

# CHAPTER I: INTRODUCTION

## 1.1 BACKGROUND

Since the crack-closure phenomenon was first observed in the late sixties, the important influence of crack-closure on fatigue life of engineering components has gradually been realized. The consideration of plasticity-induced crack-closure (PICC), the first type of crack-closure being identified and the most widely studied, has provided explanation for effects such as R-ratio and load sequence on fatigue crack growth. However, the high level of crack-closure at near-threshold region can not be explained by PICC only. Neither can PICC be held accountable for the microstructural effect on fatigue crack growth in the near-threshold region which has been observed in fatigue experiments. Instead, crack-closure caused by roughness, termed roughness-induced crack-closure (RICC) is believed to have the major influence over fatigue crack growth in the near-threshold region.

Due to the importance of RICC at near-threshold region, it becomes a key to understanding fatigue crack initiation and early growth behavior. It is hence essential to take into account RICC in high-cycle fatigue life predictions. A few numerical approaches have been developed to model RICC; yet due to the complex and chaotic nature of RICC, none of these approaches appears efficient enough to incorporate RICC into the consideration of engineering design.

## 1.2 OBJECTIVE AND SCOPE

The goal of this study is to develop a sophisticated model to simulate the complex roughness-induced crack-closure phenomenon, at the same time to keep the model easy to implement so that it can be used in engineering design to predict the long-life fatigue behavior of structural components.

Newman's modified Dugdale strip-yield model for plasticity-induced crack-closure is improved to include RICC caused by local mixed-mode sliding between crack surfaces as the result of deflected crack growth path. Various factors which influence the severity of RICC are investigated. Near-threshold fatigue behavior is predicted using the model. The validity of these predictions is verified with experimental data. The effectiveness of the model is confirmed by comparing the predictions with those made using previous RICC model. The fatigue notch size effect is investigated using the model and the results are compared with existing theories.

## 1.3 THESIS ORGANIZATION

The thesis is organized in the following order:

Chapter II Literature Review

The development of crack-closure concept is reviewed, various crack-closure mechanisms are presented, and the origin of roughness-induced crack-closure as well as different models developed for the simulation of PICC and RICC is discussed.

Chapter III Modified Dugdale Strip-Yield Model

The Dugdale-type strip-yield model developed by Newman for the modeling of plasticity-induced crack closure is presented. This presentation is followed by improvement made by Hou and Lawrence to include notch-plasticity. The insufficiency of the model in the near-threshold region is discussed.

Chapter IV Developing an Analytical PICC-RICC Model

An analytical model developed based on the strip-yield PICC model to simulate both roughness-induced crack closure and plasticity-induced crack closure, the PICC-RICC Model, is introduced.

Chapter V Preliminary Examination of the Near-threshold RICC Behavior

The effect of RICC due to crack-path deflection is simulated using the PICC-RICC model. The influences of the geometrical characteristics of the surface roughness, R-ratio and cyclic load range on the severity of RICC are investigated.

Chapter VI Investigation of the Microstructurally Sensitive Near-Threshold Fatigue Crack Growth

The microstructurally sensitive near-threshold fatigue crack growth is predicted and examined using the PICC-RICC model. The predicted results are compared with experimental data as well as the prediction made using a previous finite-difference model.

Chapter VII Investigation of the Fatigue Notch Size Effect

Existing fatigue life prediction models for notched components are reviewed. The fatigue notch size effect is re-examined using the PICC-RICC model. First, a total life model is developed as follows: A dislocation double-pile up model is employed to calculate the nucleation life of the notched component; the PICC-RICC Model is used to calculate the propagation life; the initial crack length for propagation, $a_i$, is determined based on the competition between the nucleating and propagating processes. Next, the notch fatigue

strength and fatigue notch factor are predicted using the total life model developed. The predicted results are compared with experimental data as well as those predicted using Peterson's and Neuber's empirical relationships. The existence of a "worst case notch" for notched components with variable notch root radii is confirmed.

Chapter VIII Discussion

The influence of microstructure on RICC is investigated and its three-dimensional effect on RICC is discussed. Fatigue notch size effect predicted using the PICC-RICC model and the Initiation-Propagation (I-P) model are compared.

Chapter IX Conclusions and Proposed Future Work

Conclusions from this study are drawn and topic for further investigation is proposed.

Appendix A Weight Functions for Single-Edged and Center-Cracked Specimen

Mathematical formulations of the weight functions for single-edged and center-cracked specimen are presented.

Appendix B A Double Pile-Up Dislocation Model for Crack Nucleation

A brief description of the double pile-up dislocation model used to calculate fatigue crack nucleation life.

# CHAPTER II: LITERATURE REVIEW

## 2.1 FATIGUE CRACK CLOSURE MECHANISM

Crack-closure refers to the phenomenon of premature contact between crack surfaces when far field stress is still tensile. Because of crack-closure, only a portion of the fatigue cycle will actually contribute to the advance of the crack since no fatigue crack growth is assumed until the crack tip has fully opened.

The crack closure phenomenon was first observed by Elber [1-2]. He detected a non-linearity in crack-face displacement and applied stress relation during fatigue test of a 2024-T3 aluminum alloy. Observation of the stress-displacement curve revealed that such variation in material compliance was due to the change in fatigue crack configuration. Further examination led to the conclusion that the non-linearity was caused by premature contact between crack surfaces when the far-field stress was tensile. The premature contact Elber found was the result of plastic deformation left along the crack wake: see Fig. 2.1. This kind of crack-closure mechanism was later termed "plasticity-induced crack-closure" (PICC) [3]. Since its first observation, PICC has been extensively studied both theoretically and experimentally. The concept of PICC has been used to explain many fatigue crack growth characteristics under both constant amplitude and variable amplitude loading, such as the effect of R-ratio or the load sequence effect. The extent of PICC is directly related to the bulk parameters that affect plastic deformation of the material, such as the yield strength and the applied load level, while the effect of the microstructure of the materials is not directly reflected.

Several other crack-closure mechanisms other than PICC have been identified. Since then it has become impossible to perform fatigue growth analysis without considering crack closure.

Walker and Beever [4] were the first to identify the significant effect of crack-closure arising from rough fracture surface morphology, which was later termed "roughness-induced crack closure" (RICC) [5]. Crack-tip Mode-II sliding, promoted by deflected crack growth path resulting from the surface roughness, can wedge the crack open at discrete contact points along crack faces and hence causes enhanced crack-closure: see Fig. 2.2(a). RICC has since been recognized as one of the dominant closure mechanisms in the near-threshold region. With its high sensitivity to microstructure, RICC mechanism contributes greatly to the microstructural influence on fatigue crack growth in the near-threshold region [4-13].

Another crack-closure mechanism which also plays an important role in near-threshold fatigue behavior is oxide-induced crack closure (OICC) [9, 14-15], as it was later named [3]. OICC is the result of corrosion deposits, whose size is comparable to crack-tip displacement, and which build up near the crack-tip in moist environments: see Fig. 2.2(b). Fretting oxidation [16] has been suggested as the likely cause for the formation of such corrosion deposits. OICC mechanism has since been used to provide plausible explanations of the influence of environment in the near-threshold fatigue behavior of metallic materials [9, 14-15, 17-18].

The influence of RICC and OICC on high-cycle fatigue is tremendous due to the critical roles they play in the near-threshold region. Due to the complex and chaotic nature of RICC and OICC, far less progress has been achieved in the understanding of either RICC or OICC as compared to PICC. A sophisticated and easy-to-implement model still remains to be developed before the effect of crack-closure can be estimated accurately in high-cycle fatigue regime.

Other proposed crack-closure mechanisms include: phase transformation-induced crack closure caused by a net volume increase at the crack tip during phase-transformation [19-20]; viscous fluid-induced crack-closure which could result from complete penetration of the crack by high viscosity fluid [21-22] and grain boundary-induced crack closure which arises from the possibility that the opening range of a crack may be reduced when the crack approaches a grain boundary [23-25].

The study of various crack-closure mechanisms have greatly advanced the understanding of fatigue crack growth and fracture behavior of metallic materials.

The stress intensity factor range, $\Delta K$, has been defined as

$$\Delta K = K_{max} - K_{min} \tag{2.1}$$

where

$K_{max}$ = Stress intensity factor at maximum applied stress, $S_{max}$

$K_{min}$ = Stress intensity factor at minimum applied stress, $S_{min}$

Before the crack-closure mechanisms were recognized, Paris, et al [26] suggested that $\Delta K$ be used as the linear-elastic fracture mechanics (LEFM) characterization of the "driving force" for fatigue crack growth. They proposed the following governing equation which has become well known as the Paris equation:

$$\frac{da}{dN} = C\,(\Delta K)^m \tag{2.2}$$

where:

| | | |
|---|---|---|
| $\frac{da}{dN}$ | = | Fatigue crack growth rate |
| a | = | Fatigue crack length |
| N | = | Fatigue life (cycles) |
| C, m | = | Materials constants in Paris equation |

The use of $\Delta K$ as the crack driving force, however, pertains only to the situation when the crack-tip is fully open during the entire fatigue cycle. Its use becomes inappropriate under the influence of crack-closure when the crack is fully open during only part of the loading cycle.

To reflect the effect of crack-closure, Elber [2] introduced the concept of "effective stress intensity factor range", $\Delta K_{eff}$, which is defined as the following:

$$\Delta K_{eff} = K_{max} - K_{open} \tag{2.3}$$

where

| | | |
|---|---|---|
| $K_{open}$ | = | Stress intensity factor at the crack opening stress, $S_{open}$ |

He suggested that under the influence of crack-closure, $\Delta K_{eff}$ better represent the *actual* driving force for fatigue crack growth. The followed "modified Paris equation" was proposed:

$$\frac{da}{dN} = C' (\Delta K_{eff})^m \tag{2.4}$$

where

| | | |
|---|---|---|
| C', m | = | Materials constants in the modified Paris equation |

One parameter frequently-used to represent the extent of crack-closure, the effective stress-intensity ratio, U, has been defined as:

$$U(a) = \frac{\Delta K_{eff}(a)}{\Delta K(a)} = \frac{K_{max}(a) - K_{open}(a)}{K_{max}(a) - K_{min}(a)} = \frac{S_{max}(a) - S_{open}(a)}{S_{max}(a) - S_{min}(a)} \tag{2.5}$$

in which a is the fatigue crack length. Eq. (2.3) can now be written as:

$$\frac{da}{dN} = C'(U\Delta K)^m = C'U^m (\Delta K)^m \tag{2.6}$$

Once the value of U is known, the fatigue crack growth rate behavior under the influence of crack-closure can be calculated from Eq. 2.6, and the fatigue life of the component considered can be found from the integration of Eq. 2.6.

## 2.2 Analytical and Numerical Study of Plasticity-Induced Crack-Closure

### 2.2.1 The Study of PICC of Fatigue Crack in a Smooth Specimen

PICC has been intensively studied. Both analytical and numerical approaches have been developed to estimate the extent of PICC.

The comprehensive analytical work of Budiansky and Huchinson [27], through a Dugdale-type analysis [28], provided the theoretical justification for the use of $\Delta K_{eff}$ to characterize the fatigue crack growth under plane stress state. Similar investigations have been conduct and the results of these study were used to predict fatigue crack growth under spectrum loading [29-30]; yet to date it has remained too difficult to carry out a parallel theoretical analysis of PICC under plane strain condition.

Elastic-plastic finite element analysis (FEA) was the first numerical approach developed to estimate PICC. Earlier models were built to study PICC under plain stress [31-32]. The work was later extended to consider constant and variable-amplitude fatigue under plain strain condition [34-40]. Three-dimensional FEA [41-42] was also conducted for thick plate. It has been found that the value of $S_{open}$ varies throughout the thickness of the plate. FEA proved the existence of PICC under plain strain condition. The method has been shown to be quite accurate and can deal with various geometry, materials and loads, but in general it is very complicated, requires large computing facilities and is costly. In addition, different choices of mesh design may add artificial influences to the outcome of the finite-element analysis affecting the reliability of the results [38, 42].

Attempts have been made to develop simpler models of crack-closure. Newman [43-44] first proposed the strip-yield Dugdale model. The model can be viewed as a discretized, numerical version of the analytical Dugdale-type model [27-30]. Plastically deformed material causing PICC was simulated with narrow strips attaching to the crack wake with the height of each strip equal to the amount of plastic deformation at that location. Crack opening stress, $S_{open}$, was calculated from the contact stress acting upon these strips. From $S_{open}$ the effective stress intensity factor U could then be found.

The strip-yield Dugdale model was built upon plane-stress PICC theory as a two-dimensional model. For situations where plane stress does not prevail, due to constraint from thickness direction, a higher level of applied stress will be required to achieve the same amount of plastic deformation as that under plane stress. Since the amount of plastic deformation strongly influences PICC, this three-dimensional constraint effect needs to be considered when estimating PICC of fatigue crack in a thick specimen. A constraint factor, $\alpha$, was introduced into the strip-yield model to take into account such a thickness effect. The material in the fatigue cracked plate is assumed to yield under stress equal to $\alpha\sigma_y$, where $\sigma_y$ is the yield stress of the material. Under plane stress, $\alpha$ has the lower-bound value of 1, while under plane strain, near-tip stress analysis and von-Mises criterion [45] gives $\alpha = 3$ as its upper bound. For a thick plate specimen, the stress state changes from near plane stress at the surface to near plane strain in the middle of plate, and the $\alpha$ factor represents the average constraint effect throughout the thickness of the plate. Irwin's [46] suggested the use of a modified $\alpha$ value (1.73) to represent nominal plane-strain condition to account for such through-thickness variation of stress state. Other methods, such as correlation with crack growth rate [44] or crack-tip plastic zone size [47-48] were also proposed as an attempt to determine the value of $\alpha$. Three-dimensions finite-element analysis appears to be the best way to determine the $\alpha$ value. Three-dimensions finite-element analysis was carried out to examine the influence of material behavior, load level and specimen geometry on $\alpha$ and this result was used to determine the $\alpha$ value needed in the Dugdale strip-yield model [49].

The Dugdale strip-yield model was initially developed to study PICC of compact-tension specimen [27]. With the use of a weight function method [47-48], the applicability of the model has been expanded to specimens with complicate geometry.

The strip-yield Dugdale model has been shown to be simple and easy to implement; it demonstrated its capability when applied to solve constant and variable PICC problems under both plane stress and plane strain conditions [43-44, 47-48, 50-51].

### 2.2.2 Modeling PICC of Fatigue Crack in the Vicinity of a Notch

Most fatigue cracks emanate from a notch-like defect which causes stress concentration. A short crack emanating from a notch has been observed to grow fast initially, then to exhibit growth retardation before gradually recovering to the growth rate of a long crack. Sometimes the retardation can be severe enough to cause complete arrest of the fatigue crack [52-56]. Fracture mechanics-based methods were used to correlate fatigue notch behavior and to calculate the fatigue life of notched components [52-62].

The crack-closure concept has been proposed as an explanation of the fatigue crack behavior at a notch. The transient behavior is thought to be related to the initial absence then

gradual built-up of crack closure [63]. Finite-element models were developed to study PICC at a notch [36, 40, 63-68]. Ting and Lawrence [69-71] proposed a method to consider RICC, OICC and PICC for fatigue crack initiation and propagation from notch root. In their approach, Tanaka's Equation [72] was used to estimate the effect of OICC and RICC in the near-threshold region. The effect of PICC was calculated from previous finite-element results [40]. From the calculated U factor, they further determined the crack propagation life and threshold stress of notched components. This approach was later applied by Hou and Lawrence [73] to investigate the behavior of a fatigue crack emanating from a weld toe.

The strip-yield Dugdale model [43] was modified to simulate the short crack behavior at a notch [44, 74-75]. Based on Newman's model, Hou and Lawrence [76-78] developed a Striped-Yield Model for Notched Components (SYMNC) to study PICC at the existence of a notch of arbitrary geometry. The SYMNC model successfully predicted the reduced crack growth rate as well as the "dip" in U value indicating crack growth retardation as observed in fatigue tests of notched components [63, 65, 79].

## 2.3 Roughness-Induced Crack Closure: Mechanism and Modeling

### 2.3.1 RICC Mechanism

Elber's PICC concept has helped to explain the R-ratio effect, the load sequence effect and the enhanced level of PICC at a notch. Yet PICC, which is most effective under plane stress [81], can not account for the high level of crack closure observed in the near-threshold region, which is dominated by plain-strain condition [3-13, 82-90]. PICC also fails to explain the effect of microstructure, such as grain size, on fatigue crack behavior [3-13, 82-90].

Roughness-induced crack closure has been proposed as the most important form of crack closure in a non-corrosive environment (thus excluding OICC) in the near-threshold region [4-5]. First identified by Walker and Beever [4], RICC is primarily caused by surface mismatch due to mixed-mode displacement between crack surfaces. The details of the formation of RICC are explained in the following:

In the near-threshold region the shortness of the crack-tip plastic zone compared to characteristic microstructural dimension, e.g., grain size of the material, determines that only one primary slip system will be activated. The fatigue crack is in the Stage-I [91] growth period, and its growth path is greatly influenced by the microstructure of the material. As a result, a serrated fracture surface can be found in the near-threshold region leading to a zig-zag fracture path [11, 92]. Such deflection of the crack growth path in the near-threshold has been observed in steel [11], aluminum alloy [93] and titanium [4, 94].

Due to the deflected crack path, Mode-II motion between the crack surfaces will occur even when far field stress is in Mode-I. Fig. 2.3 illustrates the presence of the local mix-moded motion using the example of a kinked crack. The angle of the deflected portion of the crack to the main crack is taken to be $\theta$. The far-field Mode-I stress intensity factor is taken to be $K_I$. The local Mode-I and Mode-II stress intensity factors are taken to be $k_1$ and $k_2$, respectively. When the length of the deflected portion of the crack is infinitesimally small compared to the length of the main crack, analytical solution exits for $k_1$ and $k_2$ which are given in the following equations [105]:

$$k_1 = \frac{1}{4}\left(3\cos\frac{\theta}{2} + \cos\frac{3\theta}{2}\right) K_I \tag{2.7}$$

$$k_2 = \frac{1}{4}\left(\sin\frac{\theta}{2} + \sin\frac{3\theta}{2}\right) K_I \tag{2.8}$$

Such mix-moded motion due to crack-path deflection have been confirmed by stereo imaging studies [95-96]. The lateral sliding between crack surfaces induces mismatch, wedges the crack open (Fig. 2.4) and hence causes RICC.

On the other hand, at a higher stress intensity range well above threshold when crack-tip plastic zone exceeds the characteristic microstructural size, multi-slip system is activated. The fatigue crack is in the Stage-II [91] growth region resulting in a much more planar fracture surface profile. Marked reductions of closure level are observed due to the gradually diminishing effect of RICC as the fatigue crack grows away from the near-threshold region, and the crack closure level approach that of pure PICC [11, 92, 97].

The existence of RICC explains the high level of closure observed within near-threshold region, which can not possibly be accounted for by PICC alone. RICC also helps one to understand the effect of microstructure on fatigue crack growth and explain some of the seemingly contradictory fatigue behavior associated with microstructure. For example, refining grain size has been regarded as beneficial in raising the endurance limit of materials with planar slip. In the near-threshold region, however, decreasing growth rate and higher threshold can be observed in coarse-grained materials [98]. Such beneficial effects of coarse-grain at near-threshold growth rate disappear at high R ratios [12, 98], indicating a strong role of crack-closure. This phenomenon is consistent with the nature of RICC, with the coarse-grain microstructure promoting a more serrated fracture surface, enhancing the closure level, and as a result reducing the fatigue crack growth rate. In fact, as the fatigue crack grows beyond the threshold region and the effect of RICC weakens, the effect of grain size on crack propagation has then been found to become negligible [98, 99].

2.3.2 RICC Modeling

Purushothaman and Tien [7] first tempted to quantify the effect of RICC. They suggested that RICC occurred when the crack-tip opening displacement was comparable to the height of the asperities. They did not consider the effect of the Mode-II motion on the extent of RICC, therefore their result only presented a lower bound of the severity of RICC.

Suresh and Ritchie proposed the so called "micromechanical model" to study RICC [84, 100-101]. A simple geometrical model was used in their study to idealize the fracture surface roughness. The model is the first attempt to quantify RICC based on the severity of surface roughness and Mode-II motion. The model provides a simple and useful tool to ascertain the roles of various factors on RICC. It reveals that a small relative motion between the crack surfaces can cause a marked enhancement of RICC. The model also predicted that the acuity of surface roughness, characterized by the angle of the deflected crack path, has the most prominent influence on RICC over other geometrical characteristics of the roughness. The model was later applied to study fatigue crack growth retardation following an overload at near-threshold region [102]. The model is limited by the fact that it didn't attempt to quantify the magnitude of the mix-moded motion resulting from the deflected crack path. As a result, the value of the ratio of Model-II and Mode-I displacements used in the model was assumed instead of being derived properly. Therefore, the model did not reflect the actual RICC behavior correctly.

An RICC model based on dislocation model was proposed by Ravichandran [103]. The model calculates the Mode-II motion through estimating the number of dislocations emitted during loading. Contrary to the results predicted by the micromechanical model, it predicts that the extent of the deflected branch, rather than the acuity of the roughness, has a stronger influence on RICC.

LLorca [104] developed a finite difference method to study the influence of surface roughness of crack-closure. The Mode-II displacement and hence the mismatch between surfaces were estimated from the deflected crack path. The model is the first numerical attempt to describe RICC behavior in terms of how it actually occurs. The main drawback of the model comes from the convergence requirement of the numerical scheme which can result in an overwhelming amount of computing time, especially if the model tempts to consider both RICC and PICC.

None of the existing RICC models takes into account the combined closure effect of RICC and PICC. As the result, the transition from RICC to PICC dominated closure has not been properly simulated.

## 2.4 SUMMARY

RICC is the dominant crack-closure mechanisms in the near-threshold region and the most significant one in a non-corrosive environment. Studying of the role of RICC in the near-threshold region will help us understand better the early fatigue crack growth behavior and the transition from fatigue crack initiation to propagation. It will also help us to predict better the fatigue life in high-cycle regime. Studying the roll of RICC will provide us with important insight on how the microstructure of the materials influences the near-threshold fatigue behavior and will help to raise the possibilities of improving fatigue performance through the modification of microstructure.

The study of RICC is still at an early stage due to its complex nature. The combined effect of PICC-RICC remains to be simulated; The relationship between RICC and the microstructure remains to be further examined; and the influence of RICC on the fatigue performance of engineering structures and components remain to be investigated.

# CHAPTER III: MODIFIED DUGDALE STRIP-YIELD MODEL

## 3.1 DUGDALE MODEL

Irwin's[46] linear-elastic fracture mechanics (LEFM) solution of the crack-tip stress field gives an unbounded stress distribution at the crack tip. In reality, the material will deform plastically under high stress, and the crack-tip stress will not exceed the yield stress of the material. By taking into account the plasticity of the material, Dugdale[28] developed a model which eliminates the singularity of the stress field at the crack tip. The idea of Dugdale model is briefly described in the following:

Based on the fact that the stress distribution should be bounded, Dugdale proposed the assumption that the unbounded stress at the crack tip in Irwin's LEFM solution should be canceled as a result of the plastic deformation ahead of the crack tip. The two stress fields balance each other; and as a result, the stress at crack tip remains finite.

Fig. 3.1 demonstrates the idea of the Dugdale model using the example of a center-cracked plate. The crack length is 2a with crack tip being located at A. The yield stress of the material is $\sigma_y$. The material is assumed to deform rigid-plastically once it yields. Under a Mode-I tensile load S, a plastic zone will form near the crack tip A. The plastically deformed material is represented by a thin layer of material shown in a dark shade ahead of the crack tip. The size of the plastic zone is assumed to be $\rho$. The far end of the plastic zone is located at B.

A fictitious crack is formed by extending the real crack through the plastic zone. The length of the fictitious crack is $2a + 2\rho$. The fictitious crack is under two stress fields: one caused by the external load S, the other by the uniform yield stress $\sigma_y$ in the plastic zone. The stress distribution of the fictitious crack can be found by superposing the LEFM solutions of the two stress fields. According to Dugdale, the unbounded stresses of the two stress fields should cancel each other to produce a finite stress at B. Hence, the governing equation of the Dugdale model is:

$$K_{I,B}(S, 2a + 2\rho) + K_{I,B}(-\sigma_y, 2a + 2\rho) = 0 \tag{3.1}$$

From Eq. 3.1, the plastic zone size, $\rho$, can be found.

Though the plastic deformation of the cracked specimen has been simplified as a thin layer of rigid-plastic material, the Dugdale model nevertheless provides an easy and physically plausible approach to estimate the plastic zone size at the crack tip. In the next

section, a strip-yield model will be presented which uses the concept of the Dugdale type crack in the study of plasticity-induced crack closure.

## 3.2 STRIP-YIELD MODIFIED DUGDALE MODEL FOR THE ANALYSIS OF PLASTICITY-INDUCED CRACK-CLOSURE

### 3.2.1 Newman's Strip-Yield Dugdale Model

To model PICC, the key issue is to estimate the correct amount of plastic deformation along the crack wake that leads to PICC. Since analytical solutions of PICC are only available for very special cases as solved by Budiansky and Huchinson [27], most PICC studies resort to numerical simulations of the crack-closure behavior.

The finite element method has been successfully applied to analyze the PICC behavior [31-32, 34-42]. The method, however, can be very laborious and time-consuming, especially under near plane-strain conditions.

Newman [43-44] first developed a modified Dugdale strip-yield model as a simpler alternative to the finite element method. A Dugdale-type crack is assumed in the model. The plastically deformed material along the crack wake is discretized into a number of thin strips, hence comes the name "strip-yield" modified Dugdale model.

A new parameter, $\sigma_0$, defined as the flow stress of the material, is introduced. $\sigma_0$ is the average of the yield stress $\sigma_y$ and the ultimate stress $\sigma_u$ of the material. Since the plastic behavior of the material is idealized as rigid-plastic, using $\sigma_0$ instead of $\sigma_y$ as the yield criterion enables the model to take into account the first-order effect of the plastic hardening behavior of an actual material.

While the PICC behavior of an actual fatigue-cracked specimen is a three-dimensional problem, the strip-yield Dugdale model converts the three-dimensional problem into a "quasi two-dimensional" one. This conversion is done by averaging out the constraint effect in the thickness direction of the specimen. The averaged thickness effect is reflected through the use of a constraint factor, $\alpha$. The strip-yield Dugdale model assumes that the material yields under tensile stress $\alpha\sigma_0$ or compressive stress $-\sigma_0$. The value of $\alpha$, varying from unity under plane stress state to near 3 under plane strain state, can be found using the finite element method. Details of the $\alpha$ calculation can be found in Ref. 49.

The main steps of the PICC calculation using the strip-yield Dugdale model are illustrated in Figs 3.2(a), (b) and (c) and are described in the following:

A single-edged specimen is chosen for the demonstration. The length of the crack is a. The tip of the crack resides at A. The crack is subject to cyclic loading varying from maximum stress $S_{max}$ to minimum stress $S_{min}$.

Under $S_{max}$, as shown in Fig. 3.2(a), the plastic zone size, $\rho$, is determined using Equation 3.1. The tip of the fictitious crack resides at B. The plastically deformed material is discretized into thin strip elements attached to the crack surfaces when it is first formed in the plastic zone. The amount of the plastic deformation of each strip element is then estimated. Notice that the strip elements behind the crack tip A have already been broken when the crack propagates through these elements, while the elements still in the plastic zone remain intact. The stress distribution between the crack surfaces is also shown in Fig. 3.2(a). Since the crack is fully open under $S_{max}$, the crack wake is in a stress-free state.

During the unloading portion of the fatigue cycle, distance between the crack surfaces is gradually reduced. Early contact occurs between the crack surfaces due to the presence of the strip elements. When the far-field stress reaches $S_{min}$, the contact stresses $\sigma_c(x)$ acting upon all the strip elements are calculated and illustrated in Fig. 3.2(b).

The last step is to find out the crack opening stress $S_{open}$ during the cycle. Notice in Fig. 3.2(c) that the immediate elements behind crack tip A are all under compressive contact stress. Upon reloading, the contact stress behind the crack tip has to be overcome before the crack can be fully open and start propagating again. Accordingly, Newman proposed the following method to estimate $S_{open}$:

The contact stress behind the crack tip produces a stress intensity factor at A, $K_{I,A}(\sigma_c)$. When the crack is reloaded from $S_{min}$ to $S_{open}$, the increase of the stress intensity factor will offset $K_{I,A}(\sigma_c)$, i. e.,

$$K_{I,A}(S_{open} - S_{min}) = K_{I,A}(\sigma_c)$$

or:

$$K_{I,A}(S_{open}) = K_{I,A}(\sigma_c) + K_{I,A}(S_{min}) \tag{3.2}$$

From Equation (3.2) the crack opening stress $S_{open}$ can be calculated. If we simplify the expression of $K_{I,A}(S_{open})$ with $K_{open}$, $K_{I,A}(S_{min})$ with $K_{min}$ and $K_{I,A}(\sigma_c)$ with $K_{cont}$, the above equation can be rewritten as

$$K_{open} = K_{min} + K_{cont} \tag{3.3}$$

The instance at which the far-field stress reaches $S_{open}$ is illustrated in Fig. 3.2(c). All the compressive stress behind the crack tip has been overcome, and the crack starts to fully reopen.

Newman's modified Dugdale model has been widely applied to study PICC. It has successfully predicted fatigue crack growth retardation due to PICC under various loading conditions [43-44, 47-48, 50-51]. Though its use of an "$\alpha$-factor" to account for the three-dimensional constraint effect of on PICC remains controversial, today the $\alpha$-factor method is still the easiest and most widely adopted method in strip-yield type PICC models.

3.2.2 Strip-Yield Dugdale Model for Notched Components

It has been observed that the PICC behavior is different when a fatigue crack is growing in the vicinity of a notch. While the strip-yield model described in the previous section concerns mainly with smooth specimens, the model can not describe properly the PICC behavior at a notch. This problem is demonstrated in Fig. 3.3. Shown in the figure is a notched specimen under cyclic loading $\Delta S$. The notch plastic zone size is illustrated in the figure. The solid curve in the figure describes the experimentally observed U value of a fatigue crack growing from a notch, where U is the effective stress intensity factor ratio defined in Equation 2.5. A "dip" is developed in the curve as the fatigue crack grows through the notch plastic zone. The formation of the dip indicates a severe PICC effect near the notch root, which is due to notch plasticity. The dotted line in Fig. 3.3 corresponds to the predicted U value made using the strip-yield modified Dugdale model. Though the predicted curve agrees well with the experimental observation once the crack has propagated away from the notch for a certain distance, the "dip" in the early U value has not been captured by the model.

Since most engineering cracks emanate from notch-like defect, it is essential for a model to take into account the increased PICC level near a notch root. For this purpose, Hou and Lawrence[76-78] set out to improve the strip-yield model. Realizing the fact that the complexity of notch PICC behavior arises from notch plasticity, Hou and Lawrence argued that the problem can be solved by taking into account the extra amount of plastic deformation attributed to notch plasticity. This idea is illustrated in Fig. 3.4. As shown in the figure, a fatigue crack of length a is propagating near a notch root. The crack-tip plastic zone size is denoted as $\rho_c$, the notch plastic zone size is denoted as $\rho_n$. The plastic deformation inside the crack tip plastic zone is defined as the Crack-Tip Plastic Stretch (CTPS). The plastic deformation inside the notch plastic zone is defined as Notch Plastic Stretch (NPS). While only CTPS is included in Newman's strip-yield model, Hou and Lawrence proposed that both CTPS and NPS should be considered in order to account for the notch effect. The Total Plastic Stretch (TPS) used to estimate PICC is then formulated as:

$$TPS = CTPS + NPS \tag{3.4}$$

When the fatigue crack propagates at the vicinity of a notch root, the crack tip plastic zone can be fully imbedded in the notch plastic zone, as shown in Fig. 3.4. Therefore major portion of the TPS is the NPS. The result is a much more severe PICC behavior; and the value of the effective stress intensity factor ratio, U, plunges much further than what it would be if the specimen were unnotched and the notch plasticity were absent. This effect is what causes the "dip" in the experimentally observed U curve shown in Fig. 3.3. As the crack grows out of the notch plastic zone, the amount of CTPS increases with crack length while the amount of NPS remains unchanged. The main constituent of TPS gradually shifts from NPS to CTPS; consequently, the influence of notch plasticity diminishes. The value of U starts to recover from the bottom of the "dip" before it eventually converges with the U curve of an unnotched specimen.

This improved strip-yield Dugdale model was named the Strip-Yield Model for Notched Components (SYMNC). It has since been used to study the fatigue behaviors of both sharp and blunt notches under different R ratios [76-78]. SYMNC has predicted that for fatigue loading of high $S_{max}$ value and R = 0 ratio, notch plasticity can cause the U value to drop for up to 25%.

The amount of NPS involved in the SYMNC calculation can be estimated using a two-step finite element method. Details of the procedure are described in Ref. 76.

## 3.3 Developing a Strip-Yield Model for Near-Threshold Crack-Closure Due to Roughness

A high level of crack-closure due to roughness in the near-threshold region has long been observed [4-13] under low R ratios. The so-called roughness-induced crack closure, RICC, arises from the early contacts of mismatch between fatigue crack surfaces.

Though the tremendous influence of RICC on early fatigue crack growth and high-cycle fatigue behavior have long been recognized, only in recent years have some attempts being made to simulate the RICC behavior due to the complex and chaotic nature of the RICC. As a result, RICC has remains far less thoroughly studied than PICC.

Considering the importance of RICC on the long-life fatigue behavior, the concept of RICC must be incorporated into the consideration of fatigue design of engineering components. For this purpose, a sophisticated and easy-to-implement model needs to be developed. The success of the strip-yield model for the simulation of PICC suggests a promising approach for the study of RICC. In the following chapter, a strip-yield type PICC-RICC model will be developed, and near-threshold RICC behavior will be simulated and examined using the PICC-RICC model.

# CHAPTER IV: DEVELOPING AN ANALYTICAL PICC-RICC MODEL

## 4.1 AN ANALYTICAL PICC-RICC MODEL WITH AN ASSUMED ZIGZAG FATIGUE CRACK GROWTH PATH

### 4.1.1 Mechanism of Fatigue Crack Path Deflection in the Near-threshold Region

The surface mismatch that leads to RICC is mainly caused by the deflection of fatigue crack growth path. The formation of such deflected path at near-threshold region can be explained using the Forsyth's fatigue crack growth theory [91] as described below:

According to Forsyth's theory, during near-threshed fatigue crack growth, the smallness of the crack tip plastic zone compared to the characteristic microstructural dimension of the material, e.g., the grain size, determines that only a single primary slip system will be activated: see Fig. 4.1. The fatigue crack advances by shearing along this primary slip system. When the crack tip grows near the grain boundary, it reorients itself to propagate along the new direction of the favorite slip system in the next grain: see Fig. 4.1. The result of this is that a fatigue crack grows along a zigzag path under a mixed-mode of Mode-I and Mode-II. This stage of fatigue crack growth is termed "Stage-I" by Forsyth. This stage, marked with a serrated fracture surface profile, has been observed in steel [11], aluminum alloys [93] and titanium alloys [4, 94]. As the fatigue crack advances further, the stress intensity factor increases accordingly. This increase results in a secondary slip system being activated: see Fig. 4.2. The fatigue growth enters the "Stage-II" period defined by Forsyth. During Stage-II the fatigue crack advances concurrently along both slip systems, resulting in a Mode-I growth that creates a planar path perpendicular to the far field tensile stress. Consequently the source which leads to RICC gradually diminishes in Stage-II. The onset of the secondary slip system is thought to be strongly correlated with the condition that the plastic zone size is on the order of the grain size: see Fig. 4.2.

### 4.1.2 Introducing a Zigzag Fatigue Crack Growth Path

Based on the Stage-I fatigue crack growth mechanism, a zigzag path is assumed to simulate surface roughness. As shown in Fig. 4.3, a zigzag path with branch length L, branch amplitude h and tilt angle $\theta$ is introduced. To reflect the absence of crack path deflection during Stage-II fatigue crack growth, in the model calculation $\theta$ is set to zero once the near-tip plastic zone size equals the grain size of the material.

The assumed zigzag path, a simplification of the actual profile of the fatigue crack surface, reflects the two main characteristics of a Stage-I fatigue crack growth path: the

deviation from a straight path normal to the far field tensile stress and the deflection induced by grain boundaries.

### 4.1.3 An Analytical PICC-RICC Model: Combining the Strip-Yield PICC Model with a Zigzag Fatigue Crack Growth Path

The zigzag path introduced in the previous section, shown again in Fig. 4.4(a), is implemented into the strip-yield PICC model described in Chapter 3, shown in Fig. 4.4(b) to form an analytical PICC-RICC model, see Fig. 4.4(c). The combined effect of PICC and RICC will be simulated naturally using this PICC-RICC model, as will be demonstrated in the next few chapters.

A modified weight function method will be used to estimate the near-tip stress and displacement field of the deflected crack. Details of the method are given in the following section.

## 4.2 Estimating the Near-Tip Stress and Displacement Fields of a Deflected Crack

### 4.2.1 Estimating the Near-Tip Stress and Displacement Fields of a Straight Crack in a Specimen with an Arbitrary Geometry Using the Weight Function Method

Shown in Fig. 4.5(a) is a straight crack in a linear-elastic specimen with arbitrary geometry. The length of the crack is a. The crack is under far-field tensile stress S. The case is equivalent to the superposition of two parts as shown in Fig. 4.5(b)-(c). Notice that the tensile stress $\sigma(x)$ acting along the crack surfaces in Fig. 4.5(c) is introduced to cancel out the internal tensile stress existing along the fictitious crack line in Fig. 4.5(b) so as to keep the crack surfaces after the superposition stress-free. The problem is now transformed into solving for the stress and displacement fields of the crack under the tensile stress $\sigma(x)$ acting along its surfaces, as shown in Fig. 4.5(c), for which an analytical solution seldom exists for a specimen with an arbitrary geometry.

The main advantage of the weight function method [116-117] is that it enables us to estimate the stress and displacement fields of a specimen having an arbitrary geometry. Using the weight function method, the stress intensity factor of the crack shown in Fig. 4.5(c) can be estimated as:

$$K_I(a) = \int_0^a \sigma(x)\, g(x, a)\, dx \tag{4.1}$$

g(x, a) in the above equation is termed "weight function." A weight function represents the contribution of a single force to the stress intensity factor. Hence the total contribution from the distributed stress σ(x) can be found through the integration given in Eq. 4.1.

The near-tip crack face displacement $u_y(x, a)$, as shown in Fig. 4.5(c), can also be estimated using the weight function method. The results are given in the following equations:

$$u_y(x, a) = \frac{1}{E'} \int_0^a \int_{a_1}^a \sigma(x_2)\, g(x, x_1)\, g(x_2, x_1)\, dx_1 dx_2 \tag{4.2}$$

In which $a_1$ is equal to the larger value of x and $x_2$, and

$$E' = \begin{cases} E, & \text{for plane stress} \\ \dfrac{E}{1 - \nu^2}, & \text{for plane strain} \end{cases} \tag{4.3}$$

E is the Young's modules and ν is the Poison's ratio of the material.

It is obvious that once the weight function g(x, a) is known, the near-tip stress and displacement field can be estimated easily using Eqs. (4.1-4.2). Weight functions can be derived from analytical solutions for a specimen with an ideal geometry or from finite-element analysis [118-119]. The weight functions for both edge and center cracks are given in Appendix A.

4.2.2 Estimating the Stress and Displacement Field Near the Tip of a Deflected Crack Using a Modified Weight Function Method

For a deflected crack, the weight function method for a straight crack needs to be modified. Cotterell and Rice [120] treated the deflection as a first order perturbation from a straight crack when the deflection is considered small compared to the length of the crack, and they estimated the subsequent effect of the deflection on the near-tip stress and displacement field. The same approach was adopted here to modify the weight function method in the case of a deflected crack. The results are presented below:

As shown in Fig. 4.6, a deflected crack is under a far field tensile stress S. Its deviation, small compared to the crack length a, is represented by λ(x). The local mixed-mode stress intensity factors are $K_I$ and $K_{II}$; the crack face displacements are $u_x(x)$ and $u_y(x)$, respectively.

The same superposition procedure is applied to the deflected crack: see Figs. 4.7(a), 4.7(b) and 4.7(c). The normal stress $T_n(x)$ and shear stresses $T_s(x)$ along the fictitious crack shown in Fig. 4.7(b) are calculated and applied to the crack surfaces in Fig. 4.7(c). Stress intensity factors $K_I$ and $K_{II}$ of the deflected crack can now be estimated from the modified weight function method using the following equations:

$$K_I(a) = \int_0^a \sigma(x)_{\text{modified}}\, g(x, a)\, dx \tag{4.4}$$

and

$$K_{II}(a) = \int_0^a \tau(x)_{\text{modified}}\, g(x, a)\, dx \tag{4.5}$$

In Eqs. (4.4 - 4.5) the weight function g(x, a) remains the same as that of a straight crack. However the original weight function method is modified through the introduction of $\sigma(x)_{\text{modified}}$ and $\tau(x)_{\text{modified}}$, which are obtained from the perturbation study of the deflected crack and can be expressed as follows:

$$\sigma(x)_{\text{modified}} = T_n(x) + \lambda(x)\, T_s'(x) + 2\, \lambda'(x)\, T_s(x) \tag{4.6}$$

and

$$\tau(x)_{\text{modified}} = T_s(x) + \lambda(x)\, T_n'(x) \tag{4.7}$$

where $\lambda'(x)$, $T_n'(x)$, $T_s'(x)$ are the first order derivatives of $\lambda(x)$, $T_n(x)$ and $T_s(x)$ respectively, with respect to x. The problem of a slightly curved crack is now approximated by a straight crack under internal loading $\sigma(x)_{\text{modified}}$ and $\tau(x)_{\text{modified}}$: see Fig. 4.8. The near-tip crack face displacements $u_x(x)$ and $u_y(x)$ of the deflected crack can now be estimated using the following two equations:

$$u_y(x, a) = \frac{1}{E'} \int_0^a \int_{a_1}^a \sigma(x_2)_{\text{modified}}\, g(x, x_1)\; g(x_2, x_1)\, dx_1 dx_2 \tag{4.8}$$

$$u_x(x, a) = \frac{1}{E'} \int_0^a \int_{a_1}^a \tau(x_2)_{\text{modified}}\, g(x, x_1)\; g(x_2, x_1)\, dx_1 dx_2 \qquad (4.9)$$

in which $a_1$ is again equal to the larger value of x and $x_2$, and the meaning of $E'$ is same as that given in Eq. 4.3.

After the Mode-II displacement is calculated using Eq. (4.9), the lengths of the strip elements in the PICC-RICC Model are adjusted based on the amount of surface mismatch caused by such Mode-II displacement. In this way the crack closure due to roughness, RICC, is simulated and quantified.

## 4.3 SUMMARY

An analytical PICC-RICC model has been developed based on the strip-yield type PICC model. A zigzag crack growth path is introduced into the model to represent surface roughness. This PICC-RICC Model can simulate naturally the combined effect of PICC and RICC, which will be demonstrated in the next few chapters. The effects of crack path deflection on the near-tip stress and displacement fields is estimated using a modified weight function method.

In the following chapters, the PICC-RICC model will be used to simulate the evolution of RICC as well as the transition from RICC to PICC dominated fatigue crack growth behaviors. The influence of various fatigue parameters such as R-ratio, cyclic stress range and the yield stress of the material on the severity of RICC will be studied. The relation between the microstructure of the material and RICC will be examined. The previously postulated fatigue notch size effect will be investigated. Near-threshold fatigue crack behaviors under the influence of RICC will be predicted using the model, and the predicted results will be compared with experimental data.

# CHAPTER V PRELIMINARY EXAMINATION OF THE NEAR-THRESHOLD RICC BEHAVIOR

## 5.1 EXAMINING THE EFFECT OF THE GEOMETRICAL CHARACTERISTICS OF THE ZIGZAG PATH ON RICC

In this chapter, the PICC-RICC Model developed will be used to study the near-threshold fatigue behavior. Influence of the geometrical characteristics of the assumed zigzag path on RICC will be first examined in this section, followed by a study in the next section of the effects of R-ratio and cyclic stress range on RICC.

As presented in the previous chapter, the zigzag path chosen as a simplification of the actual fatigue crack growth path is characterized by the following geometrical variables: branch length L, branch amplitude h and tilt angle $\theta$. The three variables are inter- dependent with one value depending on the other two: see Fig. 4.3. In this section, the influence of these variables on RICC will be examined.

A fatigue crack is assumed to propagate from an initial length of 0.5mm in an ideal single-edged specimen. The specimen is made of BS4360 50B steel, its properties are shown in Table 1. The cyclic stress range $\Delta S$ is 200MPa. The R-ratio is 0.1.

### 5.1.1 Constant Tilt Angle

First we considers the situation in which the branch length L and branch amplitude h vary while the tilt angle is held constant.

As shown in Fig. 5.1(a), three cases are compared with the tilt angle kept at 45°: case A: L = 50μm, h = 12.5μm; case B: L = 100μm, h = 25μm and case C: L = 200μm, h = 50μm. A fourth case is also presented in which h value is set to zero to represent the effect of PICC only. The $\frac{S_{open}}{S_{max}}$ ratio as well as the effective stress intensity factor ratio, U, were predicted using the PICC-RICC Model. The predicted results are plotted in Fig. 5.1(c) and Fig. 5.1(c).

First thing in Figs 5.1(b)-(c) that attracts one's attention is the pattern of crack-closure development when both RICC and PICC are considered: the crack-closure level is built up shortly after the fatigue crack starts propagating, reaching its maximum level when the crack has advanced approximately the distance of one branch length, then the crack-closure level gradually diminishes over a distance as great as ten times the branch length before it finally converges with that of pure PICC. This result is because RICC is most significant when the crack face opening displacement is small compared to the surface roughness. Therefore as the crack advances, the increase of crack face opening displacement

makes the crack less and less sensitive to RICC due to surface roughness. The closure level initially enhanced by RICC now subsidizes gradually and converges with the closure level of PICC only. Such a RICC to PICC transition has been widely documented in the near-threshold fatigue behavior of various materials, e.g., steel, titanium alloys and aluminum alloys [11, 83, 85, 92, 94], yet it was not predicted by earlier RICC models [100-101, 103-104].

Also noticed is that with the same tilt angle, the zigzag path which has a longer branch length is predicted to have a higher $\frac{S_{open}}{S_{max}}$ value and lower U value, indicating a higher amount of crack closure. For example, with a branch length four times the size of that in case A, the peak $\frac{S_{open}}{S_{max}}$ value of case C was predicted to be more than 80% higher than that of case A. Such variation of RICC with the branch length is physically reasonable and can be explained as follows:

RICC is caused by the mismatch between crack surfaces as a result of the mixed - mode displacement due to the crack path deflection. Neighboring branches with deflect angle $\theta$ and $180° - \theta$ induce shear displacements in opposite directions. A smaller branch length implies a higher frequency for the occurrence of the deflection and a greater likelihood for the neighboring branches to cancel out each other's contribution to the Mode-II motion. As the result, less amount of net shear displacement is generated for a smaller branch length than for a larger branch length. At the same time, a smaller branch length also means a lower branch amplitude when the tilt angle is kept constant; and a lower branch amplitude causes less mismatch even under the same amount of Mode-II displacement. In general, at the same tilt angle, a zigzag path with smaller branch length is less subject to RICC.

### 5.1.2 Constant Branch Length

Now we examine the RICC level when the branch length L is kept constant and the tilt angle $\theta$ and branch amplitude h are varied. The branch length is assumed to be 100μm. The following three cases are compared, as shown in Fig. 5.2(a): case A: tilt angle $\theta = 26.6°$, branch amplitude $h = 12.5\mu m$; case B: $\theta = 45°$, $h = 25\mu m$ and case C: $\theta = 63.4°$, $h = 50\mu m$. Predicted results of the $\frac{S_{open}}{S_{max}}$ ratio and the effective stress intensity factor ratio U are plotted in Figs 5.2(b-c) along with the results predicted for pure PICC.

A similar pattern of RICC evolution as shown in the previous subsection is once more predicted, so is the transition from RICC to PICC dominated fatigue crack growth: see

Figs.5.2(b-c). The peak levels of RICC again occur when the fatigue crack has advanced for a distance of roughly one branch length.

It is also noticed that the severity of RICC increases significantly from case A to case B and then increases further slightly in case C. The peak $\frac{S_{open}}{S_{max}}$ value of case C is predicted to be almost 50% higher than that of case A. Such variation of RICC can be straightforwardly explained as follows:

When the branch length is held constant, a zigzag path with a steeper tilt angle induces more Mode-II displacement between crack faces. At the same time, a corresponding higher branch amplitude causes more mismatch. Therefore, it is no surprise that the case with the steepest tilt angle and the highest branch amplitude yields the most severe RICC.

5.1.3 Constant Branch Amplitude

Lastly in this section, we look at the situation of constant branch amplitude. Branch amplitude is kept at 25μm while the following three cases as illustrated in Fig. 5.3(a) are considered: case A: branch length L = 50μm, tilt angle θ = 63.4°; case B: L = 100μm, θ = 45° and case C: L = 200μm, θ = 26.6°. The predicted results of $\frac{S_{open}}{S_{max}}$ and U for cases A, B, C as well as for PICC only are plotted in Fig. 5.3(b) and Fig. 5.3(c) for comparison.

A pattern similar to those predicted in the last two subsections is again observed in Fig. 5.3(b)-(c). The peak of the closure level occurs at crack advancement of nearly one branch length. What attracts our attention here is that though case C clearly trails the other two cases with the lowest RICC level, there is no obvious superiority between the predicted RICC levels of cases A and B. The peak RICC values predicted for cases A and B appear to be very close except that the peak arrives earlier in case B. An analysis of the predicted results is given below:

The branch length decreases from case C to case B then to case A. As described in section 5.1.1, shorter branch length has the tendency to cause less Mode-II displacement between crack faces and therefore reduces RICC. On the other hand, notice that since the branch amplitude is held constant, as the branch length decreases, the tilt angle increases. This effect in turn promotes the Mode-II displacement and enhances RICC. The combined effect of these two opposite influences makes the predicted RICC behavior looks more complicated than the two previous studies. As one further examines Figs 5.3(b-c), it appears that while a change of branch length always strongly affects the outcome of RICC, a corresponding increase of tilt angle only has a distinctive influence on RICC when the angle is below 45°. For example, when case B and case A are compared, the branch length decreases from 100μm in case B to 50μm in case A. Though the tilt angle increases from 45°

to 63.4° simultaneously, the predicted closure level in case A is still distinctively lower than that in case B due to a smaller branch length. When one compares cases C and B, however, even though the branch length is again reduced in half from 200μm in case C to 100μm in case B, it is almost fully compensated for by the corresponding increase of tilt angle from 26.6° to 45°. The predicted closure levels of case B and case C come out to be very similar except that the peak of the closure level arrives later in case C due to a longer branch length.

5.1.4 Summary of the Predicted Influence of the Geometrical Characteristics of the Zigzag Path on RICC

We summarize the RICC behavior predicted in this section as follows:

i) When RICC and PICC are both considered, RICC is predicted to be dominant in earlier fatigue crack growth and may greatly enhance the crack-closure level. The peak closure level is predicted when the fatigue crack advances for the distance of roughly one branch length. Afterwards RICC gradually diminishes until the crack-closure becomes PICC dominated. Such a transition from RICC to PICC dominated fatigue behavior has been well documented during experimental observations. The current model simulates this transition; whereas, previous RICC models did not [100-101, 103-104].

ii) For the zigzag path assumed, the PICC-RICC model predicts that RICC is influenced by the combined effect of branch length L, branch amplitude h and tilt angle θ. In contrast, most previous RICC models predicted only an effect of tilt angle. The effect of branch length was either not addressed [100-101] or barely detected [104]. It appears physically unreasonable to exclude the influence of branch length on RICC, since such an exclusion would imply that as long as the tilt angle is the same, a zigzag path with a tiny branch length, which can only be considered slightly deflected, will cause the same amount of RICC as that by a highly deflected path with very long branch length. The predicted branch length effect could also provide one of the clues as to why the same material with different grain sizes can be subject to very different amounts of RICC as will be discussed in Chapter VI.

We conclude this section with the following remarks:

The adaptation of a simple zigzag path retains the main features of a faceted fracture surface and renders physically reasonable RICC predictions. A possible relationship between the microscopic features of the material and the near-threshold RICC performance, linked through L, h and θ, will be further discussed in Chapter VI.

The zigzag fatigue crack path is assumed to be identical throughout thickness direction, which is essentially a 2-D simplification of a 3-D problem. The 3-D aspect of RICC will also be discussed in Chapter VIII.

In the next section, we will examine the variations of RICC with the R-ratio and the cyclic stress range, $\Delta S$.

## 5.2 The Influences of R-ratio and Cyclic Stress Range on RICC

In this section we examine the influence of R-ratio and cyclic stress range $\Delta S$ on RICC. The specimen is considered to be an ideal single-edged plate made of BS4360 50B steel having the properties listed in Table 1. The average branch amplitude of the zigzag path is 25μm. The tilt angle $\theta$ is assumed to be 45°. The branch length is calculated from h and $\theta$ as 100μm.

### 5.2.1 The Influence of R-ratio on RICC

First we examine the influence of cyclic stress ratio R on RICC. Cyclic stress range $\Delta S$ in the mean time is kept at 100MPa. Four sets of R values are considered: case A: R = -1; case B: R = 0.1; case C: R = 0.5; and case D: R=0.7. The effective stress intensity factor ratio U for the four cases are predicted and are shown in Fig. 5.4 along with the predictions made for PICC only as a comparison.

The predicted results in Fig. 5.4 suggest only a slight amount of RICC for either positive high R-ratio, such as in case D when R = 0.7, or negative R ratio, such as in case A when R = -1. RICC is predicted to be prominent in cases with positive low R-ratios, such as case B. The absence of RICC at either high R-ratio or negative R-ratio have been confirmed by experimental observations [11, 13, 94, 121]. The reason for this variation of RICC with R ratio is explained as follows:

Under a constant cyclic stress range, when the R-ratio increases, $S_{max}$ and $S_{min}$ increase as well as the crack face opening displacement. When the crack face opening displacement becomes much larger than the surface roughness, the crack becomes much less sensitive to RICC. In fact when the R-ratio goes beyond 0.7, the crack faces may barely come into contact which results in a total absence of RICC. In other words, a gradual reduction of RICC can be expected as the positive R-ratio increases: see cases B, C and D in Fig. 5.4.

At negative R-ratio, on the other hand, the contact between the crack faces is so strong that the surface roughness may be crushed under the compressive stress $S_{min}$ and no longer contribute to crack closure. Therefore RICC is weakened, as indicated by case A in Fig. 5.4.

As the result, the most distinctive RICC is predicted here for positive low R-ratio as has been experimentally observed [11, 13, 94, 121].

5.2.2 The Influence of Cyclic Stress Range ΔS on RICC

Next the influence of the cyclic stress range ΔS on RICC is studied. The R-ratio is kept at R = 0.1 based on the result from the previous study to ensure the presence of RICC. Three sets of cyclic stress ranges are considered: case A: ΔS = 300 MPa; case B: ΔS = 200 MPa; and case C: ΔS = 100MPa. Predicted U values are plotted in Fig. 5.5.

Fig. 5.5 clearly shows that at the same R-ratio, RICC becomes less distinctive as the stress range increases. While a significant amount of RICC is predicted for case C when ΔS=100MPa, almost no RICC is predicted for case A when ΔS = 300MPa with the predicted RICC for case B falls in the middle. Such variation of RICC with ΔS occurs because at the same R-ratio a larger ΔS implies higher cyclic stresses $S_{max}$ and $S_{min}$ which cause larger crack face displacement, which in turn weakens the relative importance of surface roughness. The absence of RICC at high stress ranges also explains why RICC is only important in the near-threshold region.

5.2.3 Summary of the Predicted Influences of R-ratio and Cyclic Stress Range on RICC

We conclude from the study in this section that both positive low R ratios and low cyclic stress ranges promote RICC.

## 5.3 CONCLUSION

The study in this chapter has demonstrated that the PICC-RICC Model developed gives physically reasonable descriptions of some basic characteristics of RICC in the near-threshold region. In the next chapter, the near-threshold fatigue crack growth that is microstructurally sensitive will be examined using the PICC-RICC Model. The effectiveness of the PICC-RICC Model will be checked with experimental data and be compared with a previous finite-difference RICC model.

# CHAPTER VI INVESTIGATION OF THE MICROSTRUCTURALLY SENSITIVE NEAR-THRESHOLD FATIGUE CRACK GROWTH

In this chapter, the high level of crack closure of three different materials in the near-threshold region will be investigated using the PICC-RICC model. The relationship between the crack-closure level and microstructure is examined. The predicted results using the PICC-RICC model will be compared with test data as well as predicted results using finite difference method.

## 6.1 NEAR-THRESHOLD HIGH LEVEL OF CRACK CLOSURE DUE TO RICC

Near-threshold fatigue tests were carried out using 2024-T351 (under-aged) aluminum alloy specimen by Ritchie, et al. [85] and these results will be reexamined in this section using the PICC-RICC model.

The single-edged 2024 aluminum alloy specimen was subjected to low $\Delta K$ value varied from 0.58MPa$\sqrt{m}$ to 0.92MPa$\sqrt{m}$. The initial crack length was 0.09mm and the final crack length was 0.23mm. The stress ratio R is 0.1. The material properties of the aluminum alloy are listed in Table 2.

The variation of $\frac{S_{cl}}{S_{max}}$ with crack length observed during the fatigue test is plotted in Fig. 6.1 along with the predicted closure level for PICC only, where $S_{cl}$ is the stress level when closure occurs.[1] It can be observed from the test result that the crack closure level is much higher than that of PICC only. The extraordinarily high level of crack closure was attributed to RICC [85]. The PICC-RICC model is applied to simulate such high level of crack closure due to RICC. A zigzag deflected crack path with constant tilt angle $\theta = 45°$ and branch length L= 80μm was introduced. The value of branch length was assumed based on the fracture surface roughness feature [85, 104]. The predicted result is also shown in Fig. 6.1 which has successfully simulated the high level of crack closure due to roughness.

The predicted closure level using a Finite Difference Method (FDM) developed by LLorca [104] is also shown in Fig. 6.1. A similar zigzag path with branch length L=80μm was used in FDM calculation. The tilt angle was initially assumed as 26.6°, then jumped to 45° after crack propagated for 0.04mm. An increase of closure level was predicted following the change of tilt angle.

The major difference between the FDM and PICC-RICC model is that the former model does not take into account PICC due to the complexity which would have been

[1] $S_{cl}$ is different from $S_{op}$, the crack opening stress but the two values are considered similar.

brought in the FDM modeling if PICC were considered. Therefore, we can expect the closure level predicted using FDM to be lower than experimental result as well as the closure level predicted using the PICC-RICC Model which takes into account the combined effect of PICC and RICC. The lack of consideration for PICC will also affect the ability of FDM to simulate the transition from RICC to PICC dominated fatigue crack growth.

It has been demonstrated in this section that the enhanced level of crack closure was due to RICC. Next, the RICC mechanism will be further applied to interpret the observed sensitive-to-microstructure near-threshold fatigue crack growth.

## 6.2 Influence of Microstructure on the Near-Threshold Fatigue Crack Growth

In this section, the influence of microstructure on the near-threshold fatigue crack growth of Ti-6Al-4V alloy and AISI 1080 steel will be examined using the PICC-RICC model.

### 6.2.1 Variation of Closure Level with Microstructure in Ti-6Al-4V Alloys

The Ti-6Al-4V alloy was heat treated in two different ways: one (AN705) was annealed at 705°C for 2hrs and air cooled; the other (AN850) was annealed at 850°C for 2hrs and air cooled. The material properties of AN705 and AN850 are given in Table 3. The near-threshold fatigue test was conducted at R=0.05.

From the microstructures of AN705 and AN850 shown in S-T (Short transverse-Transverse) direction in Ref. 94, it can be observed that the average gain size in AN850 is larger than that in AN705. The 3-D fracture surface roughness of AN705 and AN850 were reconstructed using a stereo pair of SEM micrographs[94]. The reconstructed fracture surface roughness at crack growth rate of $10^{-6}$ mm/cycle are shown in Fig. 6.2 which demonstrates a much more serrated fracture surface appearance in AN850 over AN705. The experimentally recorded variation of $\frac{S_{op}}{S_{max}}$ with $K_{max}$ is shown in Fig. 6.3. A distinctively higher level of crack closure can be observed in AN850 over AN705. The difference is clearly the result of the different amount of surface roughness in the two materials caused by the difference in their microstructure, a speculation which is consistent with the Stage-I fatigue crack growth theory proposed by Forsyth which shows the extent of crack path deflection increase with grain size: see Fig. 4.1.

The PICC-RICC model is used to simulate the different closure levels. Zigzag paths with same tilt angle(45°) but different branch amplitude were introduced: the branch

amplitudes was assumed as 12.5μm, 25μm and 50μm, respectively, to analogize the observed variation of fracture surface roughness in AN705 and AN850: see Figs. 6.2. The predicted crack closure levels are shown in Fig. 6.3. Among the three assumed paths, the one with the largest branch amplitude (h=50μm) predicts the highest RICC level which compares favorably with that observed in AN850; the one with the lowest branch amplitude (h=12.5μm) yields the lowest RICC level which compares favorably with that observed in AN705; the crack closure level predicted for the medium branch amplitude (h=25μm) falls in between. Such predicted results confirm that the different RICC level observed in AN705 and AN850 is caused by the unequal amount of surface roughness due to their microstructure difference.

Notice that the experimentally observed closure level decreases and approaches that of PICC only as the crack grows longer, indicating the transition from RICC to PICC dominated fatigue crack growth. Such a decline of RICC is also captured by the PICC-RICC model.

In this section the variation of closure level with microstructure of Ti-6Al-4V alloy in the near-threshold region has been studied. Results indicate that grain size plays an important role in RICC. In the next section, the influence of grain size in the near-threshold fatigue behavior of AISI 1080_steel will be examined.

### 6.2.2 Grain Size Effect on RICC in AISI 1080 Steel

In the experiments carried out by Gray, et al.[13], near-threshold fatigue tests were conducted for hot-rolled rail steel (conforming to AISI 1080 steel) which were coarse grained and fine grained, respectively, to examine the microstructurally sensitive fatigue crack growth. The average material properties of the AISI 1080 steel are given in Table 4. The stress ratio of the tests was R=0.1. The tests were conducted in helium to eliminate potential environmental interference such as oxide film formation.

For the AISI 1080 steel used in the test, the grain size of the fine and coarse grained were measured to be 25.5μm and 130μm, respectively [13]. The corresponding roughness height was measured to be 12.5μm~17.5μm for the fine grained and 30μm~40μm for the coarse grained. Such a variation of surface roughness with grain size, similar to that in Ti-6Al-4V alloy previously discussed, once again demonstrates the relationship between grain size and surface roughness.

In the PICC-RICC model, the roughness amplitude is represented by the branch amplitude of the assumed zigzag path, h. The value of h can be estimated through grain size based on Forsyth's Stage-I growth theory (shown in Fig. 4.1) as:

$$h = \frac{1}{2} d \sin(\theta) \tag{6.1}$$

where d is the grain size and θ is the tilt angle of the deflected path. In the PICC-RICC model, under far field tensile loading the zigzag path is assumed to be along the maximum shear stress direction with θ=45°. Plugging into Eq. 6.1 this value of θ and the measured grain size, the branch amplitude can be estimated to be 9μm for the fine grained and 46μm for the coarse grained, which are in good agreement with the measured values of roughness height. given earlier.

The test data for the variations of closure level (given in terms of $K_{cl}$ and U) with ΔK is shown in Fig. 6.4, which shows a much higher amount of crack closure in the coarse grained material. The PICC-RICC model is used to predict the variation of RICC with grain size. The initial crack length was 0.5mm. The zigzag path has a tilt angle of 45° and a branch amplitude of 9μm (for fine-grained) or 46μm (for coarse-grained). The predicted results, presented in Fig. 6.4, compare favorably with the experimental data. A higher amount of closure in the coarse-grained material over the fine-grained has been successfully captured through the use of different h values estimated using Eq. 6.1 based on grain size.

## 6.3 SUMMARY

In this chapter, the near-threshold crack closure of aluminum alloy, titanium alloy and steel was investigated using the PICC-RICC model. The PICC-RICC model successfully simulated the microstructurally sensitive fatigue-crack growth due to surface roughness variation caused by the grain-size difference. The PICC-RICC model also successfully described the experimentally observed transition from RICC to PICC dominated fatigue crack growth.

# CHAPTER VII INVESTIGATION OF THE FATIGUE NOTCH SIZE EFFECT

In reality, most fatigue cracks emanate from notch-like defect due to stress concentration. Such defects resulting from geometrical or microstructural discontinuities exist in almost all structural components. Hence it is of great importance to understand the influence of notch characteristics on fatigue behavior, especially on the extent of reduction of the fatigue strength.

In this chapter, the PICC-RICC model we have developed will be used to predict the fatigue limit of notched components with various notch geometry. The predicted results will be compared with existing empirical relationships. The predicted variation of the fatigue limit with notch size will be investigated using the model. A previously postulated existence of a "worst case notch" will be verified and explained using the model.

## 7.1 FATIGUE NOTCH SIZE EFFECT AND THE "WORST CASE NOTCH"

### 7.1.1 Fatigue Notch Size Effect

As shown in Fig. 7.1a, the theoretical stress concentration factor, $K_t$, is defined as the ratio of the maximum local stress at notch root over the far field stress as follows:

$$K_t = \frac{\sigma_{max}}{S} \tag{7.1}$$

When the fatigue limit is considered, the ratio of the fatigue limit of an unnotched component, $S_e^{(unnotched)}$, versus the fatigue limit of a notched component, $S_e^{(notched)}$ is defined as the fatigue notch factor, $K_f$:

$$K_f = \frac{S_e^{(unnotched)}}{S_e^{(notched)}} \tag{7.2}$$

$K_f$ reaches the value of $K_t$ for a full theoretical notch effect. Typically the value of $K_f$ is smaller than $K_t$. A notch sensitivity factor, q, is introduced to account for such reduction:

$$q = \frac{K_f - 1}{K_t - 1} \tag{7.3}$$

Empirical relationships have been proposed for the determination of q, the most common being the Peterson's relationship and Neuber's relationship.

Peterson relationship gives the following form for q calculation:

$$q = \frac{1}{1 + \frac{a_P}{r}} \tag{7.4}$$

where r is the notch root radius and $a_P$, Peterson's constant, is a material constant considered to be related to material strength and ductility. For low to medium strength steel, Peterson's constant has been estimated empirically as follows:

$$a_P\,(\text{mm}) = 0.0254 \left(\frac{2070}{\sigma_u\,(\text{MPa})}\right)^{1.8} \tag{7.5}$$

An alternative form to estimate q, as shown in the following, was obtained from Neuber's study:

$$q = \frac{1}{1 + \sqrt{\frac{\rho_N}{r}}} \tag{7.6}$$

where r is again the notch root radius. $\rho_N$, Neuber's constant, is a material constant which is considered to be related to the grain size of the material.

Peterson's and Neuber's relationships were obtained by empirical fit to long life fatigue data of notched and unnotched specimens; Both relationships have revealed that unlike $K_t$, whose value depends only on the geometry of the specimen and loading mode, the value of $K_f$ depends on material property and notch size as well. Such dependency of $K_f$ on material property and notch size implies that fatigue limit of a notched component can not be determined solely upon the acuity of the notch. For example, Peterson's relationship indeed suggests a "worst case notch" with lowest fatigue limit among constant depth notches which does not coincide with the sharpest notch, as will be described next.

### 7.1.2 "Worst Case Notch"

Here we describe the existence of a "worst case notch" among constant depth notch which has been previously postulated by Lawrence, et al [106-108]. For an elliptical notch as shown in Fig. 7.1b, the stress concentration factor $K_t$ can be estimated as:

$$K_t = 1 + 2\sqrt{\frac{D}{r}} \tag{7.7}$$

If one substitutes the above $K_t$ expression into Eq. 7.3, and making use of the Peterson's relationship shown in Eq. 7.4, one get the following expression for $K_f$:

$$K_f = 1 + \frac{2\sqrt{D}}{\sqrt{r} + \frac{a_P}{\sqrt{r}}} \tag{7.8}$$

which suggests the existence of a maximum $K_f$ value at $r = a_P$ with the corresponding $(K_f)_{max}$ equals to:

$$(K_f)_{max} = 1 + \sqrt{\frac{D}{a_P}} \tag{7.9}$$

The postulated "worst case notch" is just an example to demonstrate the complexity of the fatigue notch behavior. The concept of "worst case notch" is of critical importance for the safety of notched components under fatigue loading since it suggests that the lower limit of the fatigue strength should be based on the "worst case notch" instead of the sharpest notch as conventionally thought. To ensure the safety of any engineering components with notch-like defects, one needs to understand how the material properties and notch size are influencing the fatigue life of notched components and to capture the "bottom line" fatigue limit such as the "worst case notch" using a fatigue life prediction model. In the rest of this Chapter, we will apply the RICC-PICC model to investigate the contribution of near-threshold crack-closure to fatigue notch size effect as well as the cause of the "worst case notch".

## 7.2 Fatigue Life-Prediction Models for Notched Components

### 7.2.1 Partitioning of Total Fatigue Life for Notched Components

Most fatigue cracks in engineering structures emanate from notch-like defects. Total fatigue life $N_T$ of a notched component consists of the following portions:

$$N_T = N_N + N_F \tag{7.10.a}$$

$$= N_N + (N_{P1} + N_{P2}) \tag{7.10.b}$$

where $N_N$ is the portion of fatigue life to nucleate a fatigue crack and $N_F$ is the number of cycles to propagate the fatigue crack till failure. $N_F$ can be further divided into two periods: i) $N_{P1}$, the period of early fatigue crack propagation and ii) $N_{P2}$, the period of long fatigue crack propagation until failure. Both $N_{P1}$ and $N_{P2}$ are under the influence of crack closure.

In the following, the existing models for $N_T$ calculation will be described. The necessity of applying the RICC model to predict better the fatigue crack propagation life in the near-threshold region will be discussed.

7.2.2 Initiation-Propagation Model

Lawrence et al [106-108] first proposed the Initiation-Propagation (I-P) model to estimate the total fatigue life of notched components. In the model, the total fatigue life of a notched component is composed of two portions: a fatigue crack initiation periods and a fatigue crack propagation period. The total fatigue life, $N_T$, is estimated as:

$$N_T = (N_N + N_{P1}) + N_{P2} = N_I + N_{P2} \tag{7.11}$$

The initiation life, $N_I$, is considered to consist of the initiation and early growth of fatigue cracks and their coalescence into a dominant fatigue crack. The propagation life, $N_{P2}$, consists of the number of cycles to further advance this dominant fatigue crack till failure. $N_I$ is estimated using the Basquin-Morrow equation as follows:

$$N_I = \frac{1}{2}\left(\frac{\Delta S\, K_f}{2(\sigma_f' - \sigma_m)}\right)^{\frac{1}{b}} \tag{7.12}$$

where

$\Delta S$: remote cyclic stress amplitude
$K_f$: fatigue notch factor
$\sigma_f'$: fatigue strength coefficient
$\sigma_m$: mean stress
b: fatigue strength exponent

$N_{P2}$ is estimated using the Paris Law as follows:

$$N_{P2} = \int_{a_i}^{a_f} \frac{da}{C\,\Delta K^m} \tag{7.13}$$

where

$a_i$: initial crack length
$a_f$: crack length when failure is assumed

C, m: material constants in Paris Law

The I-P model has been applied to examine the fatigue life of weldments [106-108] where fatigue damage is frequently caused by notch-like defects. Similar initiation-propagation model was proposed by Dowling [59] where the stress concentration factor of the notch, $K_t$ was used instead of $K_f$ in the calculation of $N_I$.

One difficulty with the Initiation-Propagation type model is determining the value of $a_i$ which is used as the initial flaw size in the calculation of $N_{P2}$. the value of predicted $N_{P2}$ strongly depends on $a_i$. Lawrence et al. assumed an "engineering crack size" of about 0.25mm as the value of $a_i$. Dowling[59] used the concept of transition crack length, $l_t$ and estimated $a_i$ as $D + l_t$.[2] Socie [61] simplified the problem of calculating $l_t$ by assuming $a_i$=D and also obtained good predictions of $N_T$, where D is the notch depth. It appears that though the physical meaning of $a_i$ as the initial length for propagation can be easily defined, a rigorous determination of $a_i$ based on this definition has yet to be done.

Fatigue crack behavior demonstrates special features near the notch root, among them the short crack behavior, the non-propagation of a crack and the fatigue notch size effect are all believed to be strongly related to crack closure, predominantly PICC and RICC in a non-corrosive environment. In the I-P model, instead of explicitly taking into account the influence of crack closure, $N_I$ is estimated using the strain-life approach to avoid the consideration of short crack behaviors while the fatigue notch sensitivity and fatigue notch size effect are reflected through the use of the empirical fatigue notch factor $K_f$. Hence a crack closure model which is capable of describing the near notch closure phenomenon should provide us with a rationalized explanation and better understanding of the fatigue notch behavior and enables us to predict better the total fatigue life of notched components.

### 7.2.3 Crack-Closure at a Notch Model

Realizing the importance of crack closure to fatigue notch performance, Ting and Lawrence [69-71] further proposed the Crack-Closure at a Notch model. The so-called CCN model incorporates the idea of crack-closure into Eq. 7.10b to estimate the total fatigue life, in which the crack nucleation life, $N_N$ is estimated using the Basquin-Morrow Equation as:

$$N_N = \frac{1}{2}\left(\frac{\Delta S\, K_t}{2(\sigma_f' - \sigma_m)}\right)^{\frac{1}{b}} \tag{7.14}$$

---

[2] $l_t$ is defined as the crack length from notch root beyond which the crack is believed to have grown out the notch-stress zone.

The propagation life, $N_F$, is estimated separately in two parts: $N_{P1}$ and $N_{P2}$. PICC was considered the dominant form of crack closure during the period of $N_{P1}$ when the fatigue crack is subject to the enhanced stress field near the notch root, followed by the coexistence of RICC and PICC during the period of $N_{P2}$. The effective stress intensity factor ratio $U_1(x)$ used to estimate $N_{P1}$ was obtained from FEM calculation of PICC by Sun and Sehitoglu [40]. The amount of RICC/OICC was estimated by converting Tanaka's empirical fatigue threshold ($\Delta K_{th}$ ) equation [72]. The stress intensity factor $U_2(x)$ used to estimate $N_{P2}$ was then formed by combining the RICC/OICC and PICC results based on the assumption that RICC/OICC dominates in the near-threshold region and PICC dominates in regime far away from threshold, with an assumed exponential variation in between. $N_{P1}$ and $N_{P2}$ can then be calculated using the following equations:

$$N_{P1} = \int_{l_t}^{x^*} \frac{dx}{C_1'(U_1(x)\,\Delta K)^{m_1}} \tag{7.15}$$

$$N_{P2} = \int_{x^*}^{c_f} \frac{dx}{C_2'(U_2(x)\,\Delta K)^{m_2}} \tag{7.16}$$

where $C_1'$, $C_2'$, $m_1$, $m_2$ are material constants for the modified Paris Equation. $x^*$ is the notch stress field boundary defined by Tanaka [72].

Hou and Lawrence [76-78] later further developed a Strip-Yield Model for Notched Components (SYMNC) and modified the $U_1(x)$ calculation by including the notch plasticity, as described previously in Chapter III.

The CCN model takes into account PICC (analytically) and RICC/OICC (empirically) in the calculation of the propagation life. However, the simulation of RICC in the near-threshold region and the transition between RICC and PICC dominated fatigue behavior can be improved through the use of a more sophisticated model.

In the next section, a total life model for notched components will be introduced. A dislocation model [109-111] will be employed to calculate the nucleation life; The PICC-RICC model will be used to calculate the propagation life. The initial crack length for propagation, $a_i$, will be determined based on the competition between the nucleation and propagation processes.

## 7.3 Predicting the Total Fatigue Life of a Notched Component Using the PICC-RICC Model Developed

In this section, the total fatigue life will be estimated using a nucleation-propagation model. A fatigue crack nucleation model based on dislocation concepts will be employed to estimate the nucleation life, $N_N$. The combined PICC-RICC effect during fatigue crack propagation will be simulated naturally using the PICC-RICC model developed earlier, and the fatigue crack propagation life $N_F$ will be calculated accordingly. The total fatigue life can then be estimated using Eq. (7.10.a). The initial crack length for propagation will be determined through the competition between the nucleation and propagation processes.

### 7.3.1 Estimating Fatigue Crack Nucleation Life Using A Dislocation Model

A dislocation model for the calculation of fatigue crack nucleation life was first proposed by Tanaka and Mura[109]. They assumed that when the stored strain energy due to dislocations accumulated after N cycles became equal to fracture surface energy, the layers of dislocation dipoles can be transformed into a free surface. As the result, a shear crack is formed along the layers of dislocation pile up. For more details of the model, see Appendix B.

Using the energy criterion stated above, Tanaka and Mura derived the following equation for fatigue crack nucleation life calculation:

$$N_N = \frac{8Gw_c}{d(1-\nu)(\Delta\tau_\psi - 2\tau_c)^2} \tag{7.17}$$

where

- $G$: shear modules of the material
- $\nu$: Poisson's ratio
- $w_c$: specific fracture energy for a unit area
- $\tau_c$: critical stress to initiate slip
- $d$: grain size of the material
- $\psi$: inclination angle of the slip plane
- $\Delta\tau_\psi$: range of the cyclic resolved shear stress along the slip plane

Eq. 7.17 was applied to calculate the fatigue nucleation life under multi-axial loading by Socie, et al. [110-111]. In their study, slip planes with a random distribution of inclination angle $\psi$ was assumed over a 2-D body under multi-axial loading. Here in our

fatigue notch study under mode-I loading, the scenario of nucleation is simplified as follows: an average inclination angle of 45° is assumed according to the maximum shear stress direction under far-field Mode-I loading. Possible crack nucleation sites in the 2-D body other than that along the symmetry line of the notch root (which is subject to the most severe stress concentration) will not be considered. Hence the fatigue crack is assumed to nucleate along a zigzag path of 45° inclination angle with the deflected branch length simulating the grain size d: see Fig. 7.2a.

Along the assumed slip plane with 45° inclination angle, the resolved shear stress can be evaluated in terms of local tensile stress; and Eq. 7.17 can be rewritten as:

$$N_N = \frac{8Gw_c}{d(1-\nu)\left(\frac{\Delta\sigma}{2} - 2\tau_c\right)^2} \tag{7.18}$$

where $\Delta\sigma$ is the range of local tensile stress.

Socie, et al. [111] estimated the value of $w_c$ to be $2 \times 10^3$ J/m$^2$ based on the knowledge that $w_c$ is about $10^3$ times greater than the surface energy (which is about 2 J/m$^2$ in ordinary metals). In our following study, the properties of ASTM A36 steel will be used as a reference. The average grain size is assumed to be 30μm. The value of $\tau_c$ is estimated using long life fatigue data as 105MPa. For details of how to estimate $\tau_c$, see Appendix B.

### 7.3.2 Estimating Fatigue Crack Propagation Life Using the PICC-RICC Model

The crack is assumed to propagate along the zigzag path once the nucleation period ends: see Fig. 7.2b. The effective stress intensity factor U(x) throughout the period of the propagation is estimated using the PICC-RICC model. In this way, the combined effect of PICC-RICC is simulated naturally. The propagation life, $N_F$, is then estimated using the modified Paris equation as follows:

$$N_F = \int_{a_i}^{a_f} \frac{dx}{C'(U(x)\,\Delta K)^m} \tag{7.19}$$

### 7.3.3 Determination of the Crack Length $a_i$ at the Transition of Nucleation to Propagation Dominated Crack Growth

A competition concept was used in an earlier study by Hoshide and Socie [110] to pinpoint the occurrence of transition from initiation to propagation dominated cracking. In their study, two types of crack growth curves, one due to crack coalescence and the other due

to crack propagation, were defined and compared. The crack growth behavior is determined by choosing the faster growth curve.

In our study here, the crack length $a_i$ which marks the transition from nucleation to propagation dominated crack growth will be determined using a similar concept except that the comparison of the two growth curves is done at an interval of one grain diameter each. The procedure is illustrated in Fig. 7.2b and is described below:

Starting from the notch root, the crack is let to advance for a distance of one grain diameter at a time along the slip plane. Eq. 7.18 is employed to calculate the number of cycles needed to advance through the grain via nucleation. Meanwhile Eq. 7.19 is also used to calculate the number of cycles needed to advance through the same distance via propagation. The two calculated results are then compared. The transition from nucleation to propagation dominated cracking is considered to take place at the ith grain (located between A and B as illustrated in Fig. 7.2b) when for the first time $N_F^i$ no longer exceeds $N_N^i$, i.e., when the following inequality which indicates a faster growth via propagation is satisfied:

$$\int_A^B \frac{dx}{C'(\Delta K_{eff})^m} < \Delta N_{nucleation}^{A \to B} \tag{7.20}$$

where N represents the fatigue cycles consumed. The length of the crack when it first encounters the ith grain is defined as the initial crack length for propagation, $a_i$.

In the next section, the PICC-RICC model combined with the dislocation model will be used to look at, from the point of view of crack closure, the magnitude of fatigue notch size effect and what leads to the "worst case notch." The length of $a_i$ will be determined by the procedure described above. The predicted fatigue strength and fatigue notch factor $K_f$ will be checked with experimental data from literature and will be compared with values suggested by empirical notch-size-effect relationships.

## 7.4 Examination of the Fatigue Notch Size Effect and the "Worst Case Notch"

In this section, the fatigue notch size effect will be investigated for the following two types of geometry: i) notches with a constant depth and different $K_t$ values and ii) notches with a constant $K_t$ but varying depth. The fatigue strength $S_e^{(notched)}$ and the fatigue notch factor $K_f$ at a life of $10^7$ cycles will be predicted and compared with test data as well as

existing empirical relationships. The previously postulated "worst case notch" will be examined.

7.4.1 Predicting the Fatigue Strength and Fatigue Notch Factor of Notched Specimens

The fatigue strength of the notched specimen at a life of $10^7$ cycles and the corresponding fatigue notch factors are predicted here using the total life model introduced in the previous section. The R-ratio of the cyclic load is -1. The failure of the specimen is assumed when the crack length reaches 0.5 mm. The material used is ASTM A36 steel. The materials constants are listed in Table 5.

The study will be carried out for two cases: i) specimens with a constant notch depth as shown in Fig. 7.3a, and ii) notched specimen with a constant $K_t$ value as shown in Fig. 7.3b. The result of the study is described in the following two sections.

7.4.2 Constant-Depth Notches with Varying Stress Concentration Factor $K_t$

First, the fatigue behavior of a group of notches with constant notch depth is examined. The elliptical notch, as shown in Fig. 7.3a, has a constant notch depth of 0.2". The stress concentration factor $K_t$ of the notches considered varies from 2 to 30. The zigzag path used in the prediction of propagation life has a constant tilt angle of 45° and a deflected branch length analogy to the assumed grain size of 30μm.

The initial crack length for propagation, $a_i$, is estimated and is shown in Fig. 7.4 as a function of $K_t$. The predicted result shows that when $K_t$ is less than 3, the value of $a_i$ increases noticeably as the notch gets sharper, indicating the postponing of the transition from nucleation to propagation dominated growth. This effect is because while both nucleation and propagation are promoted during this initial $K_t$ increase, the change is more prominent for nucleation and hence causes a delay of the nucleation-propagation transition. After this initial increase, the $a_i$ value decreases slightly and remains relatively constant as the notch gets further sharper, indicating a balance between nucleation and propagation. The slight decrease of $a_i$ is due to the reduction of the nucleating rate as the amplitude of the local shear stress approaches the frictional stress $\tau_c$. Also shown in the figure is the customarily assumed $a_i$ value of 0.01" in the I-P model which is close to the stabilized $a_i$ value predicted here.

The fatigue strength for the above case is also predicted and plotted in Fig. 7.5 together with experimental data [112]. The predicted result compares favorably with the test data. Another important feature of Fig. 7.5 is the verification of the existence of a "worst case notch" with the lowest value of $S_e^{(notched)}$, which for this case occurs around notch root

radius equal to 0.4mm. The cause of this dip in the notched fatigue strength will be examined later in this section.

$K_f$ values corresponding to the predicted fatigue strength of the notched components are shown in Fig. 7.6. The fatigue strength of a smooth specimen ($S_e^{(unnotched)}$) needed for the calculation of $K_f$ is estimated to be 215MPa from the test results [112]. Apart from experimentally recorded $K_f$ data, also presented in Fig. 7.6 are two curves of $K_f$ values estimated using the Peterson's and Neuber's relationships, respectively. Test data appear to fall between the prediction made using the nucleation-propagation model and the prediction made using the Peterson's relationship, with both predictions indicate the existence of a $(K_f)_{max}$ value. On the other hand, the Neuber's relationship does not suggest the existence of such a "worst case notch" and it predicts the $K_f$ values to be increasing with $K_t$, which appears to deviate from experimental results.

The existence of a "worst case notch" is further demonstrated using the example of the constant depth notches under a same set of load with R-ratio equal to -1 and $S_{max}$ equal to 55 MPa. The predicted nucleation life $N_N$, propagation life $N_P$ and total life $N_T$ are shown in Fig. 7.7. It is shown in Fig. 7.7 that under the applied load, the nucleation life of notched specimens changes only slightly with $K_t$, while the propagation life reaches its minimum at $K_t$ around 8, or notch root radius around 0.4mm. The predicted total fatigue life also reaches a minimum as the result. Obviously such minimum life is the cause of the lowest fatigue strength $S_e^{(notched)}$ among the notches, or the "worst case notch" as described earlier. The U shape $N_F$ curve which is the cause of all this can be explained as follows: the initial loss of propagation life is attributed to the acceleration of fatigue crack growth as the notch gets sharper. However, a counter effect of a sharper notch as opposed to a higher $K_t$ value is that it also introduces a higher stress gradient which leads to a quicker decline of stress once away from the notch root. Hence as the sharpness of the notch increases, a larger portion of the fatigue crack growth will be under a lower stress and will consumes more fatigue cycles, which leads to the rebound of $N_F$ after the initial drop.

### 7.4.3 Notches with a Constant Stress Concentration Factor and Varying Notch Depth

In this section the fatigue behavior of a group of notches with the same stress concentration factor $K_t$ are examined. The elliptical notches as shown in Fig. 7.3b has a constant $K_t$ value of 7.5. The depth of the notches varies from 2.5mm to 10mm. Again an zigzag path as shown in Fig. 7.2(a-b) is adopted in the nucleation-propagation model calculation.

The variation of initial crack length for propagation, $a_i$ with notch depth is predicted and plotted in Fig. 7.8. $a_i$ is predicted to increase as the geometrically similar notch deepens

due to the fact that a larger portion of the notch will be subject to enhanced stress which promotes the nucleation process over the propagation process. The average $a_i$ value for notch root radius less than 1mm is around 0.01", the customarily assumed value used in the previous I-P model calculation [106-108].

The predicted $K_f$ values for the geometrically similar notches are shown in Fig. 7.9 with experimental data [112] available only for similar $K_t$ values. The comparison between the predicted results and test data shows good agreement. The $K_f$ values estimated using the Peterson's and Neuber's relationships are also given in Fig. 7.9. The predicted results all suggest that for fatigue specimens with geometrically similar notches, the $K_f$ value increases monotonically with the notch depth D. The $K_f$ curve predicted using the nucleation-propagation model is closer in value to that given by the Peterson's relationship but has a slope more similar to that given by the Neuber's relationship.

## 7.5 SUMMARY

In this chapter, an important feature of the fatigue behavior of a notched component - the fatigue notch size effect, has been re-examined. A total life model is developed for this purpose: A dislocation double-pileup model is employed to calculate the nucleation life; The PICC-RICC Model is used to calculate the propagation life; The total fatigue life is then estimated as the summation of the predicted nucleation life and propagation life. The following conclusions can be drawn based on this study:

i) The initial crack length for propagation, $a_i$, can be estimated based on the competition between nucleation and propagation dominated fatigue crack growth. The predicted $a_i$ value of constant depth notches remains a relative invariant. For geometrically similar notches, the predicted $a_i$ value increases slightly as the notch gets deeper. For both cases, the study shows that the average $a_i$ value is around 0.01", the value assumed in the I-P model.

ii) The fatigue notch size effect predicted using the PICC-RICC model compares favorably with test data. For a constant depth notch, the prediction made using the nucleation-propagation model is closer to that made using the Peterson's relationship; Both the nucleation-propagation model and the Peterson's relationship suggests the existence of a $(K_f)_{max}$ value which indicates a "worst case notch" scenario while the Neuber's relationship predicts a monotonic increase of $K_f$ with $K_t$. For geometrically similar notches, the predictions made using the three methods are close, all suggesting a continuous increase of $K_f$ with notch depth.

iii) The existence of a "worst case notch" among notches with constant depth, as previously postulated and confirmed using the RICC-PICC model, is the result of the variation of propagation life with $K_t$ under the strong influence of near-threshold crack closure including RICC.

There are still many aspects of the fatigue notch behavior which remain poorly understood. For example, Neuber and Peterson's empirical relationships both suggest that notch sensitivity depends on material properties, reflected by the inclusion of material constants $a_P$ or $\rho_N$. One of the material properties that has been linked to notch sensitivity is the grain size. Such influence may be interpreted in terms of the difference of RICC level resulted from different grain sizes. More discussion concerning the influence of grain size will be carried out in the next chapter.

# CHAPTER VIII DISCUSSION

## 8.1 INTRODUCTION

In this chapter the following topics will be discussed: i) the implication of the 3-D nature of roughness on 2-D RICC modeling; ii) The comparison of the predicted fatigue notch behaviors using the PICC-RICC Model and the I-P Model; and iii) the influence of grain size on fatigue notch strength.

## 8.2 EFFECT OF THE 3-D NATURE OF ROUGHNESS ON RICC MODELING

The 2-D analysis carried out by the PICC-RICC model presented in our study is an idealized simplification of the 3-D nature of surface roughness. Under the 2-D assumption, the geometric characteristics of roughness remains identical throughout thickness: this idea is illustrated in Fig. 8.1 in which the lower surface of a crack under such 2-D assumption is depicted. The crack is under far-field tensile load along the y-axis; and the crack is growing in the x direction. The thickness of the plate is (t) and lies on z axis. The crack grows along a zig-zag path in the x-y plane but remains identical along the z-axis.

In reality, fracture surface roughness is a 3-D phenomenon. Using the same coordinate system, the variation of surface roughness in the thickness direction is illustrated in Fig. 8.2. The roughness profiles at $z = z_1$ and $z = z_2$ are depicted to demonstrate the difference in their appearances. Complexity arises from such three-dimensionally distributed roughness as discussed below:

The direct consequence of a varying roughness profile in thickness direction is that the Mode-II sliding displacement which causes RICC will be reduced due to the tendency of a "twisting" motion in the x-z plane. The cause of such twisting motion is explained in Fig. 8.3(a-b) with the example of the different roughness profiles at $z = z_1$ and $z = z_2$ previously shown in Fig. 8.2. It is demonstrated in Figs. 8.3(a-b) that, due to the different slopes observed in roughness profiles at $z = z_1$ and $z = z_2$, the Mode-II displacements under the same far field tensile load S at these two locations are opposite to each other. Although in reality the neighboring "layers" of fractures surfaces in the thickness direction may not always be so drastically different as to cause the complete opposite sliding displacements shown in Fig. 8.3(a-b), we can expect that due to the irregularity of roughness profile, "layers" lying at different thickness locations will interfere and restrain the Mode-II motion of each other. As a result, internal twisting among these layers is created; and the net

Mode-II displacement is reduced. In our 2-D PICC-RICC model, we could take into account such twisting motion featured in 3-D by choosing roughness parameters θ and h of the crack path so that the predicted Mode-II displacement using these parameters can reflect its mean value across the plate thickness. However at this point, this task has not been achieved.

Aside from reducing the Mode-II displacement, the twisting motion described above also introduces a Mode-III torsion stress as well as the possibility of additional RICC in x-z plane due to the lateral contact between crack surfaces [101]. However these contributions are considered less significant than the contribution from Mode-I and local Mode-II displacements in x-y plane and are therefore neglected in our RICC calculation.

In summary, we conclude that the 2-D RICC model can be used to describe the main features of 3-D RICC if the roughness parameters used in the calculation represent the average roughness features throughout the thickness direction.

## 8.3 Comparison of the PICC-RICC Model and the I-P Model Predictions for Fatigue Notch Strength

The Initiation-Propagation (I-P) Model was previously described in Section 7.2.2. The I-P model has been frequently used to predict the fatigue life of notched welded components [106-108, 113-114]. The I-P model takes into account the short crack behaviors through the use of the fatigue notch factor $K_f$ derived from Peterson's empirical relationship, instead of explicitly simulating the small crack behavior as in the PICC-RICC Model. Another feature of the I-P Model is the use of an "engineering size crack" of about 0.01" as the length of initial crack length for propagation: see Section 7.2.2. In this section both the I-P Model and the PICC-RICC Model will be used to predict the fatigue strength of a notched component with constant depth and the predicted results will be compared.

### 8.3.1 Comparison of the Initial Crack Length for Propagation, $a_i$, and the Fatigue Notch Strength Predicted Using the I-P Model and the PICC-RICC Model

The fatigue notch behavior of the ASTM A36 steel specimen with elliptical notch of constant depth (0.2") as shown in Fig. 7.3a is investigated using both models. The R-ratio considered is -1. The material constants are listed in Table 5.

Predicted values of $a_i$ for different $K_t$ using the PICC-RICC Model are plotted in Fig. 8.4 with the "engineering size crack" used in I-P model. The PICC-RICC model predicted results show a good agreement with the $a_i$ value of ~0.25mm (0.01") customarily assumed in the I-P Model.

Predicted values of fatigue strength at $10^7$ cycles are shown in Fig. 8.5. Both models give favorable predictions compared with test data [112]. The existence of a "worst case notch" is predicted using both models, which is consistent with the occurrence of $(K_f)_{max}$ value suggested by Peterson's empirical relationship: see Fig. 8.5.

### 8.3.2 Summary of the PICC-RICC Model and the I-P Model Predictions

The comparison of the PICC-RICC Model and the I-P Model predictions reveals that while the short crack behavior has been taken into account through different approaches, the predicted fatigue strength using these two models show good agreement. The initial crack length for propagation $a_i$ predicted using the PICC-RICC Model confirms the use of the "engineering-sized crack" of 0.01" as a good approximation. The existence of a "worst case notch" previously postulated using the I-P Model [106-108] is also confirmed by the PICC-RICC Model.

## 8.4 Effect of Grain Size on the Fatigue Notch Size Effect

In this section, the PICC-RICC model will be used to investigate the influence of grain size on notch fatigue strength. Grain sizes of 10μm, 30μm, 50μm and 70μm will be considered. The predicted results are shown in Figs. 8.6-8.7 for stress ratio R equal to -1 and 0, respectively.

Eq. 7.18 was used in the PICC-RICC model to calculate the nucleation life, $N_N$. Eq. 7.18 suggests that for same material (by this we assume that the frictional stress to activate dislocation, $\tau_c$, remains the same), a larger grain size leads to shorter nucleation life. When one looks at the propagation life, however, results in Section 5.1.1 and Chapter VI suggest that materials with a larger grain size are subject to a higher amount of retardation due to RICC, which in turn prolongs the propagation life. When the initial crack length for propagation $a_i$ is concerned, since larger grain size reduces the number of cycles needed to nucleate a crack while increases the retardation for propagation, materials with a larger grain size tend to stay in the nucleation mode longer and put off the process of propagation. Therefore $a_i$ will be longer for larger grain size, which in turn further promotes the nucleation life and shortens the propagation life. Considering these sometimes opposite effects of grain size on $N_N$ and $N_F$, there is unlikely to be an apparent relationship between grain size and the fatigue strength of the notched members. The speculation that the (grain size - notch fatigue strength) relationship is complicated was confirmed by experimental observation [122] which demonstrated that the fatigue strength did not vary with grain size in a monotonic

manner. For example, the best fatigue performance did not occur at either the large or small grain sizes, but instead occurred at some intermediate grain size.

The PICC-RICC model was used to predict the variation of fatigue notch strength with grain size. To limit the consideration at this point to grain size only, the change of the flow stress with grain size was not considered. The predicted results are shown in Fig. 8.6 and Fig. 8.7 for stress ratio R=-1 and R=0, respectively.

The predicted results show that the variation of fatigue strength with grain size is more distinct for R=-1 than for R=0. This result is because that RICC is more prominent for R=0 than for R=-1 as previously demonstrated in Fig. 5.4, therefore at R=0 the increase of $N_F$ with grain size due to RICC overcomes the decrease of $N_N$ more effectively. As the result, the difference in fatigue strength due to different grain sizes is reduced when R=0.

The PICC-RICC model prediction also suggests that, as shown in Figs. 8.6-8.7, the "worst case notch" occurs at approximately the same location regardless of the grain size of the material.

For R= -1, where the difference of fatigue strength between various grain size is more distinct than R=0, the fatigue strength of grain size equal to 50μm is predicted to gradually exceed those of other grain sizes (10μm, 30μm or 70μm) as the notch gets sharper, which is consistent with the experimental observation [122] that medium grain size materials sometimes have a higher fatigue notch strength than either the fine-grain-size materials or the large-grain size materials.

Notice that in the above discussion the variation of flow stress $\sigma_0$ with grain size, which in turn influences the amount of PICC and subsequently $N_F$, is not addressed because of the lack of a Hall-Petch type equation describing the relationship between the grain size and the flow stress. One way for us to roughly estimate such relationship is by using Eq. 7.18. Substituting into Eq. 7.18 the empirical estimation that the fatigue strength at $N_N = 10^6$ cycles is roughly equal to $0.5\sigma_u$ [115] and rearranging Eq. 7.18, one gets the following estimated relationship between the ultimate strength ($\sigma_u$) and the grain size (d) for the ASTM A36 steel (the values of material constants $\tau_c$, $w_c$, G and ν used in the derivation were listed in Table 5; the grain size d is assumed to be 30μm):

$$\sigma_u\,(\text{MPa}) = 420 + \frac{84.44}{\sqrt{d\,(\mu\text{m})}} \tag{8.1}$$

Further more, using the empirical estimation of $\sigma_y = \frac{5}{9}\sigma_u$, where $\sigma_y$ is the yield strength of the material, and noticing that the flow stress $\sigma_0$ is defined as the average of the yield strength and the ultimate strength of the material, one gets:

$$\sigma_0 \text{ (MPa)} = 327 + \frac{65.68}{\sqrt{d\ (\mu m)}} \tag{8.2}$$

The above equation, however, yields only a small variation of flow stress with grain size. E. g., between grain sizes of 10μm and 100μm, the difference in flow stress is estimated to be only 14.2 MPa using Eq. 8.2. This small amount of variation of the flow stress will cause only tiny difference in the PICC level in the strip-yield model prediction [33]: see Fig. 8.8, and is unlikely to lead to major difference in the propagation life prediction.

Since Eq. 8.3 was developed based on several empirical assumptions which may affect the accuracy of the estimation, a more reliable relationship between the grain size and the flow stress is needed before the effect of grain size on the propagation life and notch fatigue strength can be estimated more accurately.

## 8.5 SUMMARY

The discussion in this chapter can be summarized as the following: i) The current 2-D model PICC-RICC Model is capable of representing the features of the average RICC through thickness direction if average roughness parameters are used in the model; though, at this point, the mean values of these roughness parameters (i.e., θ, L and h used in the PICC-RICC Model) have not been quantified; ii) The fatigue behavior of notched components predicted using the PICC-RICC Model and the I-P Model show good agreement. The use of the "engineering-sized crack" of ~0.01" as $a_i$ in the I-P Model and the existence of a "worst case notch" previously postulated using the I-P Model were both confirmed using the PICC-RICC Model; iii) The PICC-RICC Model predicts that the influence of the grain size on the fatigue strength is more distinct for stress ratio R=-1 than for R=0. When the change of flow stress due to grain size is not considered, the PICC-RICC model also predicts that the "worst case notch" occurs at approximately the same notch-root radius regardless of the grain size.

# CHAPTER IX CONCLUSIONS AND PROPOSED FUTURE WORK

## 9.1 CONCLUSIONS

1. Near-threshold fatigue analysis showed that RICC is the most important form of crack-closure in this region. The influence of RICC does not diminish until PICC becomes the main source of crack closure. Therefore to describe realistically the near-threshold crack-closure behavior the influence of RICC needs to be taken into account in conjunction with PICC. An analytical PICC-RICC Model has been developed in this study. The PICC-RICC Model is powerful and unique in that it combines the effects of RICC and PICC. Thus, the gradual transition from RICC to PICC dominated crack closure behavior is handled naturally by this model.

2. The near-threshold fatigue behavior of aluminum alloy, titanium alloy and steel was predicted using the PICC-RICC Model. The predicted result shows a high crack-closure level due to RICC during early fatigue crack growth, followed by a gradual decrease of crack closure as the influence of RICC weakened and as the closure level converged with that of PICC.

3. The influence of various fatigue parameters on RICC was examined using the PICC-RICC Model. Predicted results suggest the following:

   - RICC is promoted by longer branch length (L), higher branch amplitude (h) and steeper tilt angle ($\theta$). The final outcome of RICC is subjected to the combined effect of L, h and $\theta$;
   - RICC was most severe at positive low stress ratio (R) and under low cyclic stress ranges ($\Delta S$);
   - The effect of grain size on fatigue behavior in the near-threshold region was investigated using the model. The predicted RICC behavior is consistent with the experimental observation that during early fatigue crack propagation coarse-grained materials exhibit more severe RICC-induced crack retardation over fine-grained materials.

4. The PICC-RICC Model prediction of the fatigue notch size effect compared favorably with the I-P Model prediction. The initial crack length for propagation $a_i$ predicted using the PICC-RICC Model agrees with the $a_i$ value customarily assumed based on the "engineering size crack" in the I-P Model. The predicted fatigue notch

strength using both models also show good agreement. The "worst-case-notch" previously postulated in the I-P Model was confirmed using the PICC-RICC Model. The agreement of the predictions made using the two models confirms the use of the Peterson's empirical relationship in the I-P Model as an effective and efficient way to characterize the fatigue notch behavior.

## 9.2 PROPOSED FUTURE WORK

1. The relationship between surface roughness and the grain size considered in the PICC-RICC Model study was based on the Forsyth Stage-I crack growth theory as suggested by previous RICC research. For a better understanding and a more sophisticated correlation of the relationship between surface roughness and the material microstructural features including grain size, additional experimental work, e.g., a con-focus microscope study of the fracture surface roughness, is very much desired.

2. The current PICC-RICC model is a 2-D RICC analysis. How to determine the values of the roughness parameters L, h and $\theta$ so as to reflect the mean RICC level across thickness direction and to simulate the 3-D nature of RICC requires further study.

3. In the study of the influence of grain size on fatigue notch strength, the variation of the flow stress with grain size was neglected due to the unavailability of a reliable (grain size-flow stress) relationship for the material considered. For further investigation in the future, the variation of the flow stress with grain size needs to be better quantified and taken into account.

# TABLES

Table 1 Material properties of BS4360 50B steel [123].

| | |
|---|---|
| Yield strength, $S_y$ (MPa) | 345 |
| Ultimate strength, $S_u$ (MPa) | 555 |
| Young's modulus, E (GPa) | 200 |

Table 2 Material properties of 2024-T351 aluminum alloy [85].

| | |
|---|---|
| Yield strength, $S_y$ (MPa) | 360 |
| Ultimate strength, $S_u$ (MPa) | 488 |
| Young's modulus, E (GPa) | 70 |

Table 3 Material properties of Ti-6Al-4V alloys [94].

| | AN705 | AN850 |
|---|---|---|
| Yield strength, $S_y$ (MPa) | 880 | 848 |
| Ultimate strength, $S_u$ (MPa) | 933 | 944 |
| Young's modulus, E (GPa) | 106 | 110 |



Table 4 Material properties of AISI 1080 steel [13].

| | |
|---|---|
| Average yield strength, $S_y$ (MPa) | 521 |
| Average ultimate strength, $S_u$ (MPa) | 934 |

Table 5 Material properties of ASTM A36 steel [115].

| | |
|---|---|
| Young's modulus, E(MPa) | 189 |
| Shear modulus, G (GPa) | 78.5 |
| Yield strength, $S_y$ (MPa) | 531 |
| Ultimate strength, $S_u$ (MPa) | 669 |
| Specific fracture energy, $w_c$ ($J / m^2$) | $2 \times 10^3$ [111] |
| Frictional stress, $\tau_c$ (MPa) | 105 [110] |
| Modified Paris equation constant, C′ | $3.3 \times 10^{-10}$* [79] |
| Modified Paris equation constant, m | 4.0 [79] |
| Peterson's constant, a (mm) | $0.025\left(\frac{2070}{S_u\ (MPa)}\right)^2$ |
| Neuber's constant, $\sqrt{\rho}$ ($\sqrt{in}$) | 0.115 [124] |
| Strength coefficient, K (MPa) | 2110 |
| Cyclic strength coefficient, K' (MPa) | 1489 |
| Strain hardening exponent, n | 0.102 |
| Cyclic strain hardening exponent, n' | 0.215 |
| Fatigue strength coefficient, $\sigma'_f$ (MPa) | 724 |
| Fatigue ductility coefficient, $\varepsilon'_f$ | 0.218 |
| Fatigue strength exponent, b | -0.066 |
| Fatigue ductility exponent, c | -0.492 |

* The values listed give the unit of da/dN in mm/cycle.

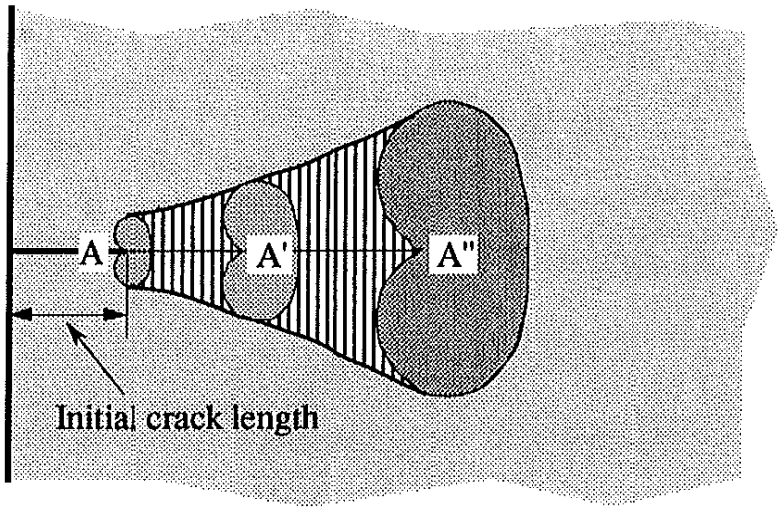


A, A', A" Locations of crack tip during fatigue crack propagation

Plastic zones formed during fatigue crack propagation for crack lengths A, A', A"

Plastically deformed material left along the fatigue crack wake, source of PICC

Figure 2.1 Plastic deformation in the crack wake which becomes the source of PICC.

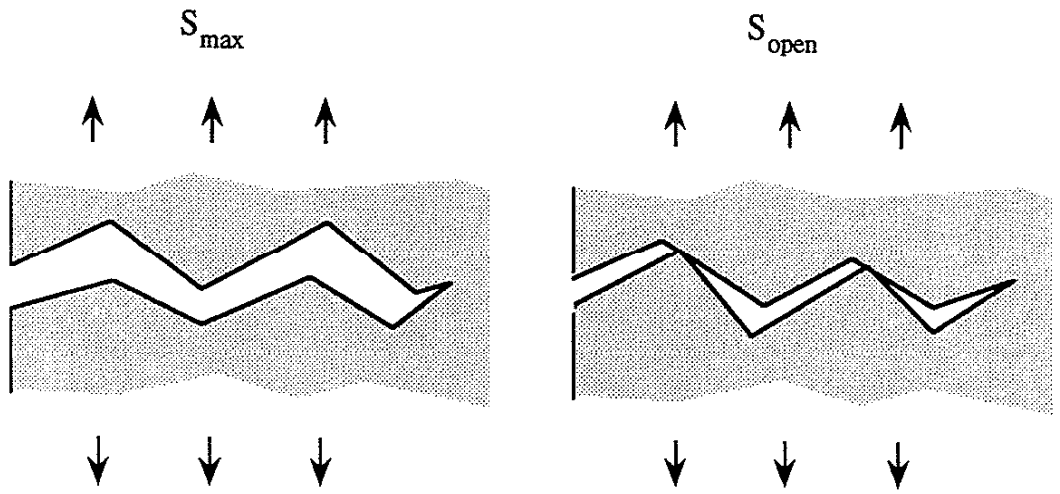


(a)

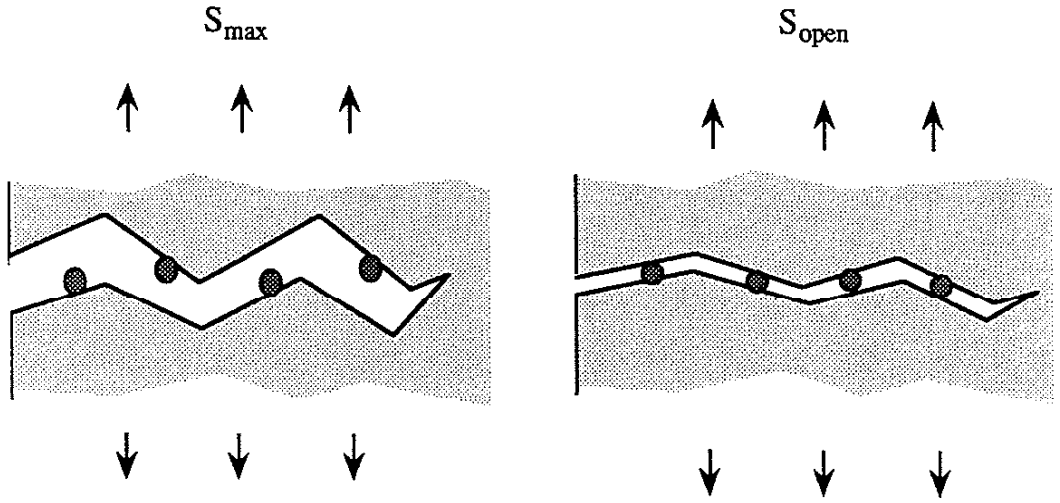


(b)

Fig. 2.2(a-b) Two of the main near-threshold crack-closure mechanisms: (a) Roughness-induced crack closure; (b) Oxide-induced crack closure.

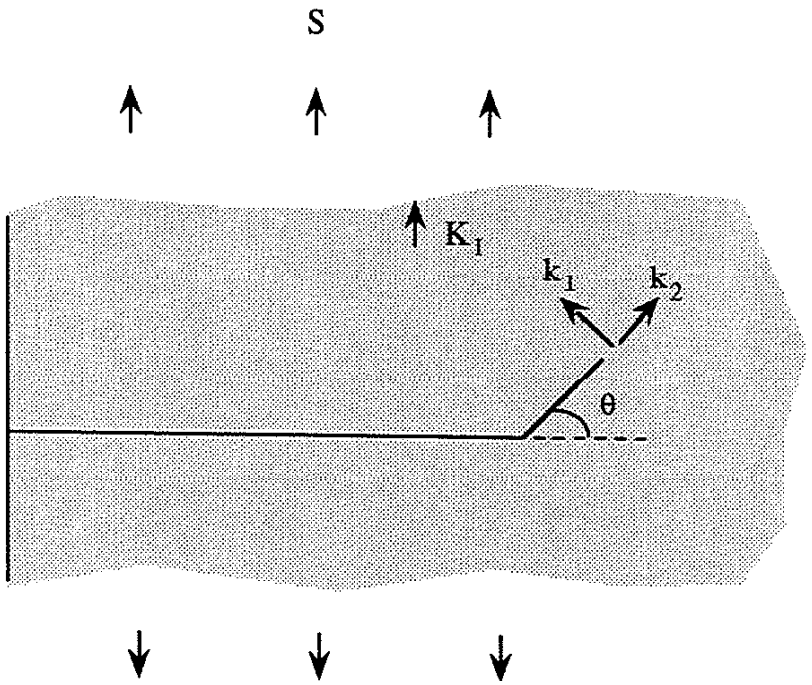


Fig. 2.3 Near-tip mixed-mode motion under far field Mode-I loading due to crack-path deflection.

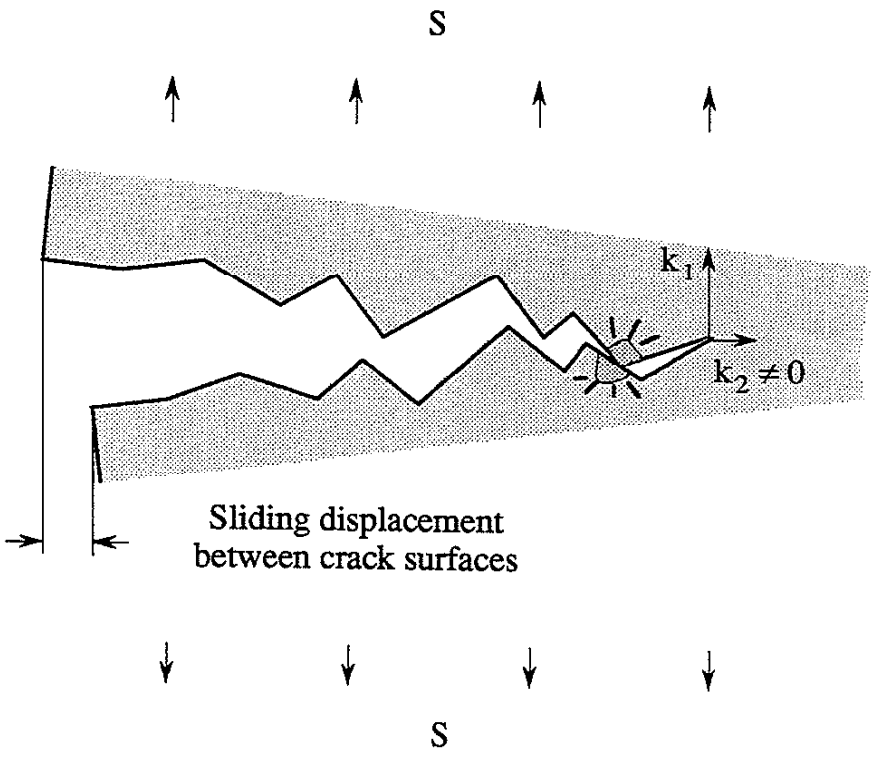


Fig. 2.4 Crack surface mismatch due to the near-tip mixed-mode loading. The lateral sliding displacement between crack surfaces wedges the crack open and leads to earlier crack-closure on unloading.

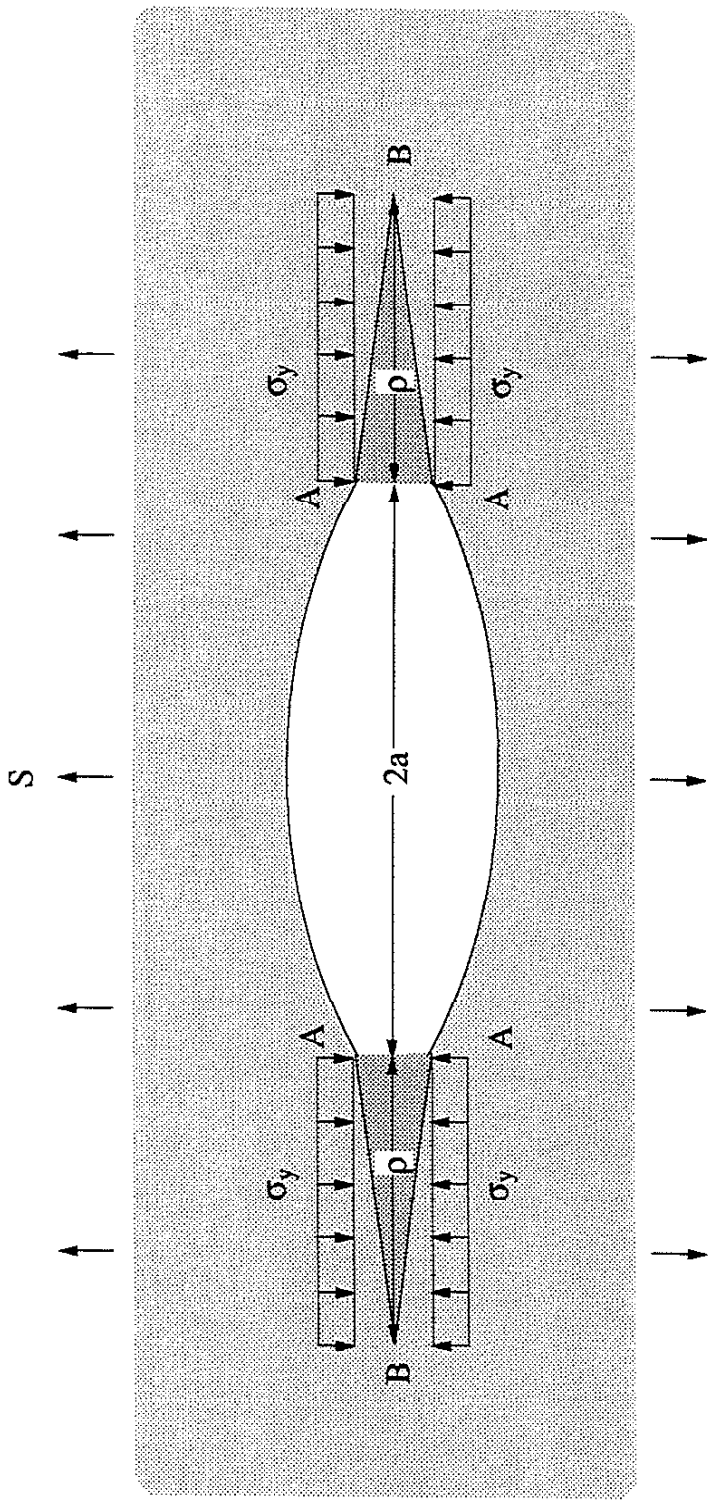


Fig. 3.1 The Dugdale model.

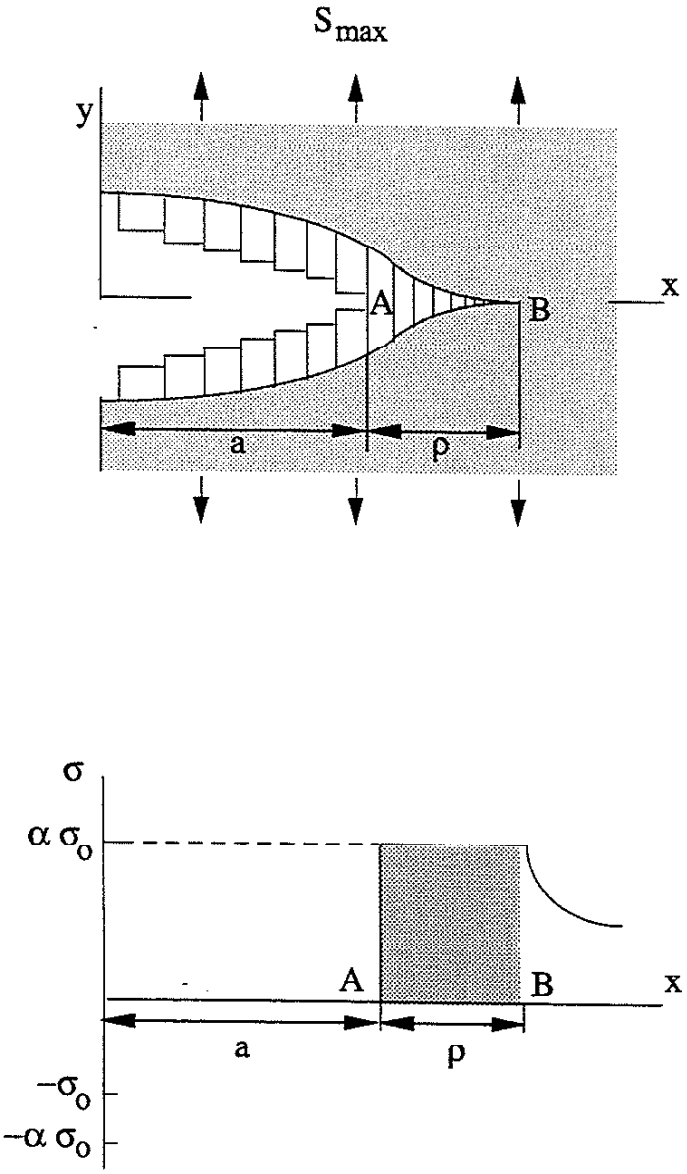


Fig. 3.2(a-c) Three steps of the PICC calculation using the strip-yield Dugdale model: (a) Under $S_{max}$, determine the plastic zone size as well as plastic deformation within the plastic zone.

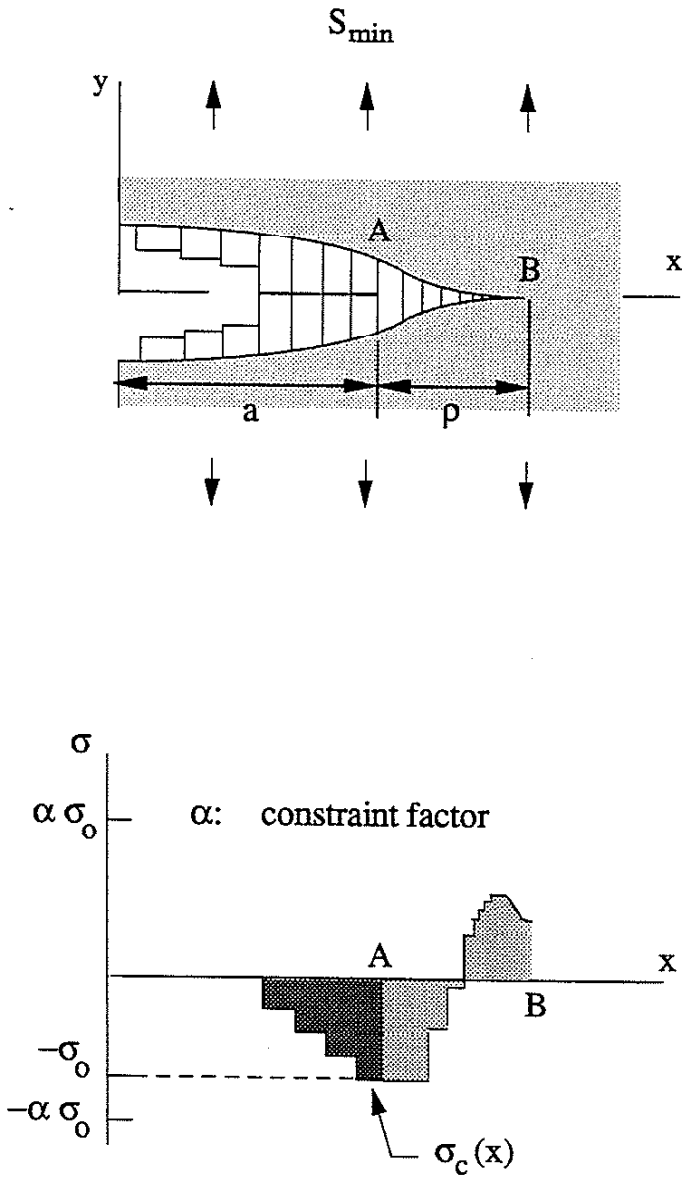


Fig. 3.2 (b) Under $S_{min}$, determine the contact stress along the plastic wake

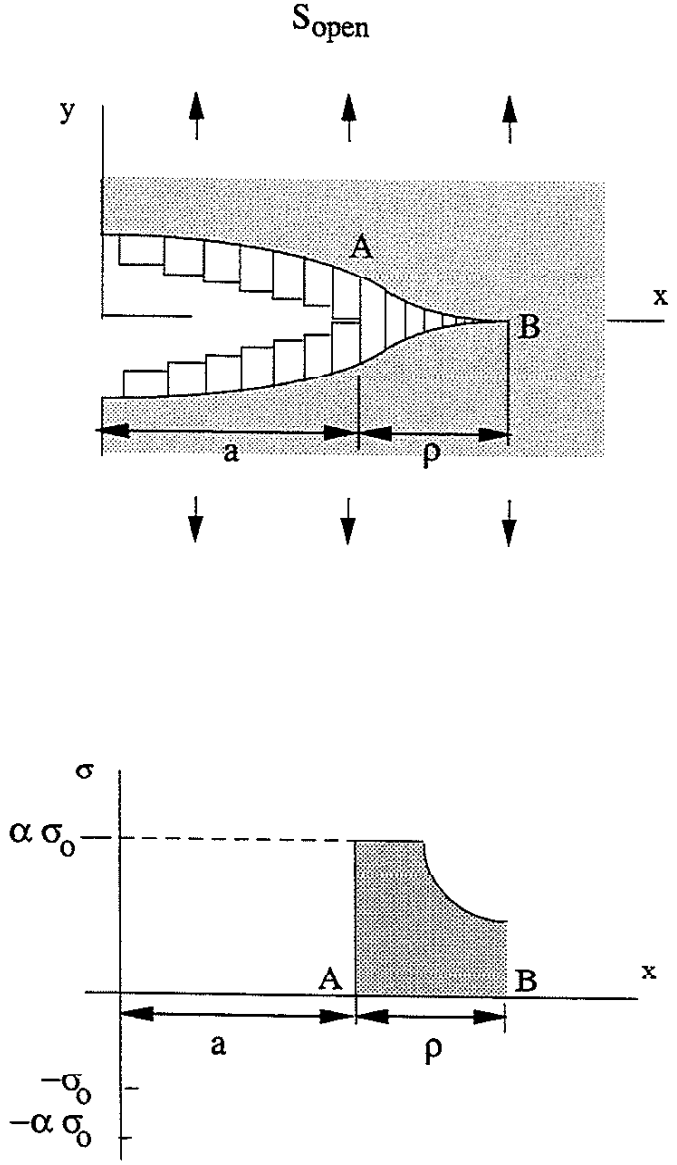


Fig. 3.2 (c) Determine the crack opening stress $S_{open}$.

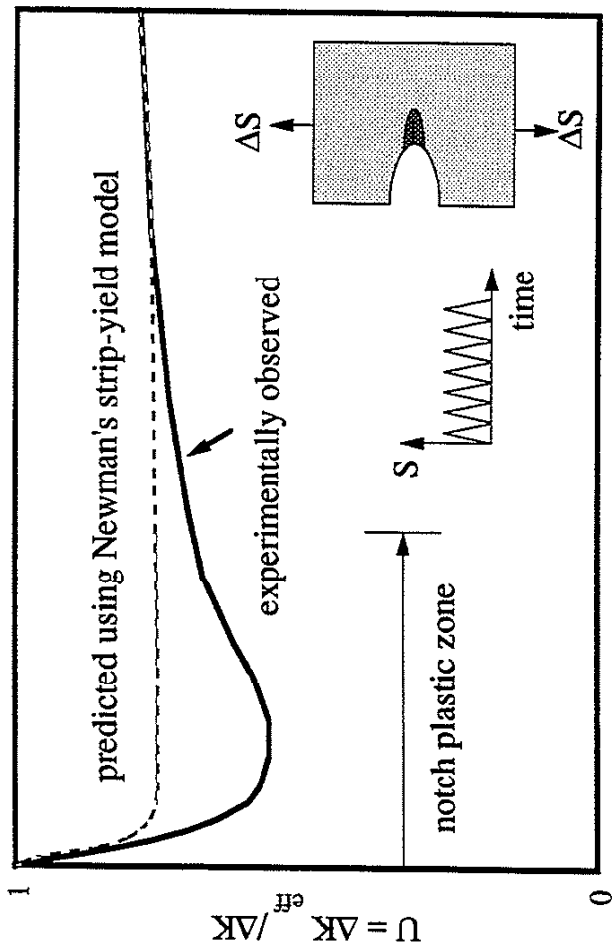


Fig. 3.3 Comparison of the experimentally observed U value for a notched specimen and that determined using the original strip-yield model.

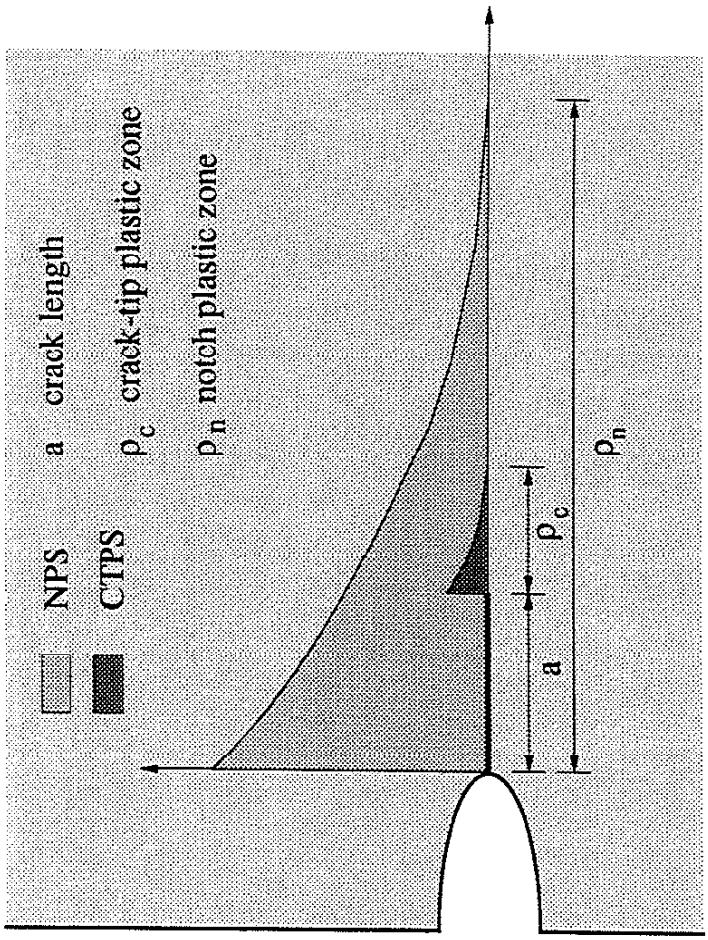


Fig. 3.4 Calculation of total plastic stretch of a notched specimen to include notch plasticity in Strip-Yield Model for Notched Component (SYMNC).

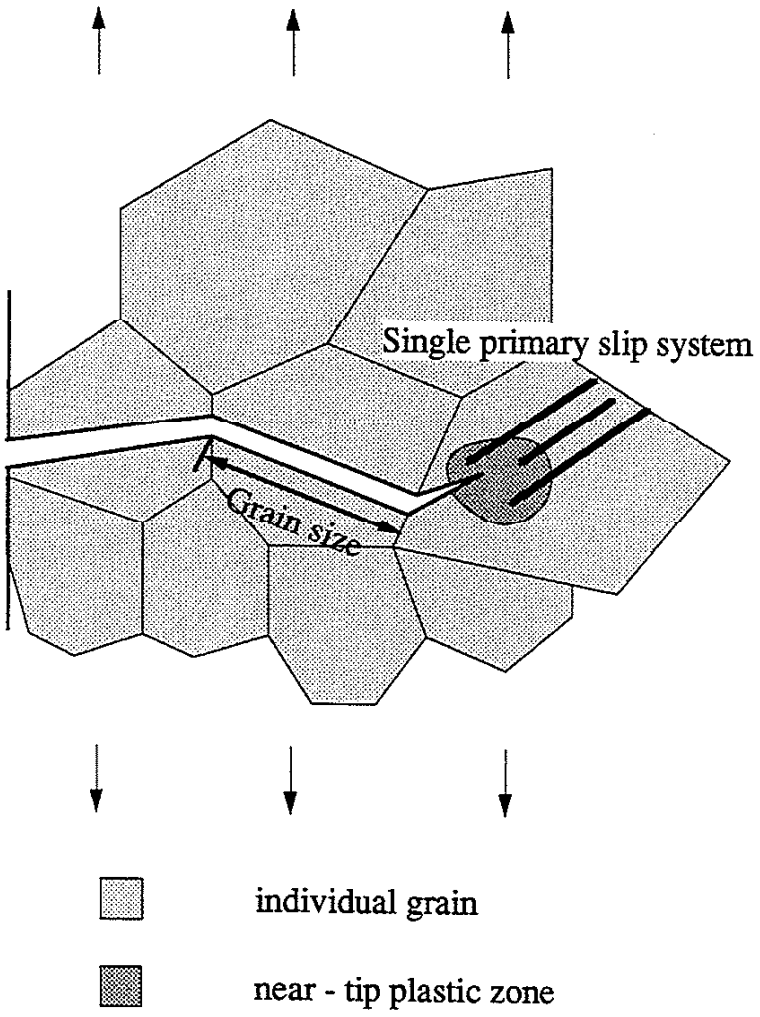


Fig. 4.1 Stage-I fatigue crack growth as described in Forsyth's theory. A single, primary-slip system is activated in this stage.

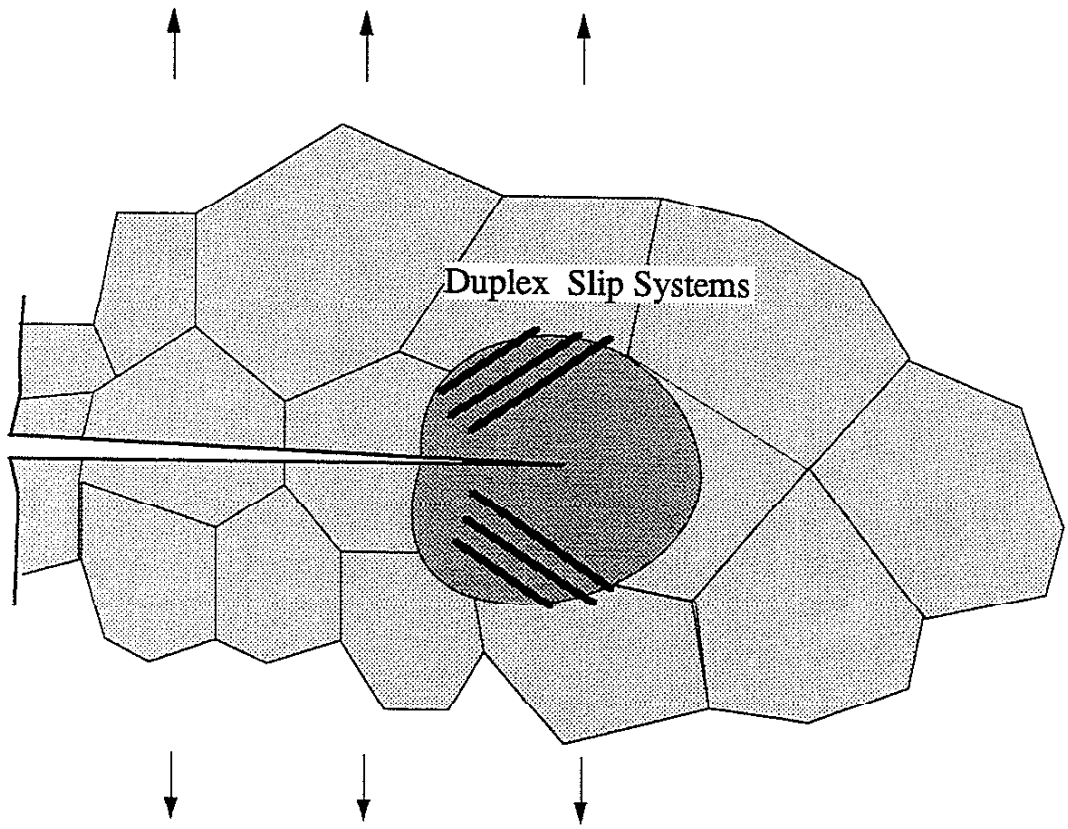


Fig. 4.2 Stage-II fatigue crack growth as described in Forsyth's theory. Multiple slip systems are activated in this stage.

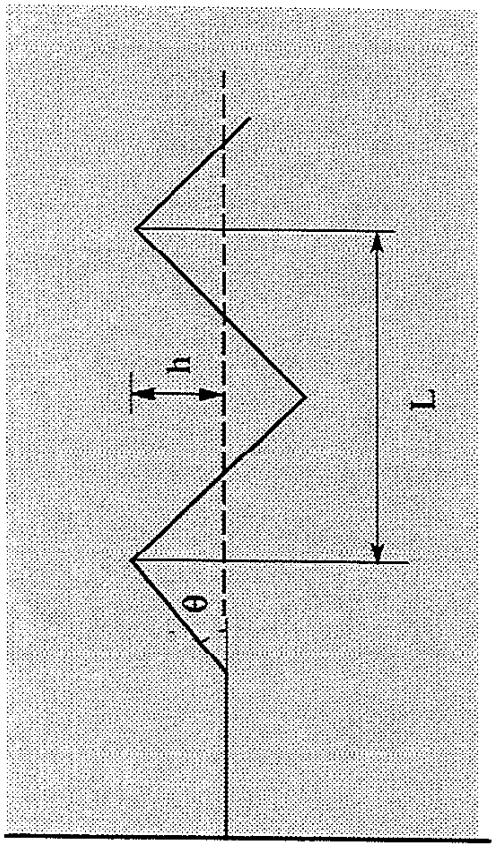


Fig. 4.3 Geometrical features of the zigzag path assumed in PICC-RICC model.

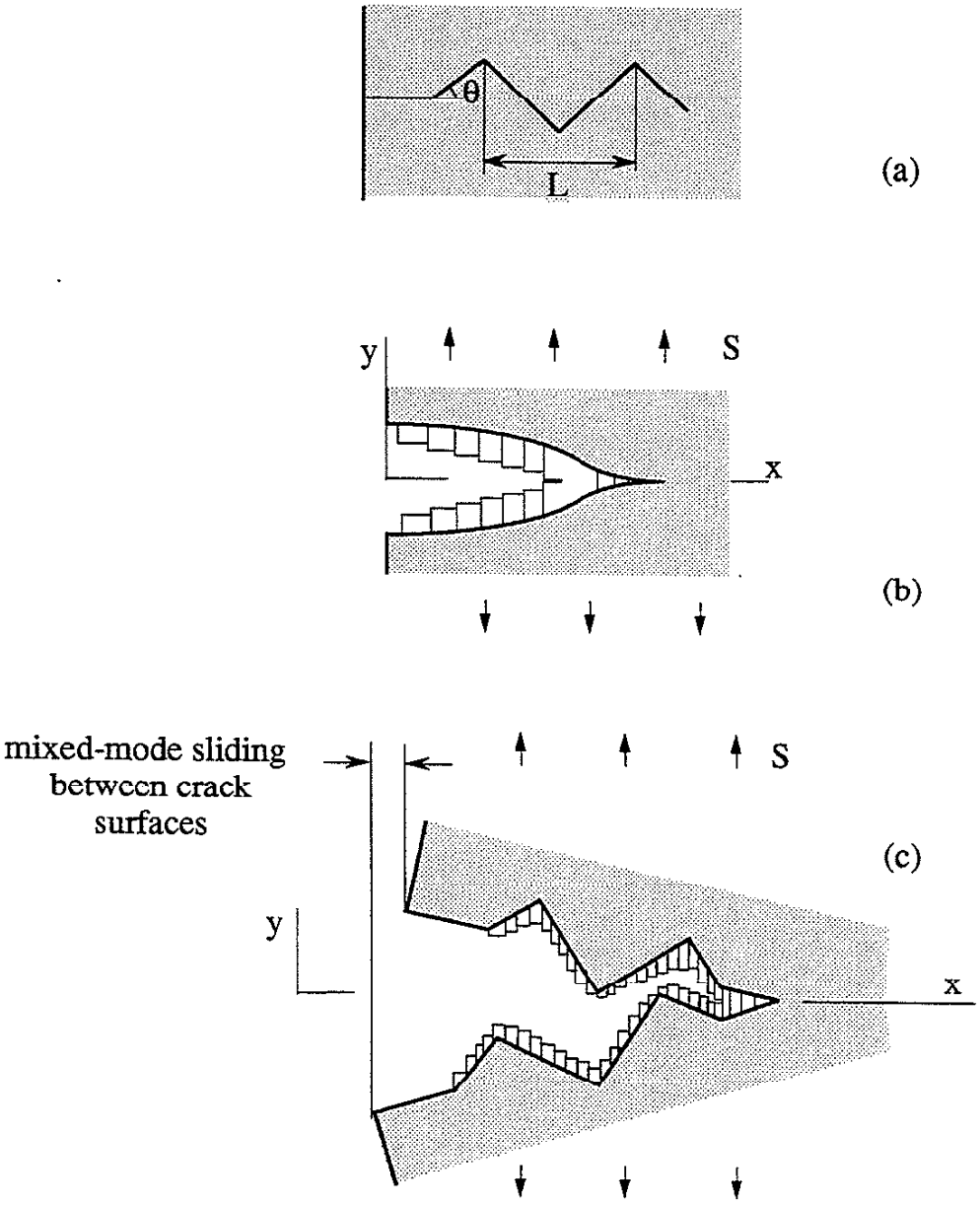


Fig. 4.4(a-c) Illustration of the PICC-RICC model: (a) Assumed zigzag shape deflected path; (b) Strip-yield Dugdale model; (c) an analytical PICC-RICC model combining (a) with (b).

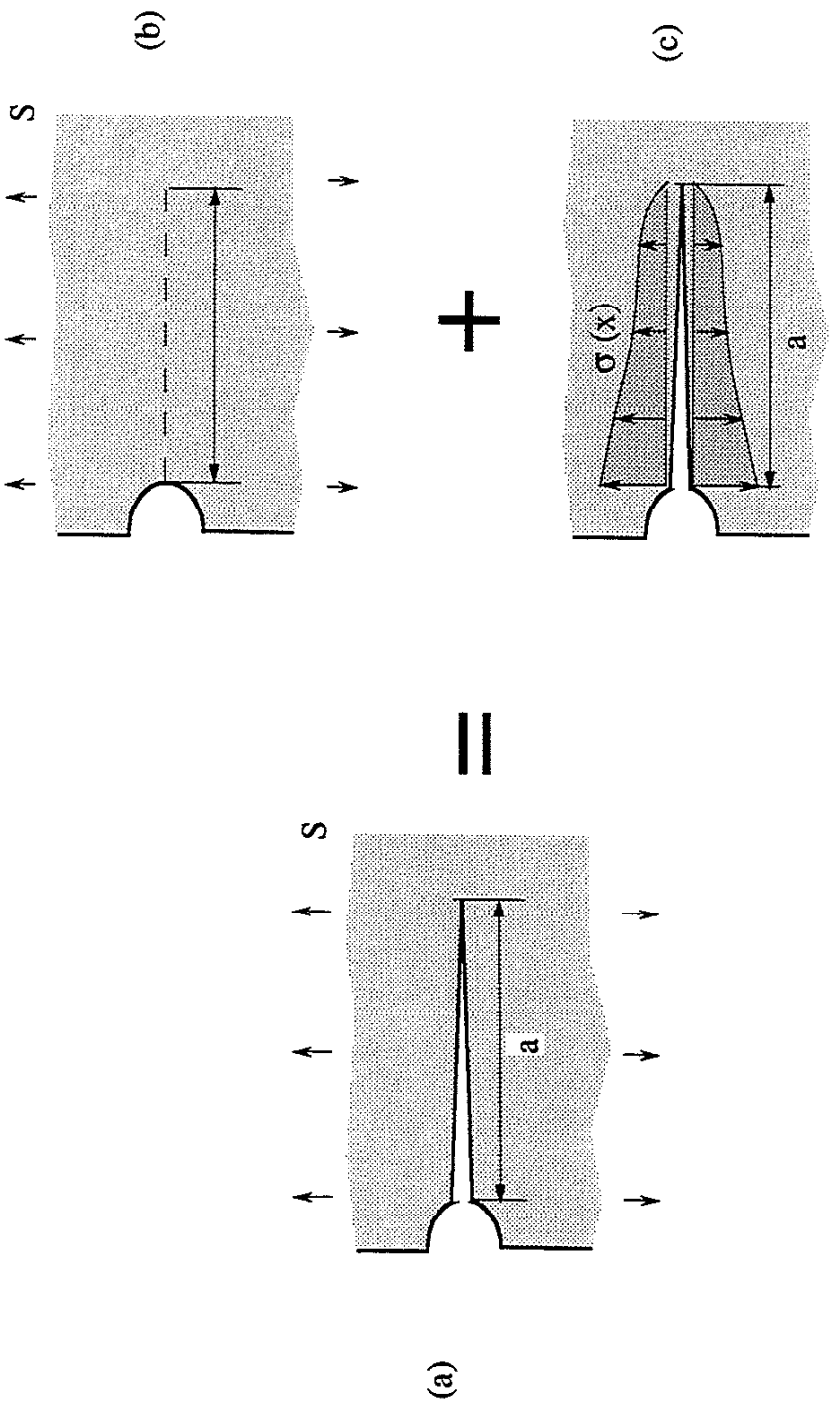


Fig. 4.5(a-c) Superposition of the stress field of a crack under far-field loading: (a) A straight crack of length a in a specimen with arbitrary geometry, which is equivalent to the superposition of (b) crack-free specimen under same far-field loading and (c) the cracked specimen under internal tensile stress σ(x) acting upon the crack faces.

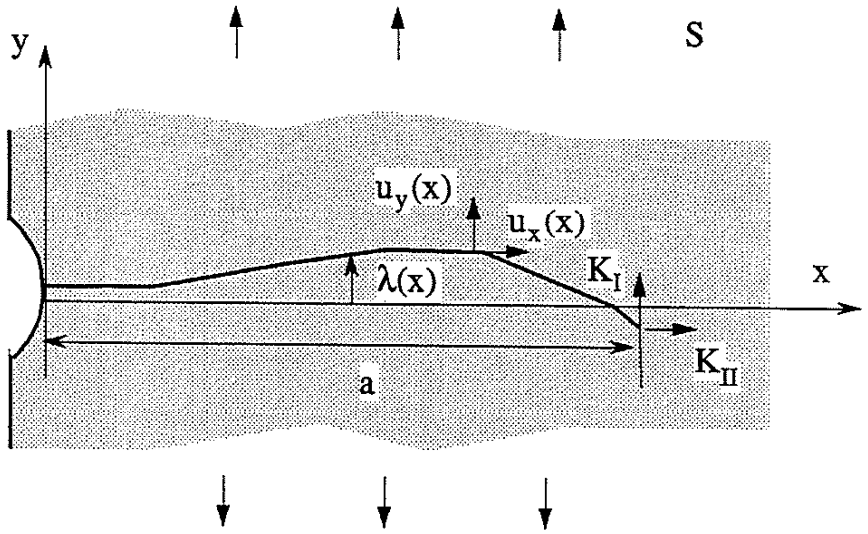


Fig. 4.6 For a deflected crack under far field tensile stress, the deviation of the crack from straight line $\lambda(x)$, the mixed-mode stress intensity factor at the crack tip $K_I$ and $K_{II}$, and the mixed-mode displacements along the crack surface $u_x(x)$ and $u_y(x)$ are illustrated.

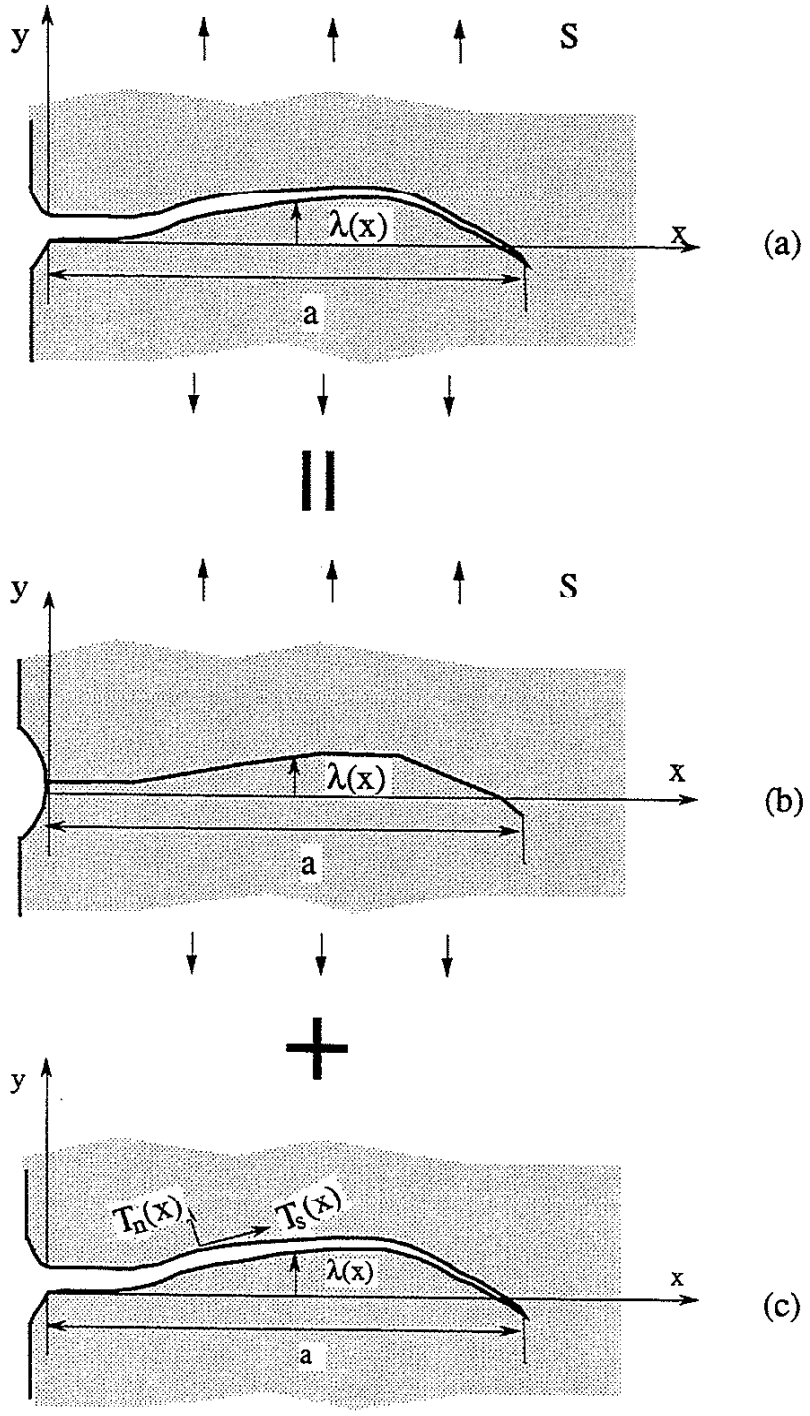


Fig. 4.7(a-c) Superposition of the stress field of a deflected crack under far-field Mode-I loading: (a) The deflected crack in a specimen with arbitrary geometry which is equivalent to the superposition of (b) a crack-free specimen under same far-field loading and (c) the specimen with the deflected crack under internal normal and shear stresses $T_n(x)$ and $T_s(x)$ acting upon the crack faces.

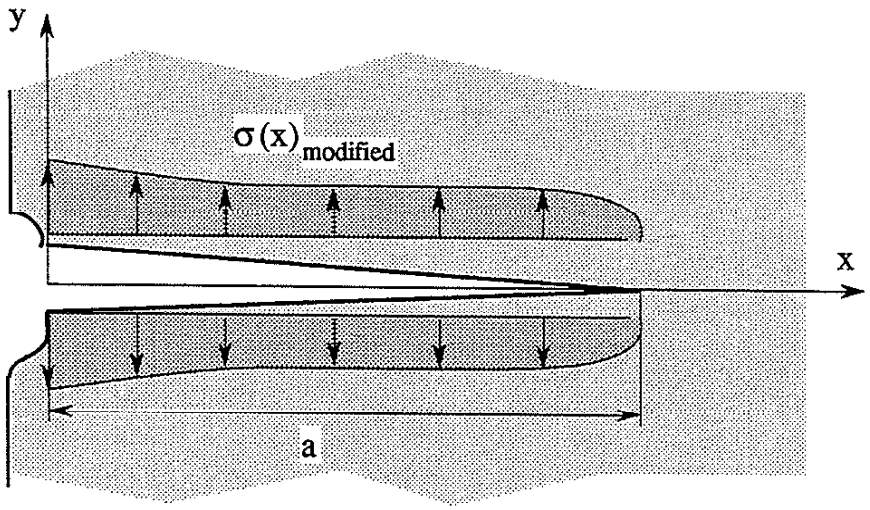


(a)

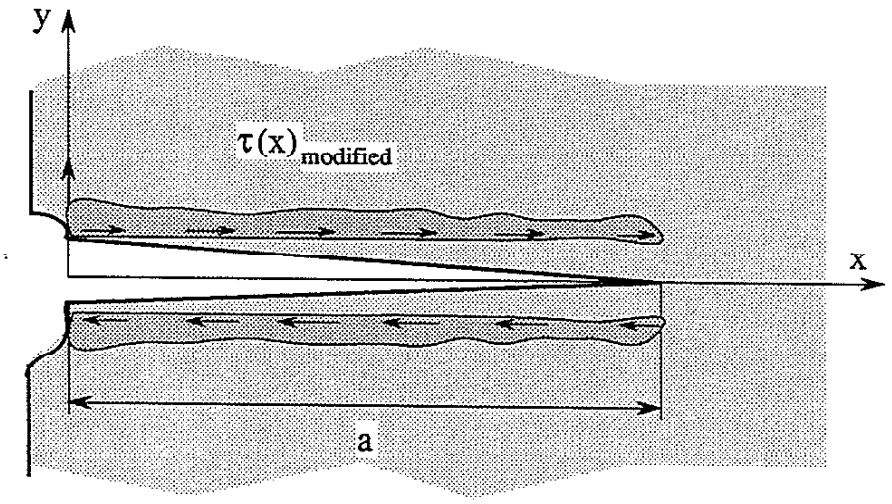


(b)

Fig. 4.8(a-b) A straight crack under internal (a) tensile stress $\sigma(x)_{modified}$ and (b) shear stress $\tau(x)_{modified}$ after transforming the deflected-crack problem (as shown in Fig. 4.7(c)) into a straight crack one.

| | | h | L | θ |
|---|---|---|---|---|
| – – – – | 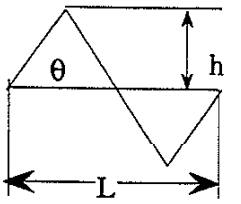 | 12.5μm | 50μm | 45° |
| ——— | 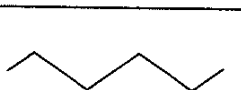 | 25μm | 100μm | 45° |
| ..... |  | 50μm | 200μm | 45° |
| — - — |  | 0 | ∞ | 0 |

Fig.5.1(a-c) Predicted influence of the geometrical features of the assumed zigzag path on RICC - case I, constant tilt angle: (a) Illustrations of three zigzag paths (with constant 45° tilt angle) and an undeflected crack path (for the case of PICC only) for comparison.

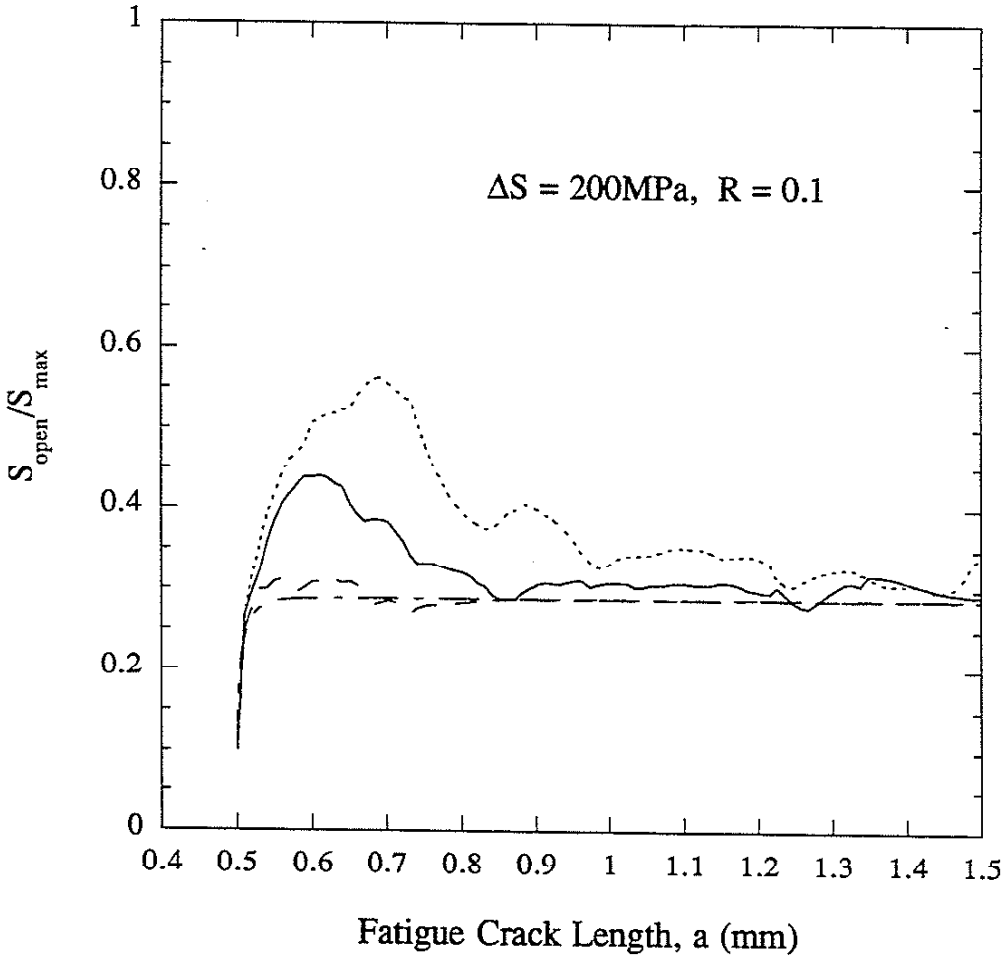


Fig. 5.1(b) Predicted variation of $S_{open}/S_{max}$ with crack length using the four paths, respectively.

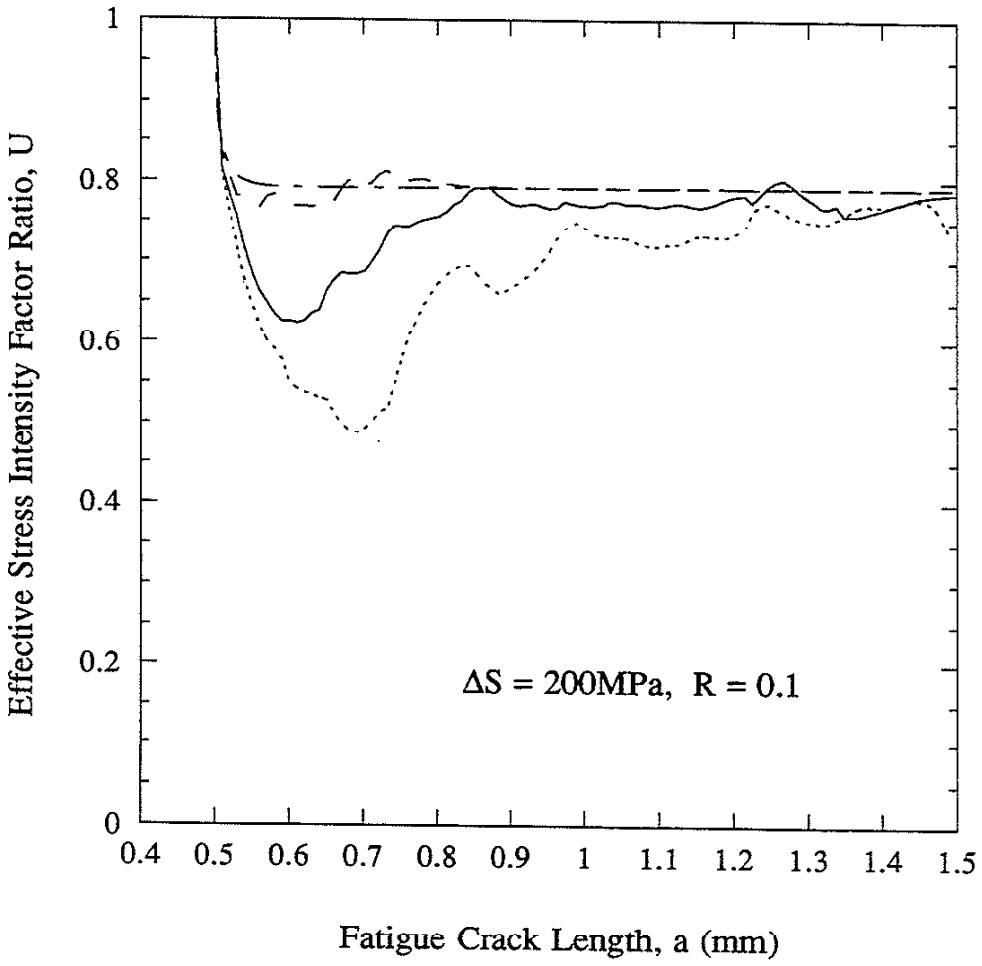


Fig. 5.1(c) Predicted variation of U with crack length.

| | | h | L | θ |
|---|---|---|---|---|
| | 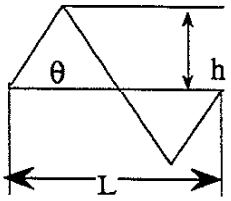 | 12.5μm | 100μm | 26.6° |
| |  | 25μm | 100μm | 45° |
| |  | 50μm | 100μm | 63.4° |
| |  | 0 | ∞ | 0 |

Fig.5.2(a-c) Predicted influence of the geometrical features of the assumed zigzag path on RICC - case II, constant branch length: (a) Illustrations of three zigzag paths (with constant branch length L=100μm) and an undeflected crack path (for the case of PICC only) for comparison.

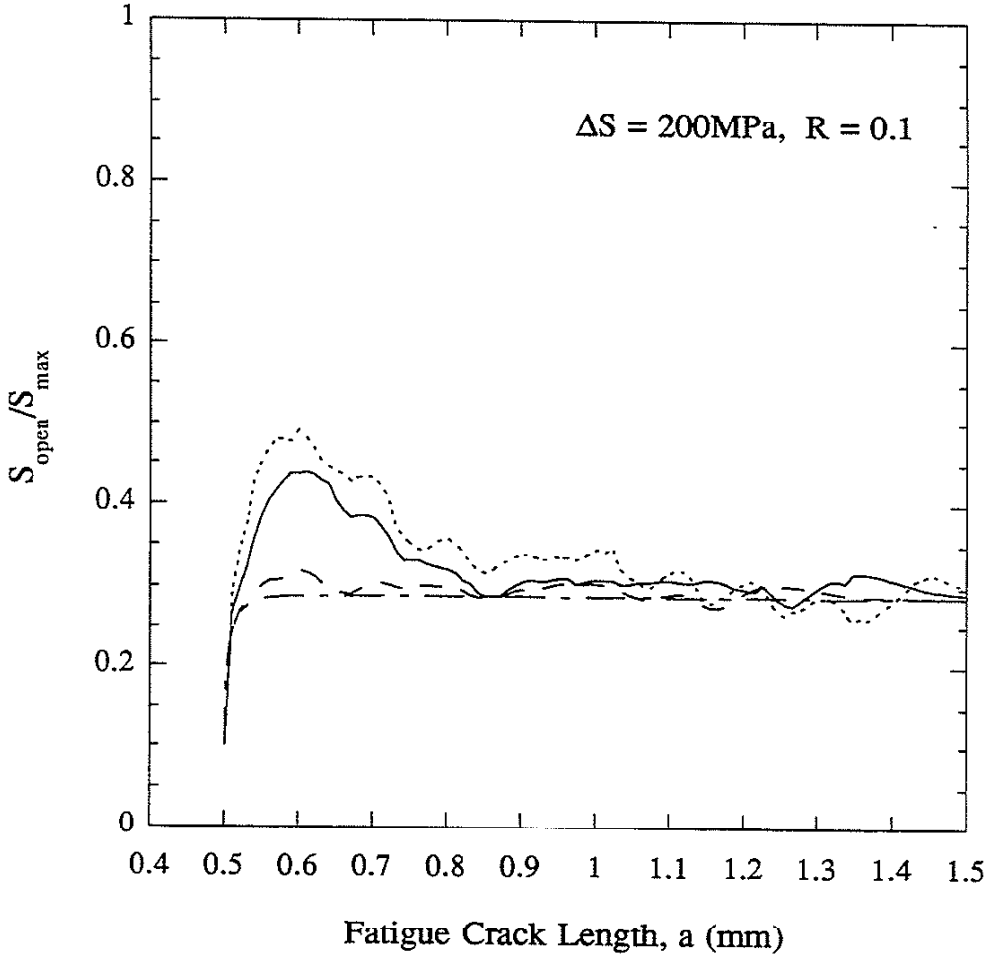


Fig. 5.2(b) Predicted variation of $S_{open}/S_{max}$ with crack length using the four paths, respectively

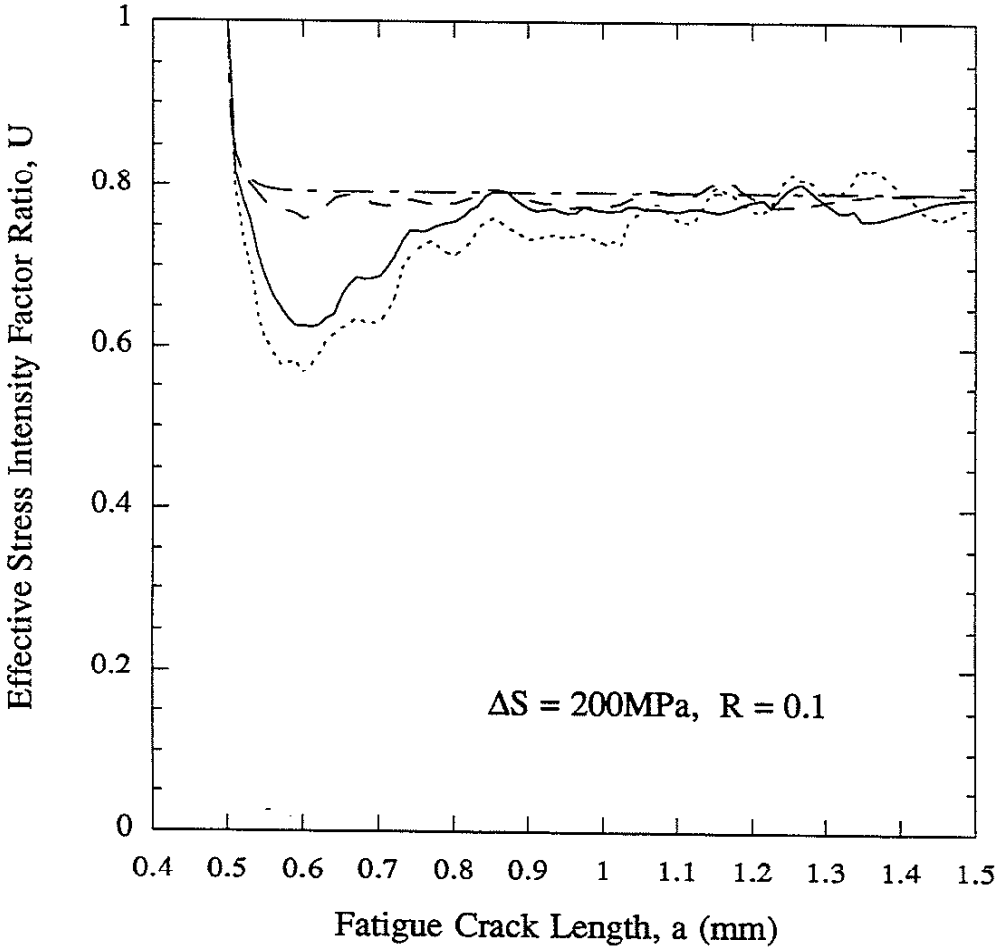


Fig. 5.2(c) Predicted variation of U with crack length.

| | | h | L | θ |
|---|---|---|---|---|
| | 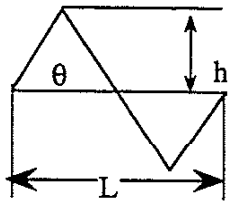  | | | |
| – – – – |  | 25μm | 50μm | 63.4° |
| ——— |  | 25μm | 100μm | 45° |
| ..... | 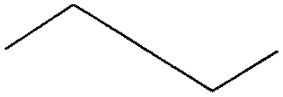 | 25μm | 200μm | 26.6° |
| — - — |  | 0 | ∞ | 0 |

Fig.5.3(a-c) Predicted influence of the geometrical features of the assumed zigzag path on RICC - case III, constant branch amplitude: (a) Illustrations of three zigzag paths (with constant branch amplitude h=25μm) and an undeflected crack path (for the case of PICC only) for comparison.

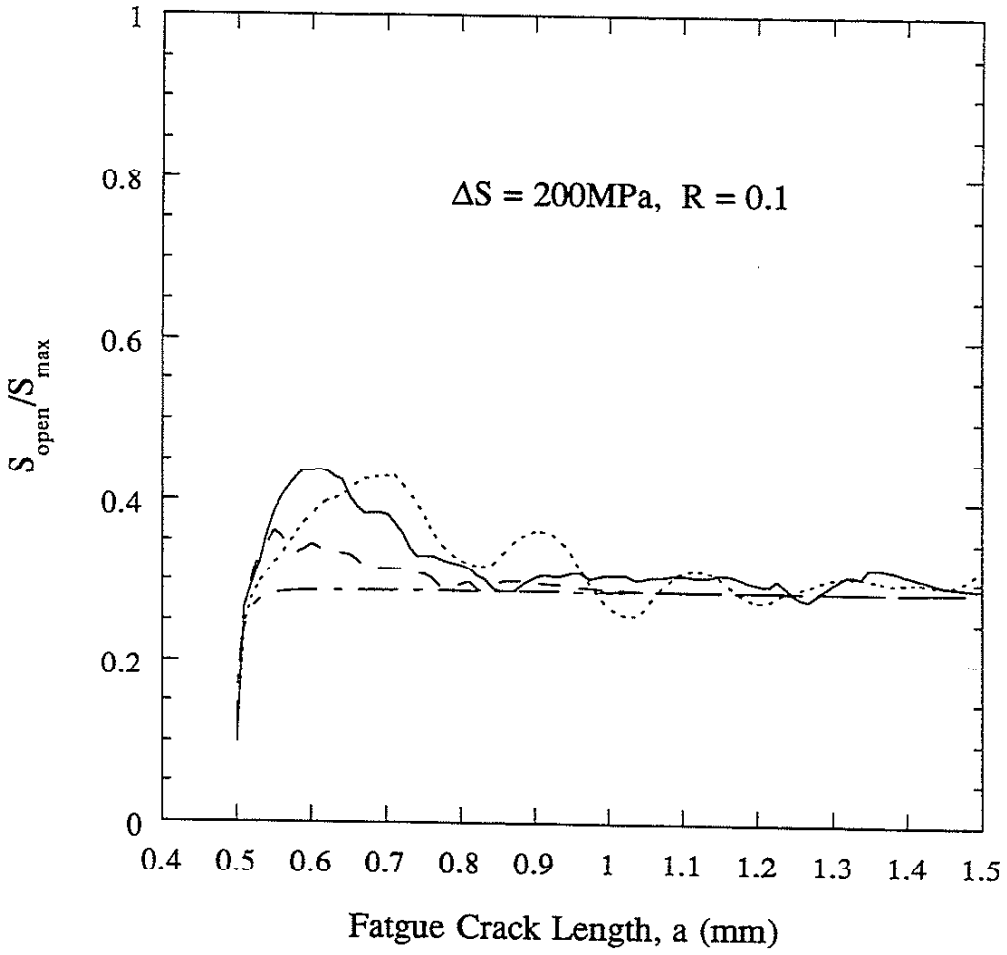


Fig. 5.3(b) Predicted variation of $S_{open}/S_{max}$ with crack length using the four paths, respectively.

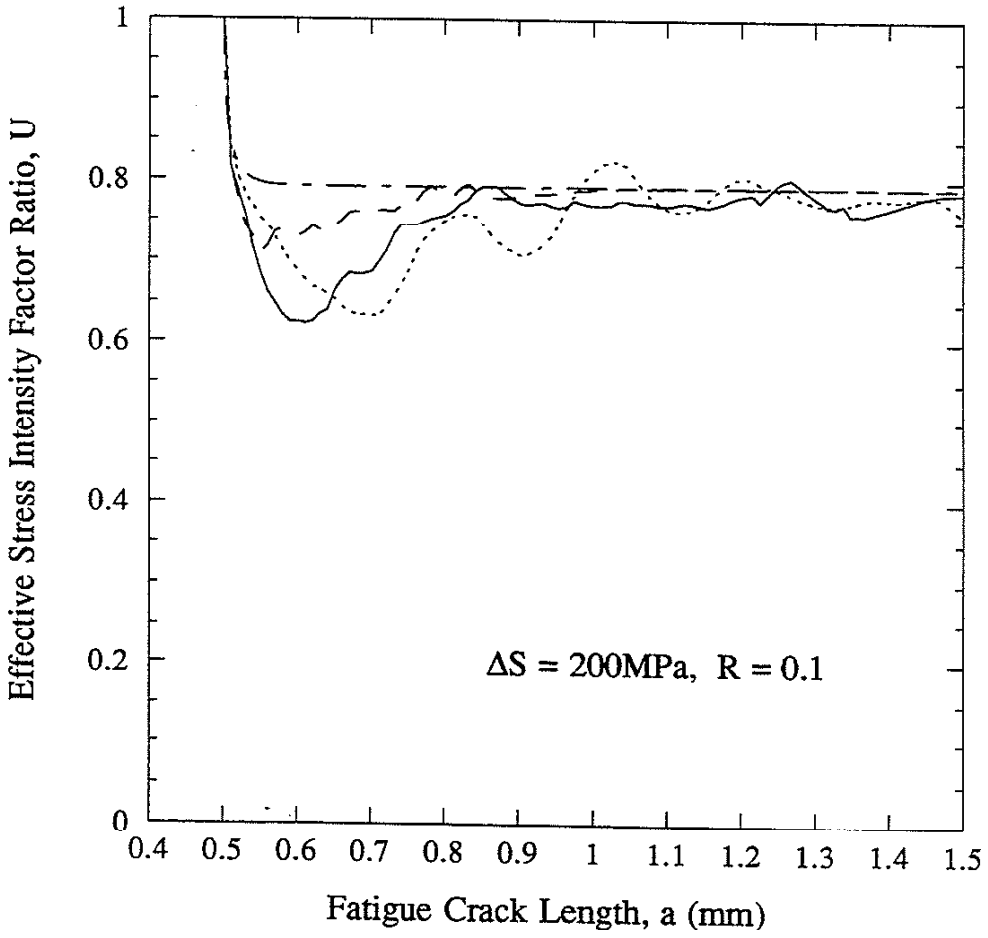


Fig. 5.3(c) Predicted variation of U with crack length.

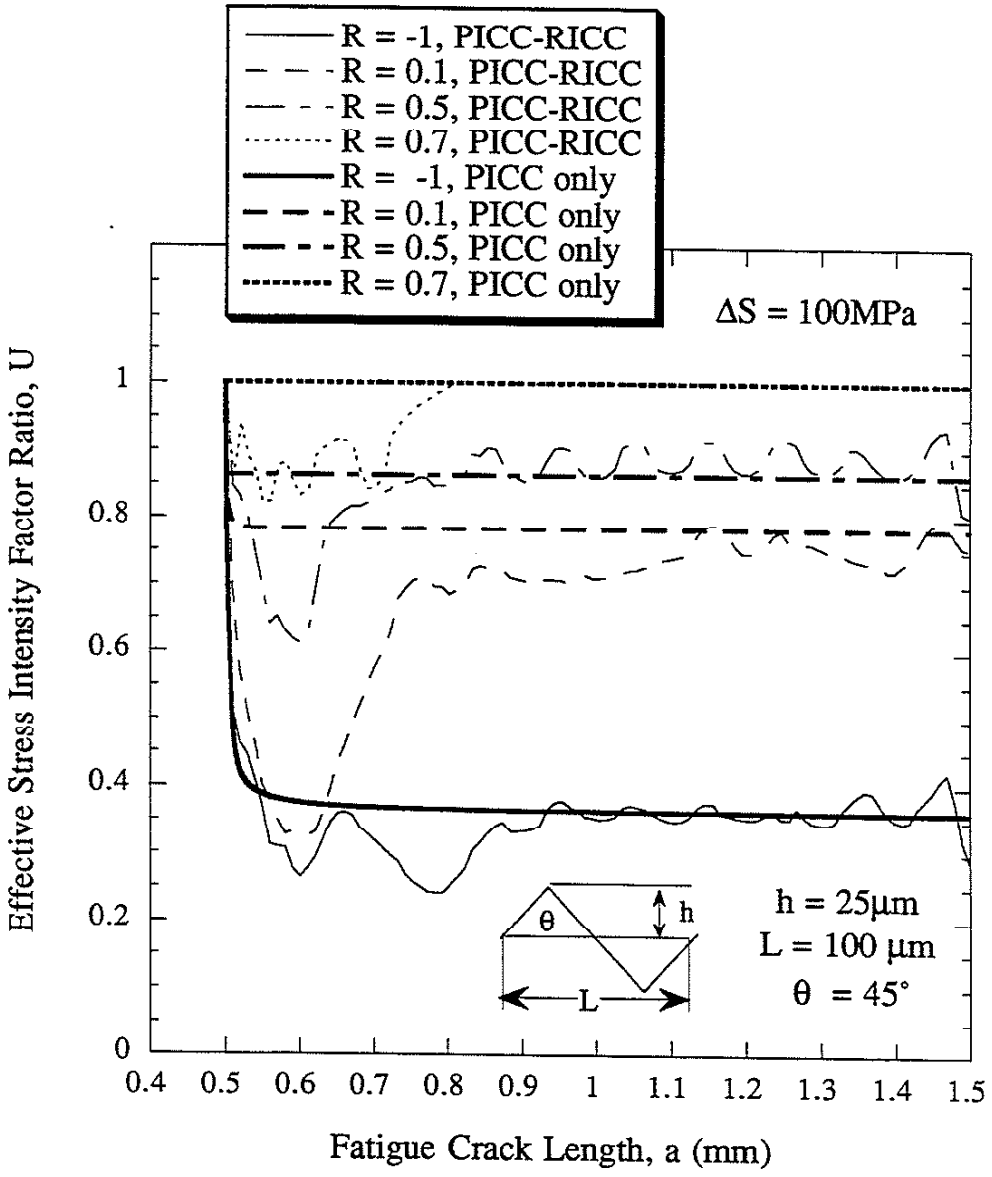


Fig. 5.4 Predicted influence of R-ratio on RICC.

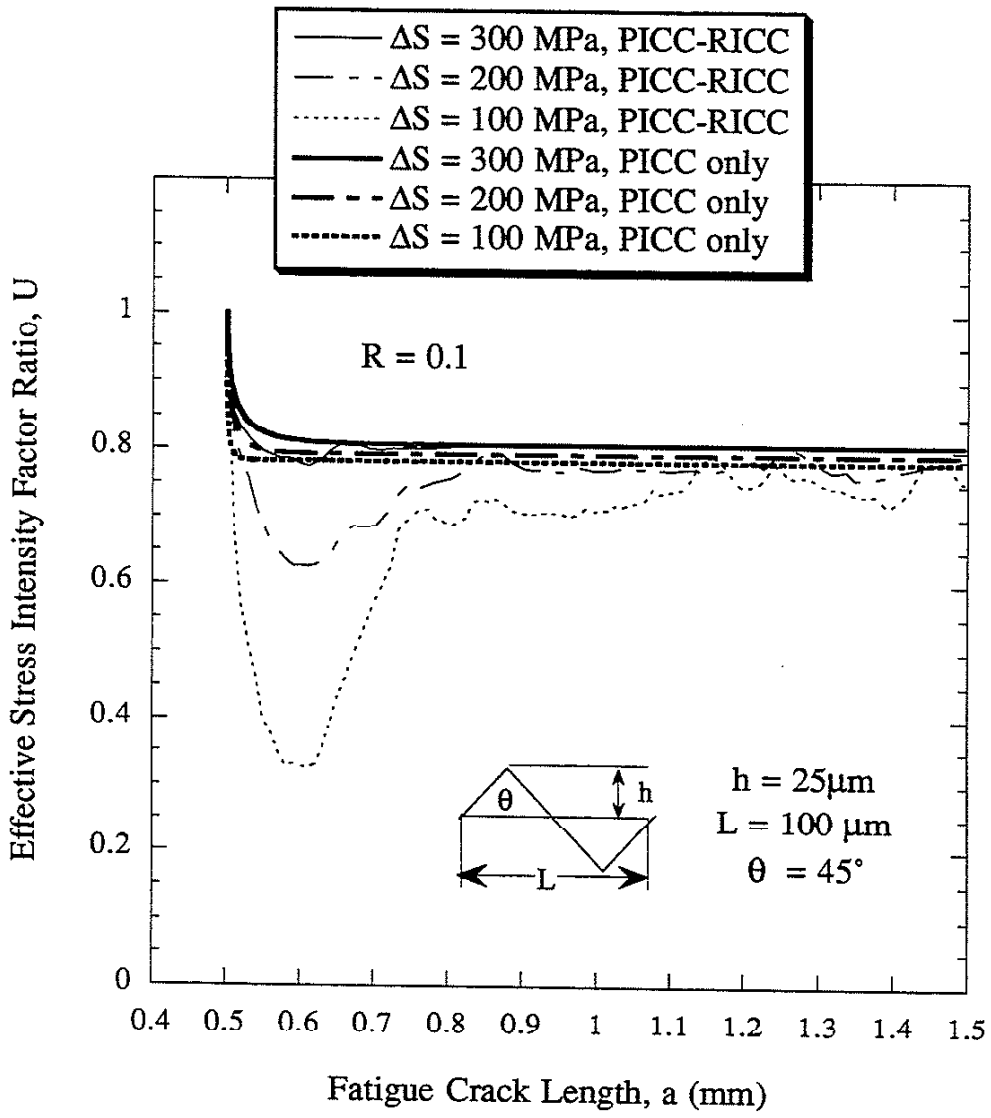


Fig. 5.5 Predicted influence of stress range on RICC.

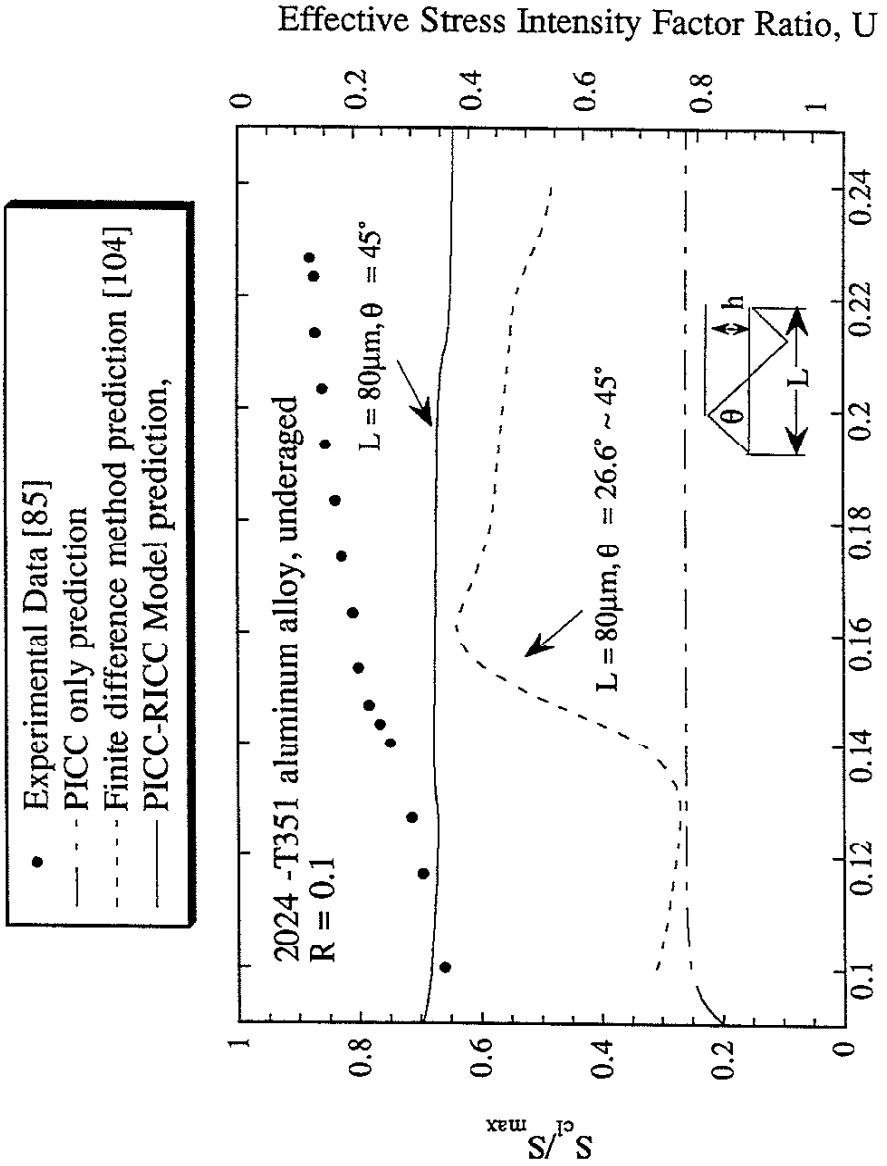


Fig. 6.1 Comparison of the experimentally observed near-threshold closure of 2024-351 aluminum alloy with the predicted results using the PICC-RICC model and finite difference method.

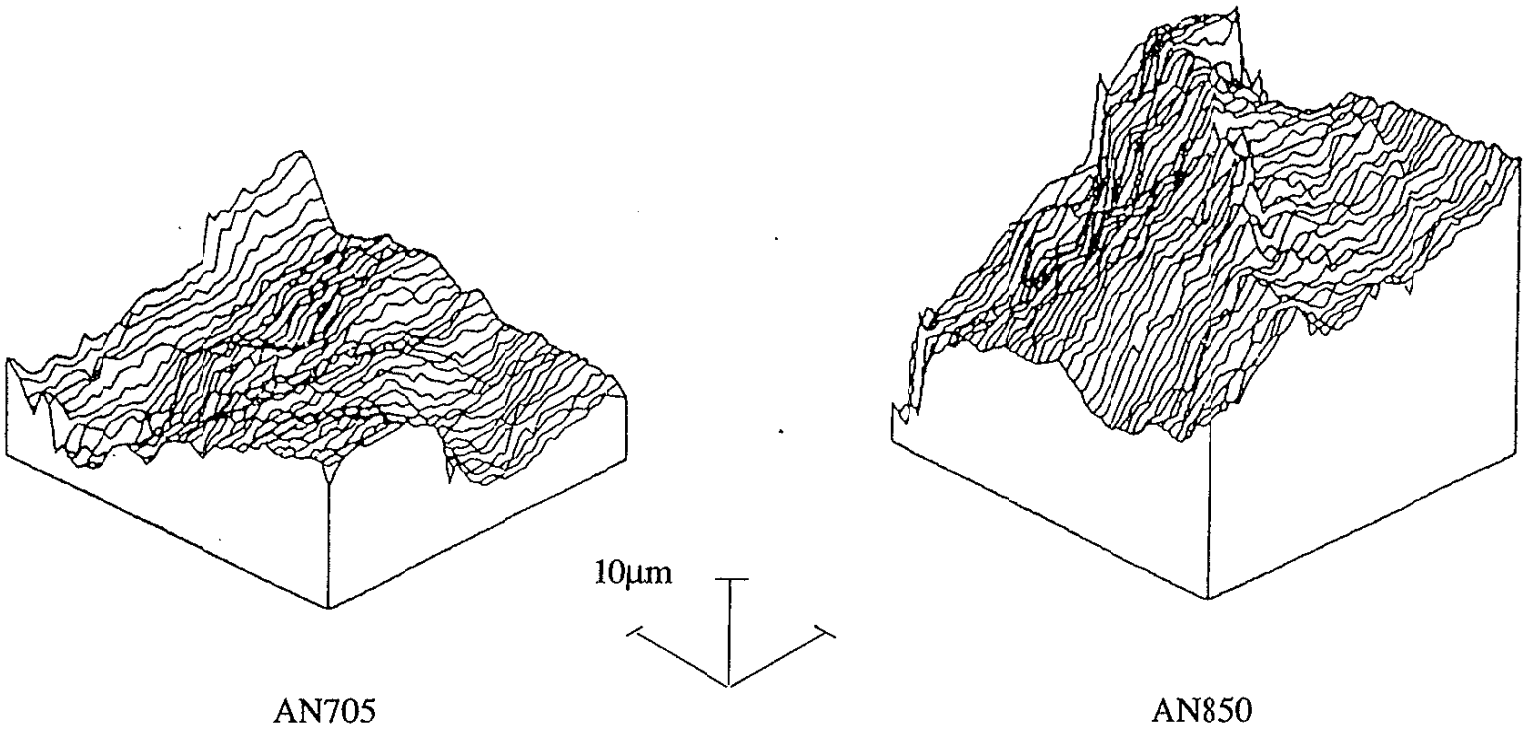


Fig. 6.2 Reconstructed 3-D fracture surface roughness of AN705 and AN850, respectively.

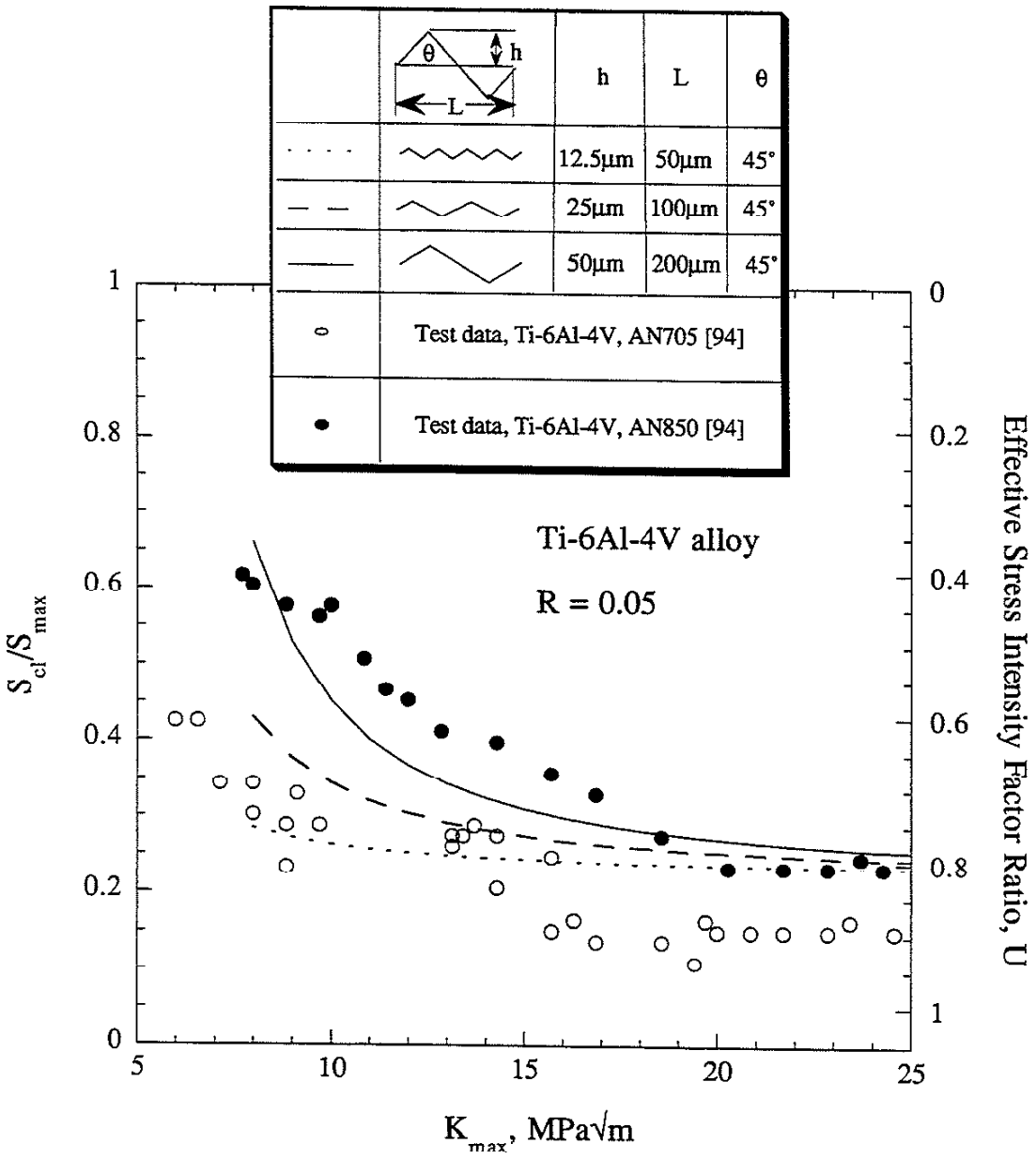


Fig. 6.3 The experimentally observed variation of the near-threshold closure levels of AN705 and AN850 compared with the predicted results using PICC-RICC model.

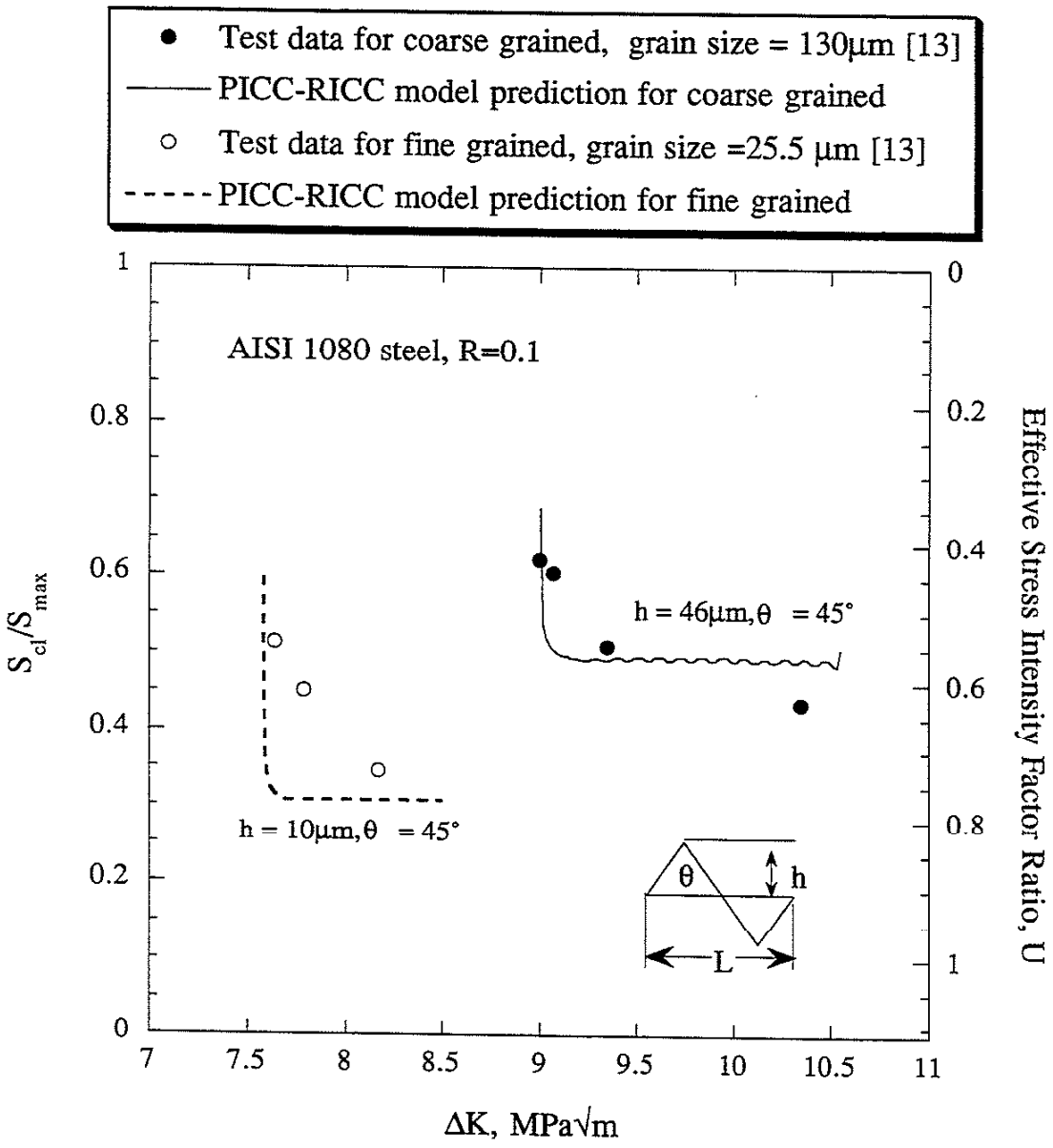


Fig. 6.4 Predicted grain size effect on RICC in AISI 1080 steel using the PICC-RICC model and compared with test data.

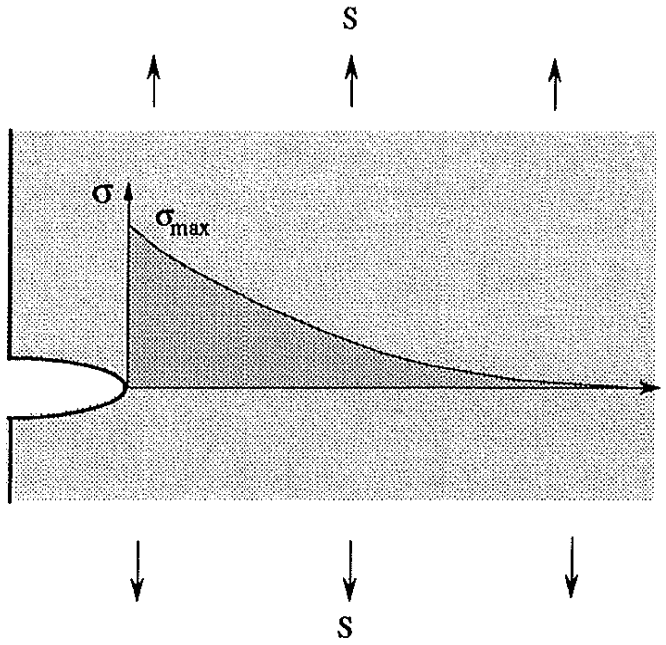


(a)

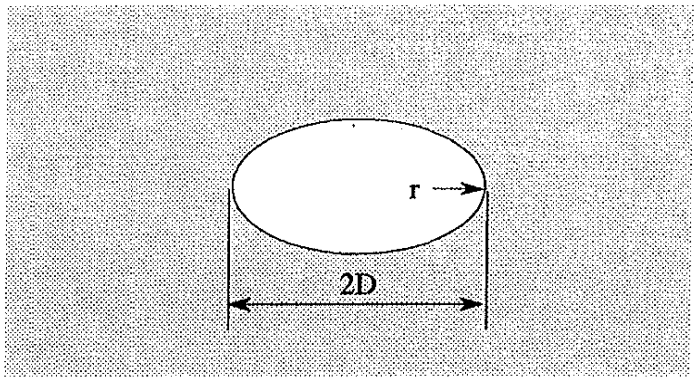


(b)

7.1(a-b) (a) Definition of the stress concentration factor, $K_t$; (b) Illustration of an elliptical notch specimen.

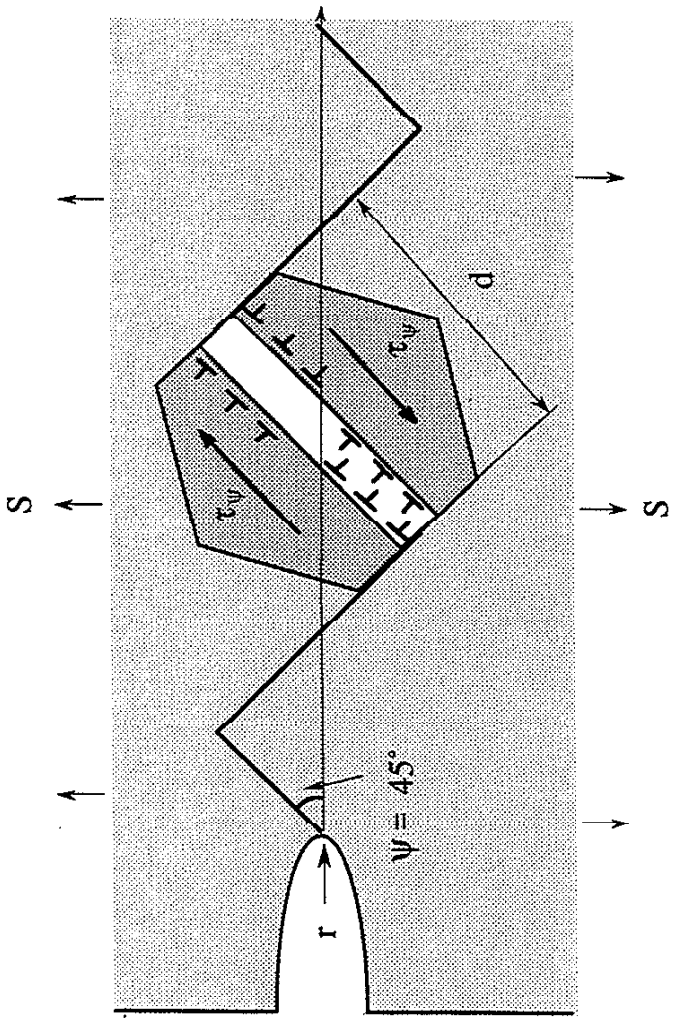


Fig. 7.2(a) Determination of the fatigue crack nucleation life using a dislocation double-pileup model.

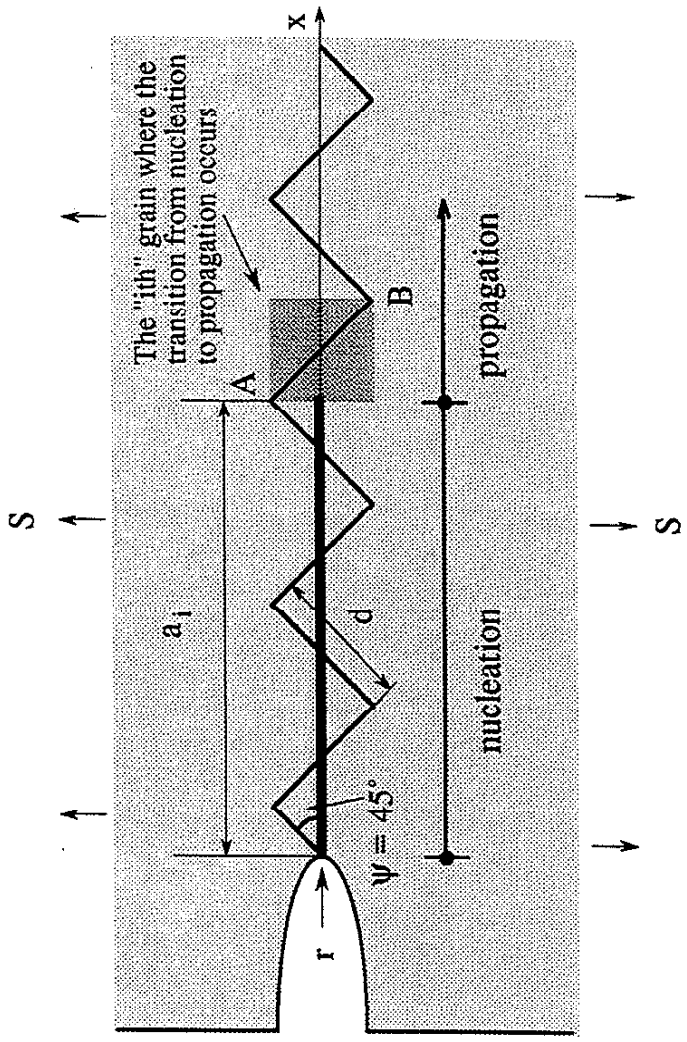


Fig. 7.2(b) Determination of the propagation life (using the PICC-RICC Model) and initial crack length for propagation, $a_i$.

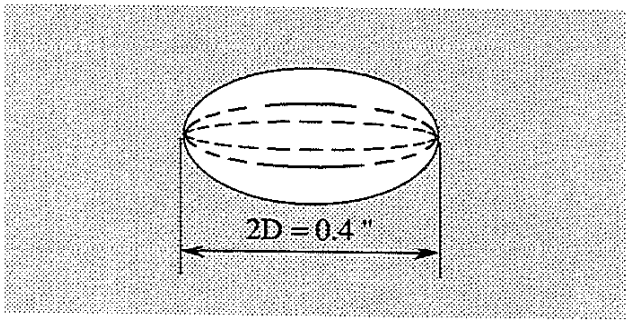


(a)

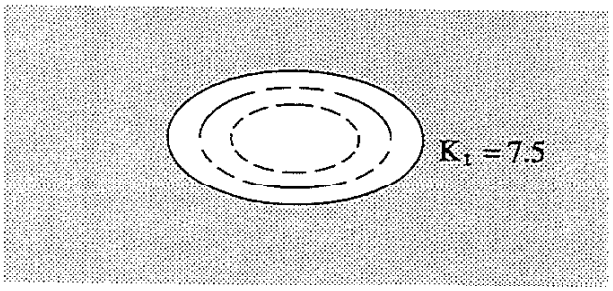


(b)

7.3 (a-b) Illustration of two sets of elliptical notch specimens considered: (a) Constant depth notch with notch depth equal to 0.4"; (b) Geometrically similar notch with constant Kt = 7.5.

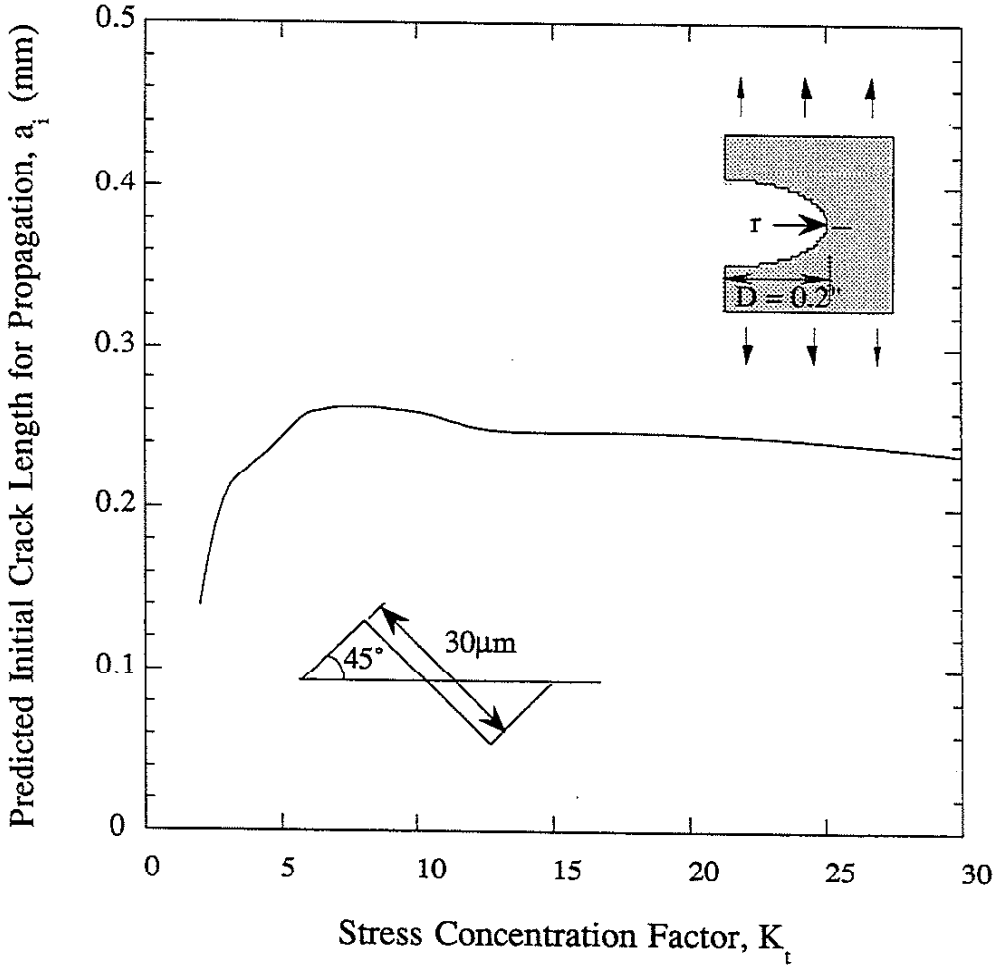


Fig. 7.4 Initial crack length $a_i$ predicted using the total life model for the constant-depth notched specimens including PICC and RICC.

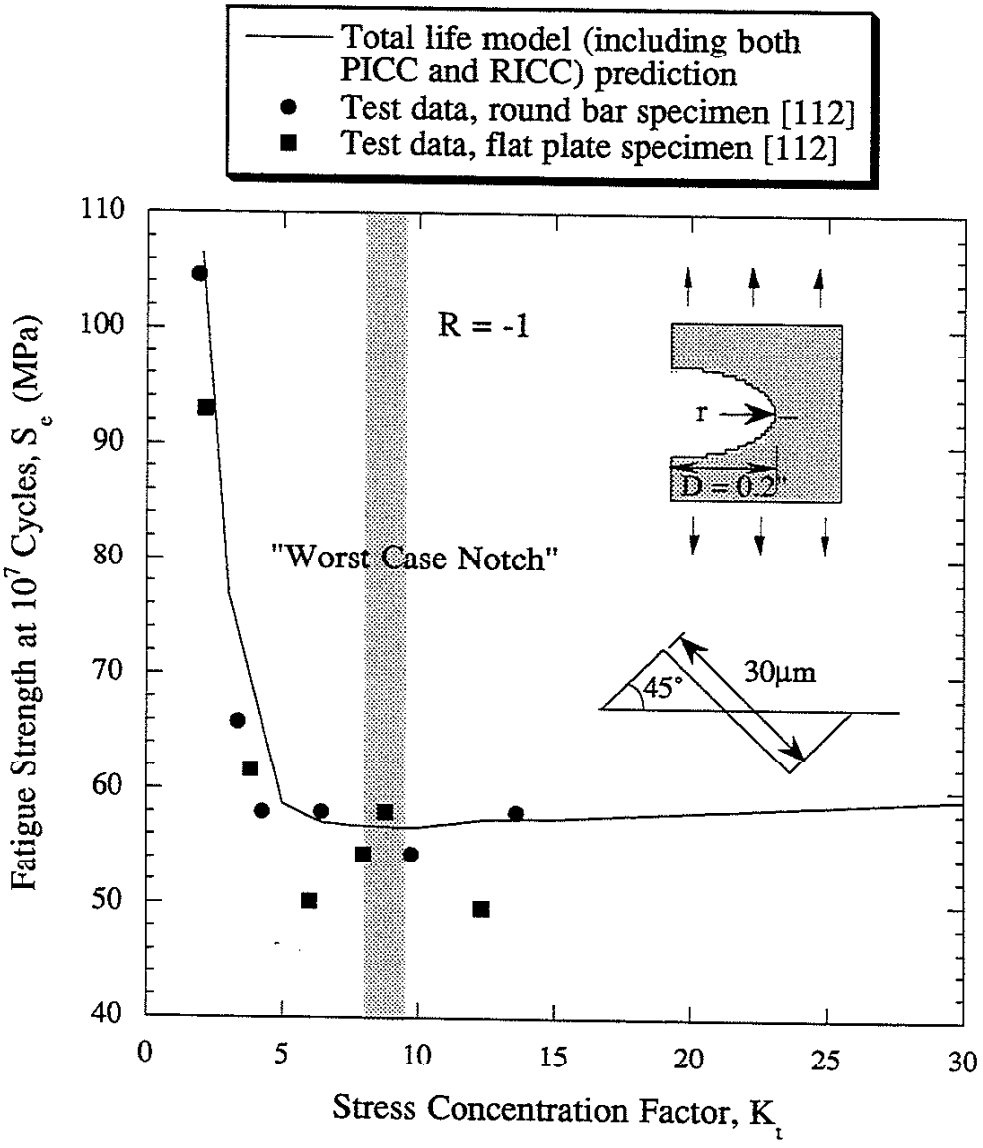


Fig. 7.5 Comparison of the notch fatigue strength of the constant depth notched specimens observed in the experiment with that predicted using the total life model (including PICC and RICC).

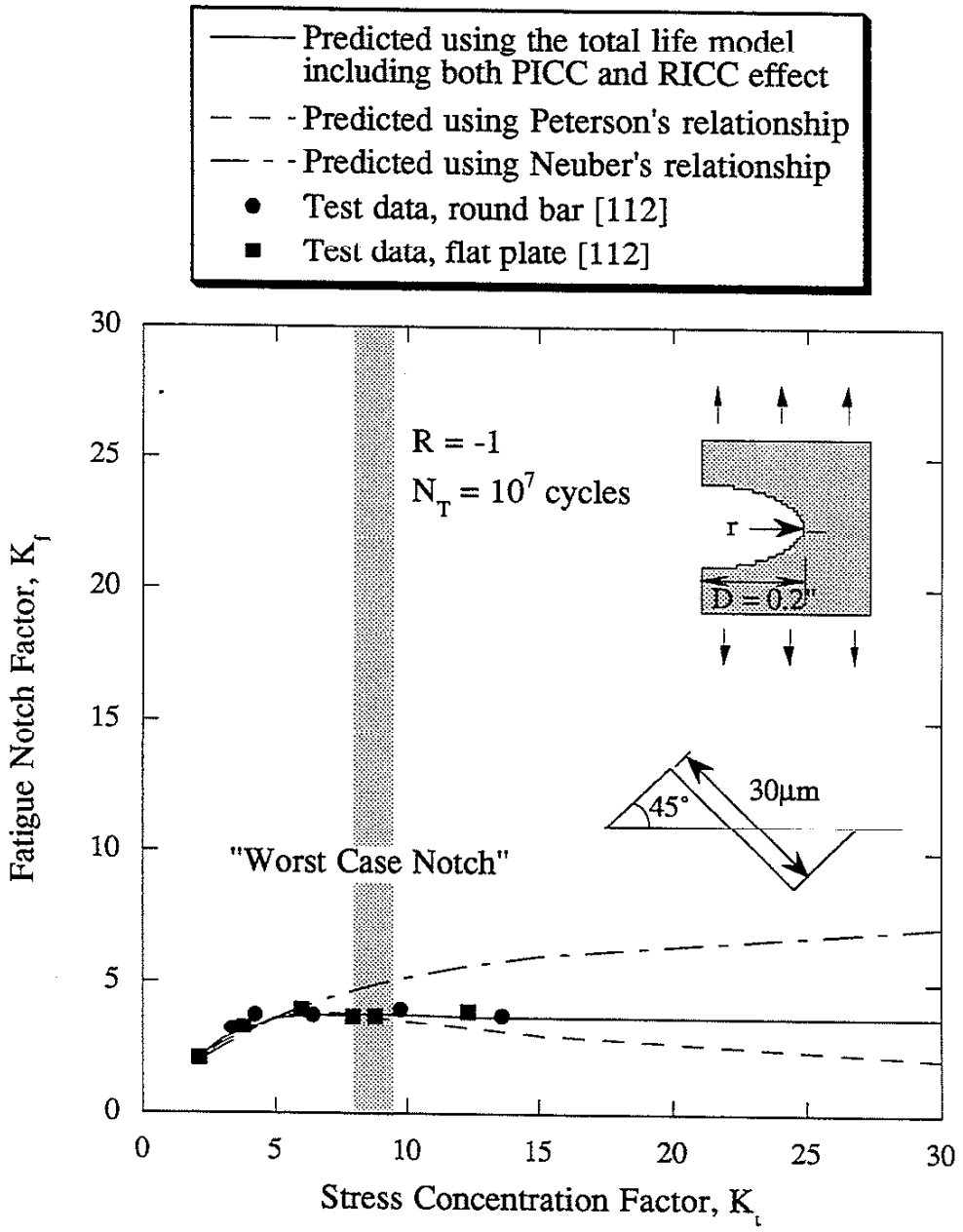


Fig. 7.6 Comparison of the fatigue notch factor $K_f$ of the constant depth notched specimens predicted using the total life model (including both PICC and RICC), Peterson's relationship and Nueber's relationship, respectively and compared with test data [112].

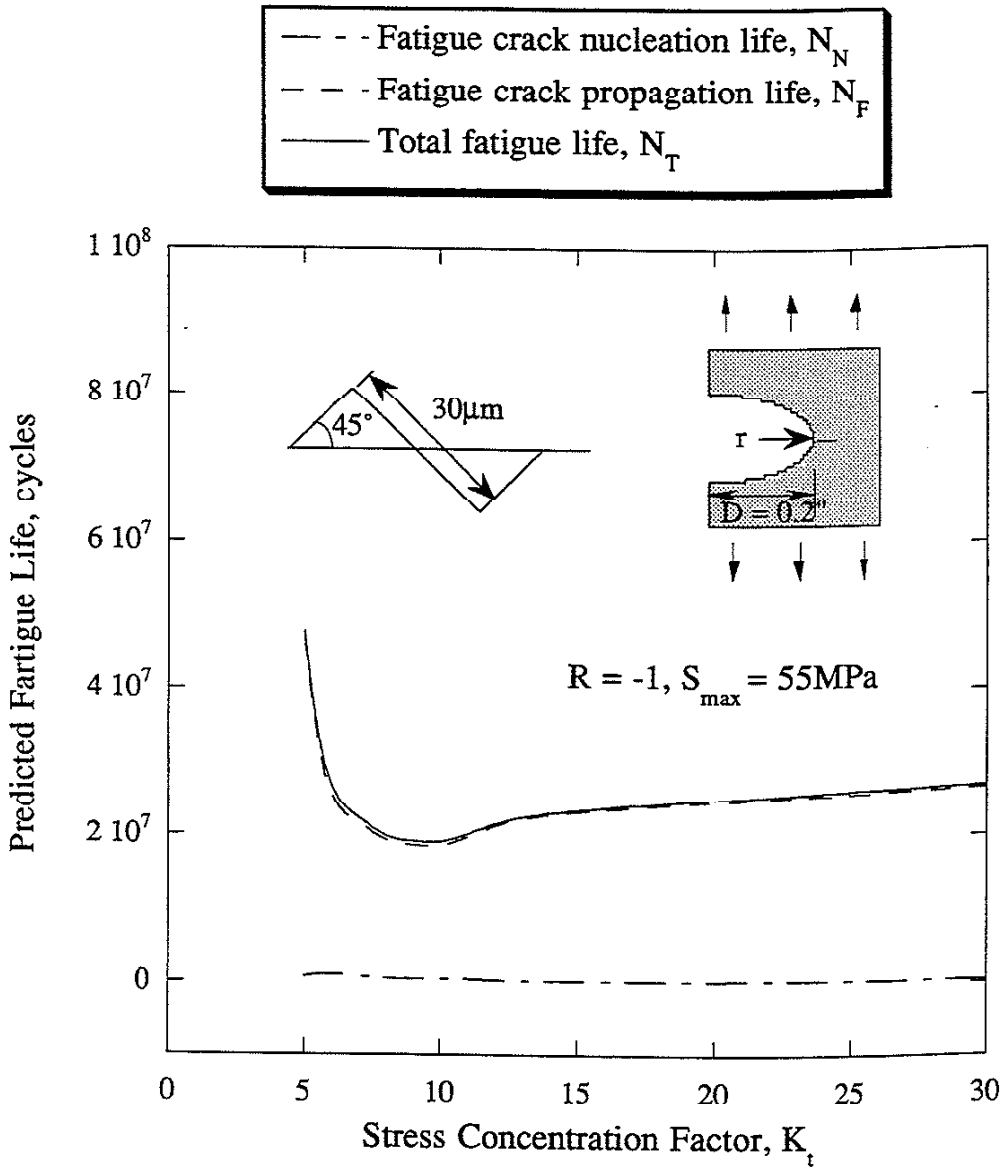


Fig. 7.7 Predicted fatigue crack nucleation life, propagation life and total life for the constant depth specimens subject to the same loading.

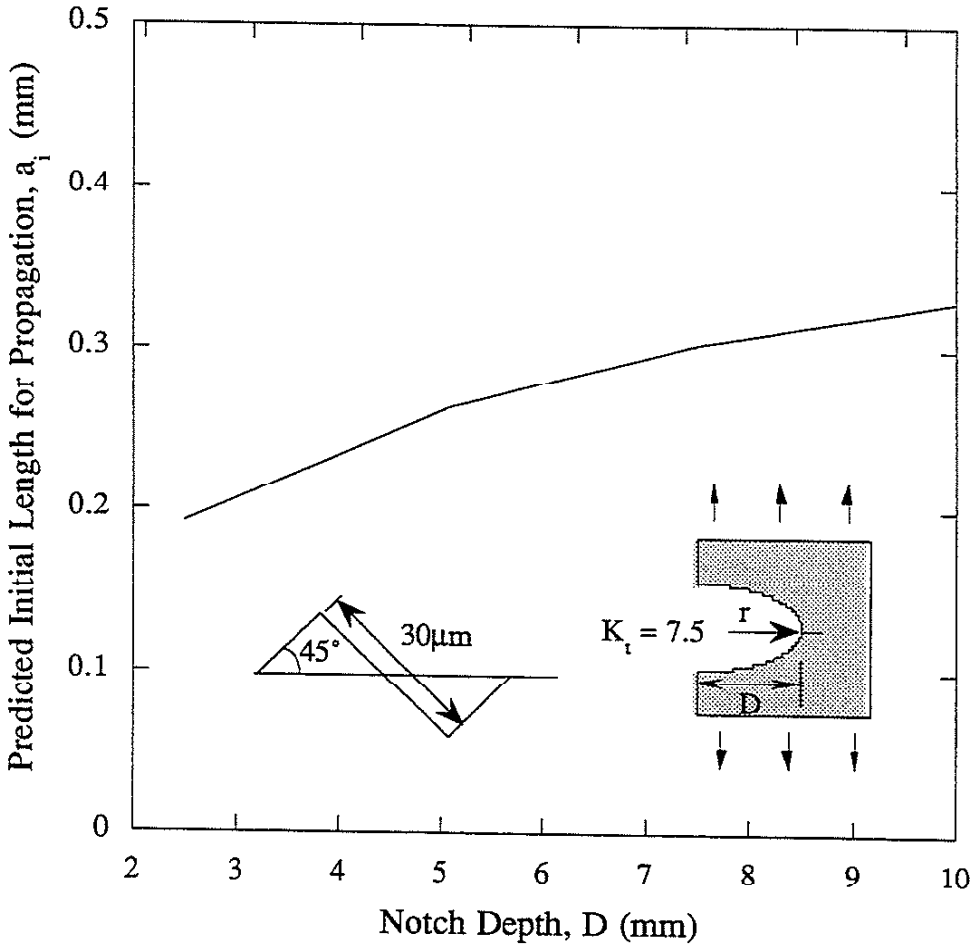


Fig. 7.8 Initial crack length $a_i$ of the geometrically similar notched specimens predicted using the total life model including PICC and RICC.

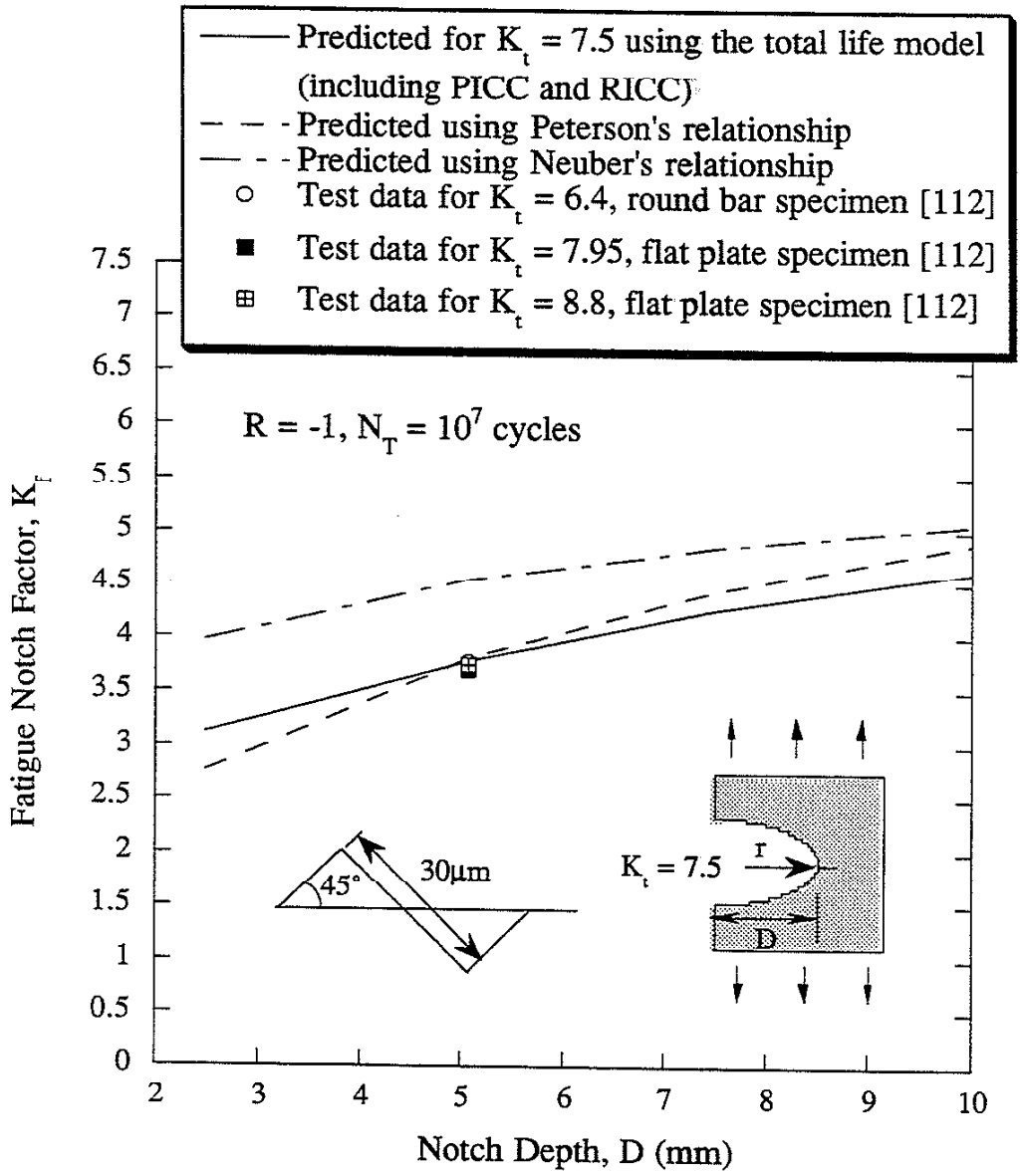


Fig. 7.9 Comparison of the fatigue notch factor $K_f$ of the geometrically similar notched specimens predicted using Peterson's relationship, Nueber's relationship and the total life model (including PICC and RICC), respectively and compared with test data.

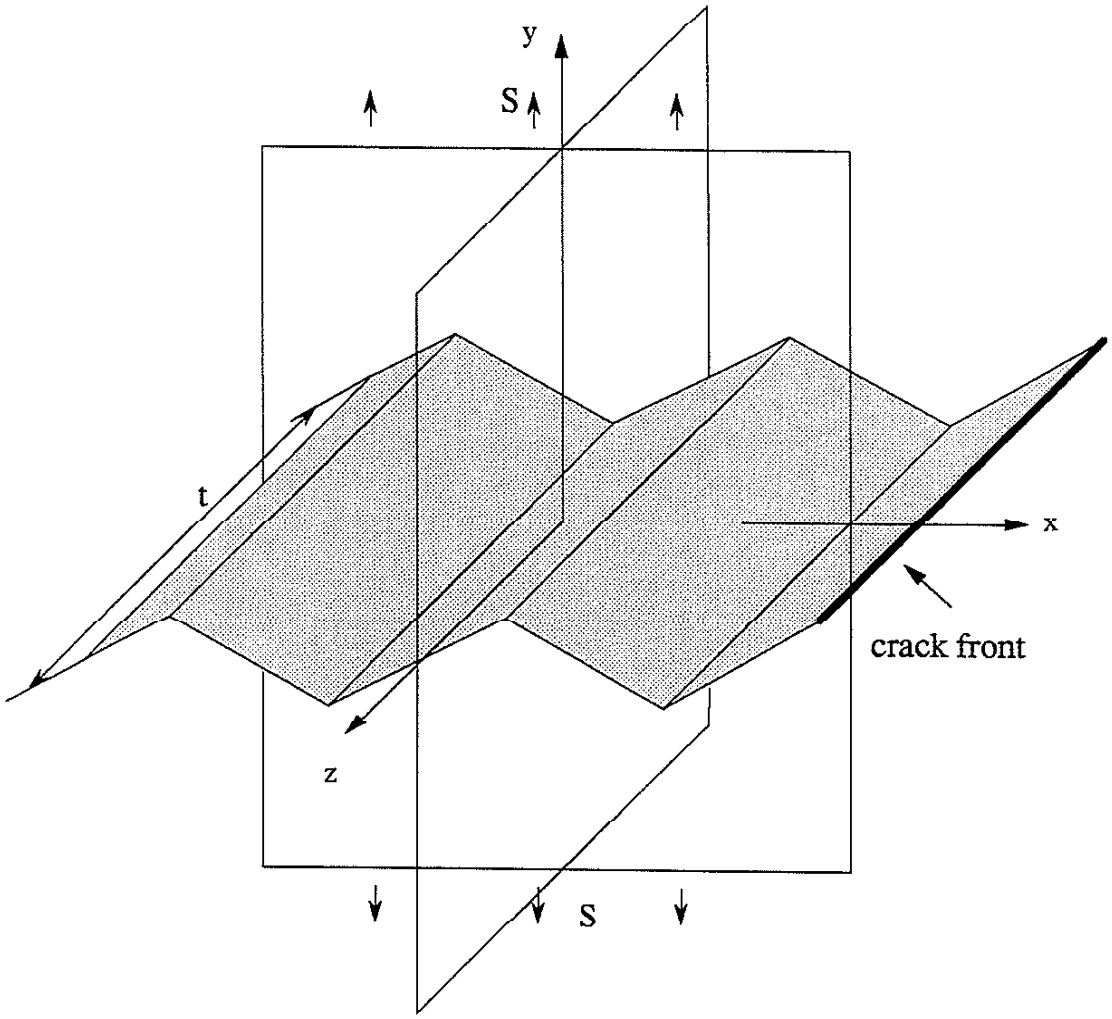


Fig. 8.1 Illustration of the identical appearance of surface roughness along the thickness direction under 2-D assumption.

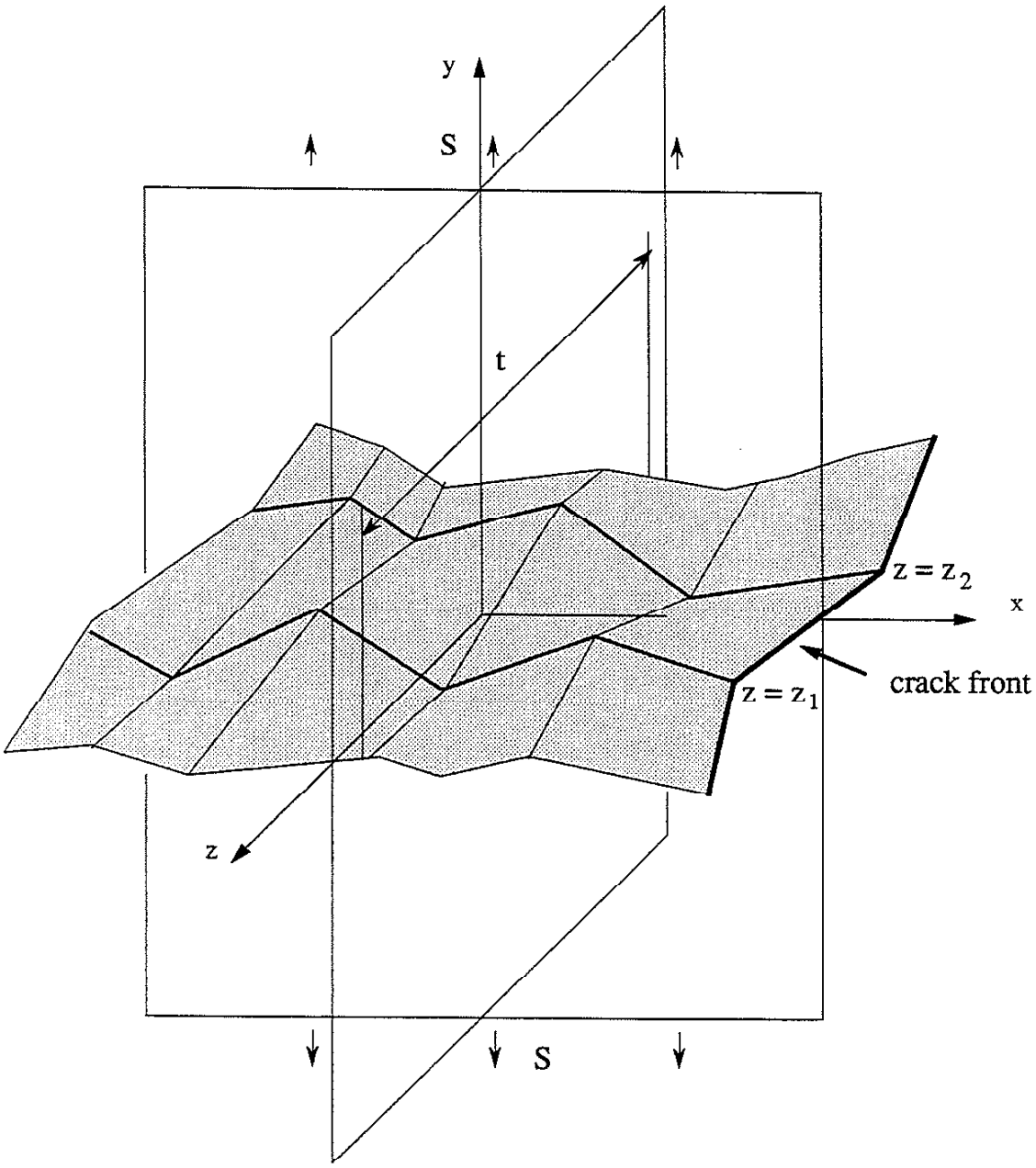


Fig. 8.2 Illustration of the variation of the 3-D surface roughness appearance along the thickness direction.

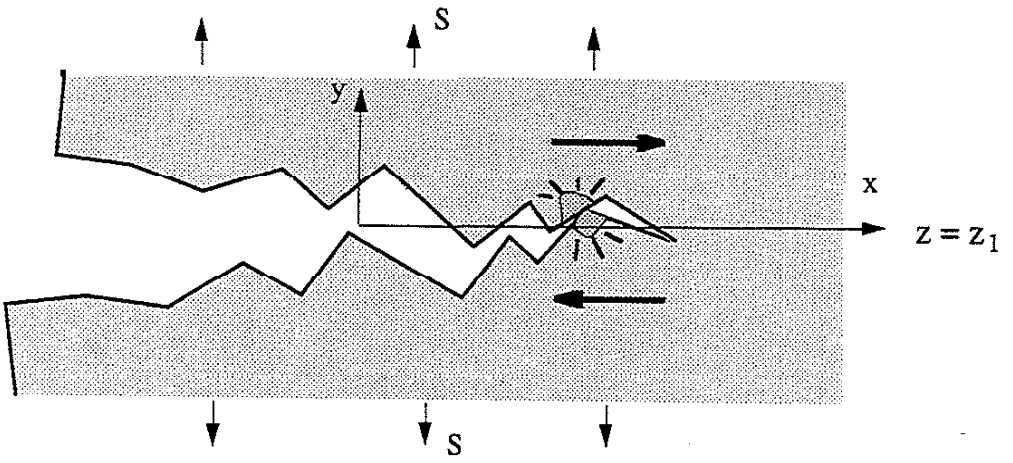


(a)

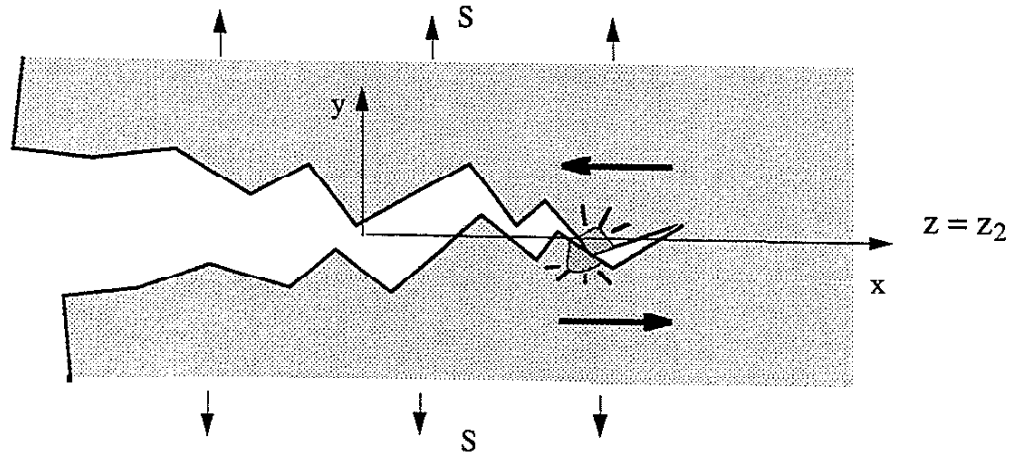


(b)

Fig. 8.3(a-b) Tendency for opposite sliding displacement in (a) and (b) among layers along the thickness direction due to their dissimilar surface appearances.

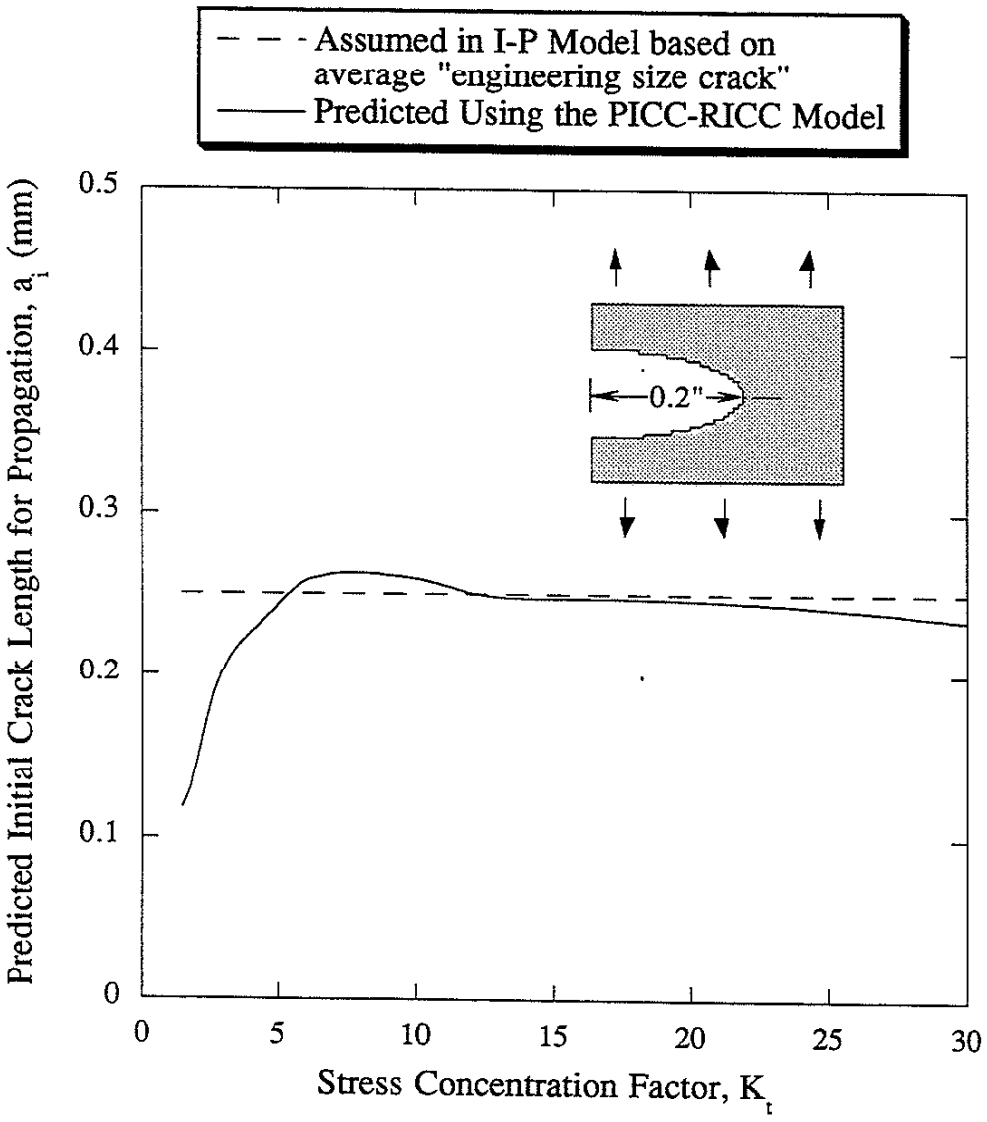


Fig. 8.4 Comparison of the initial crack length $a_i$ customarily assumed in the I-P model with that predicted using the PICC-RICC model, for the specimens with constant depth notch.

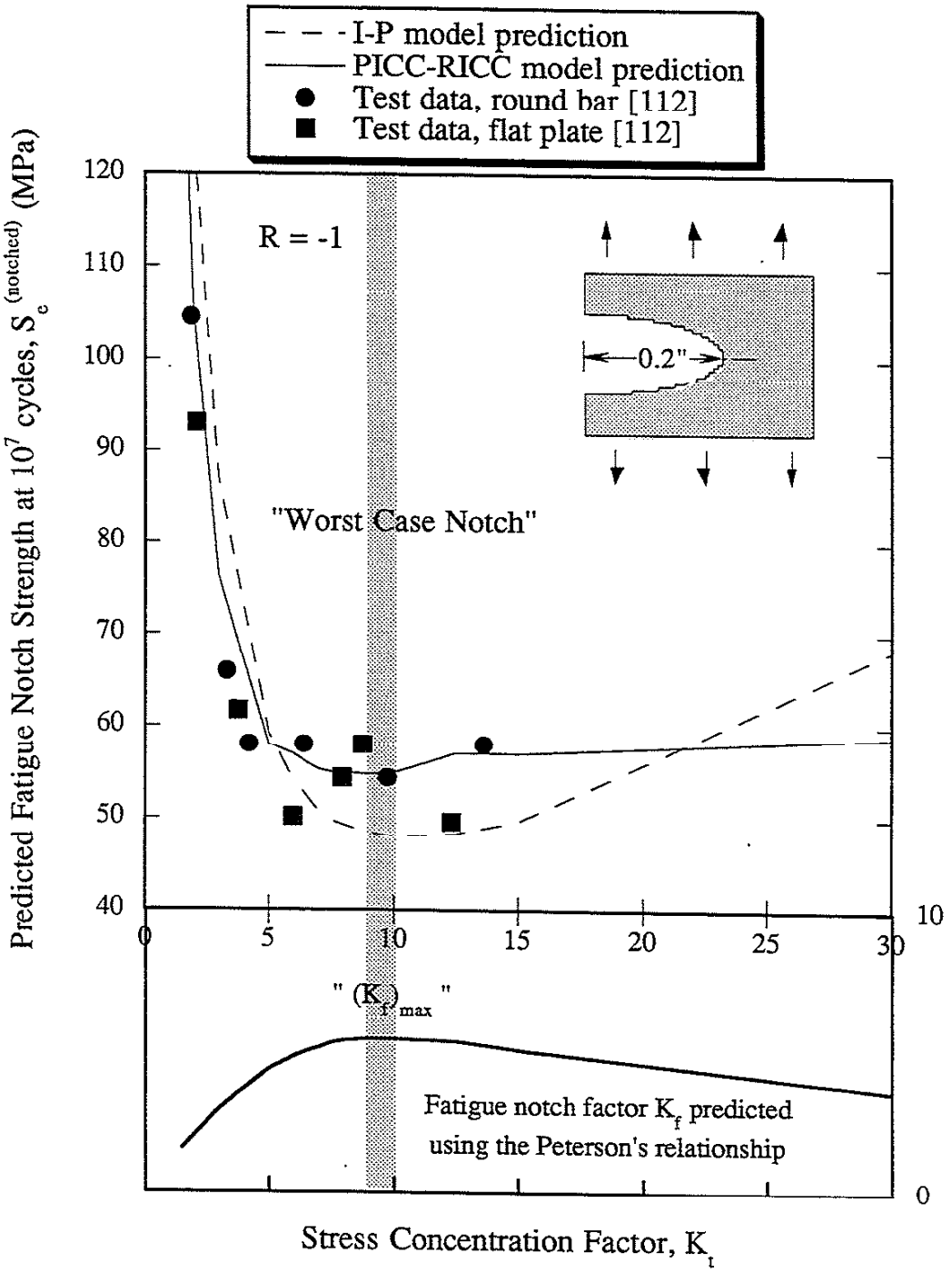


Fig. 8.5 Comparison of the fatigue notch strength predicted using the I-P model and the PICC-RICC model, respectively. The predicted "worst case notch" is consistent with the $(K_f)_{max}$ value indicated in the Peterson's empirical relationship.

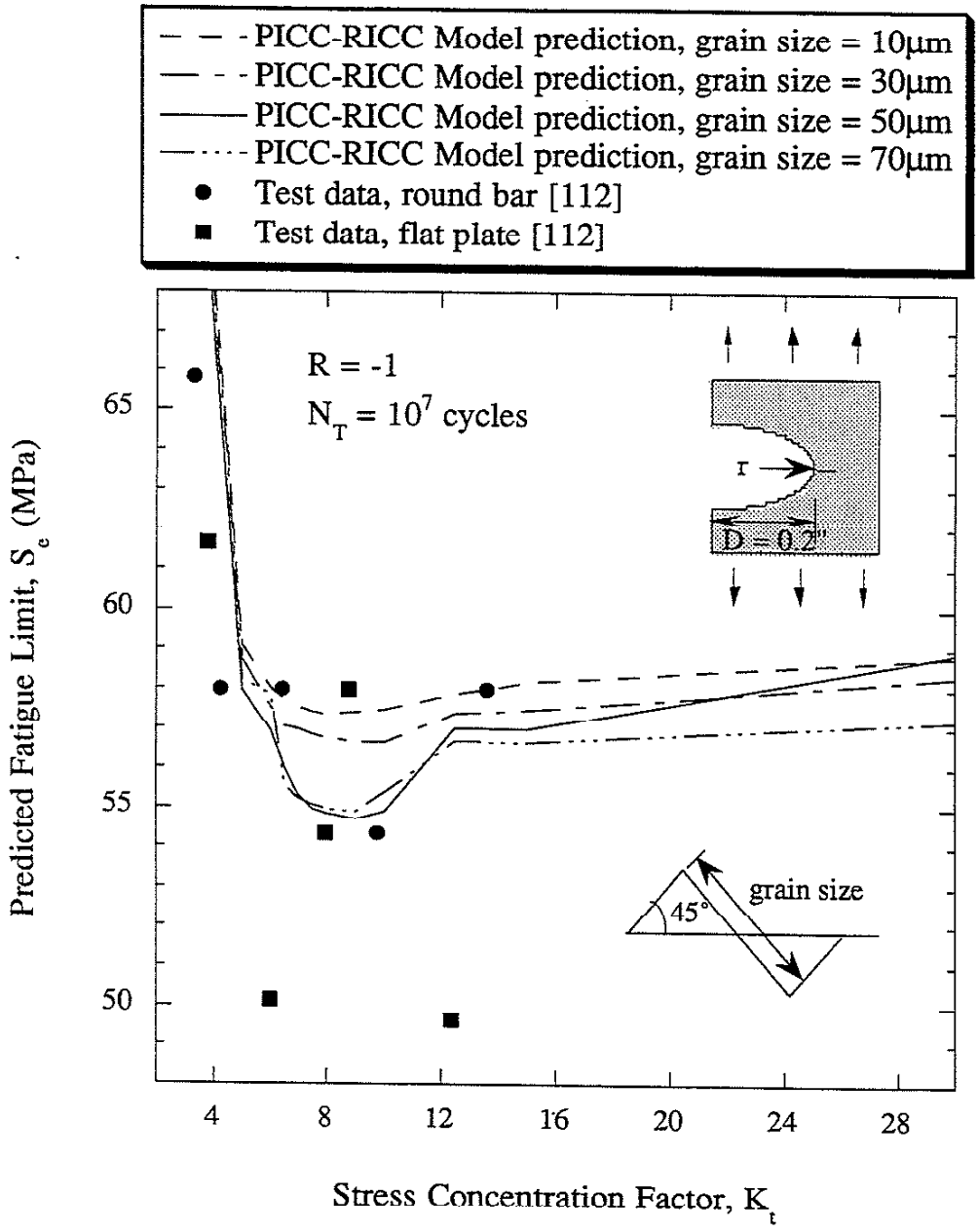


Fig. 8.6 Predicted variation of fatigue notch strength with grain size for stress ratio R=-1 using the PICC-RICC model and compared with test data.

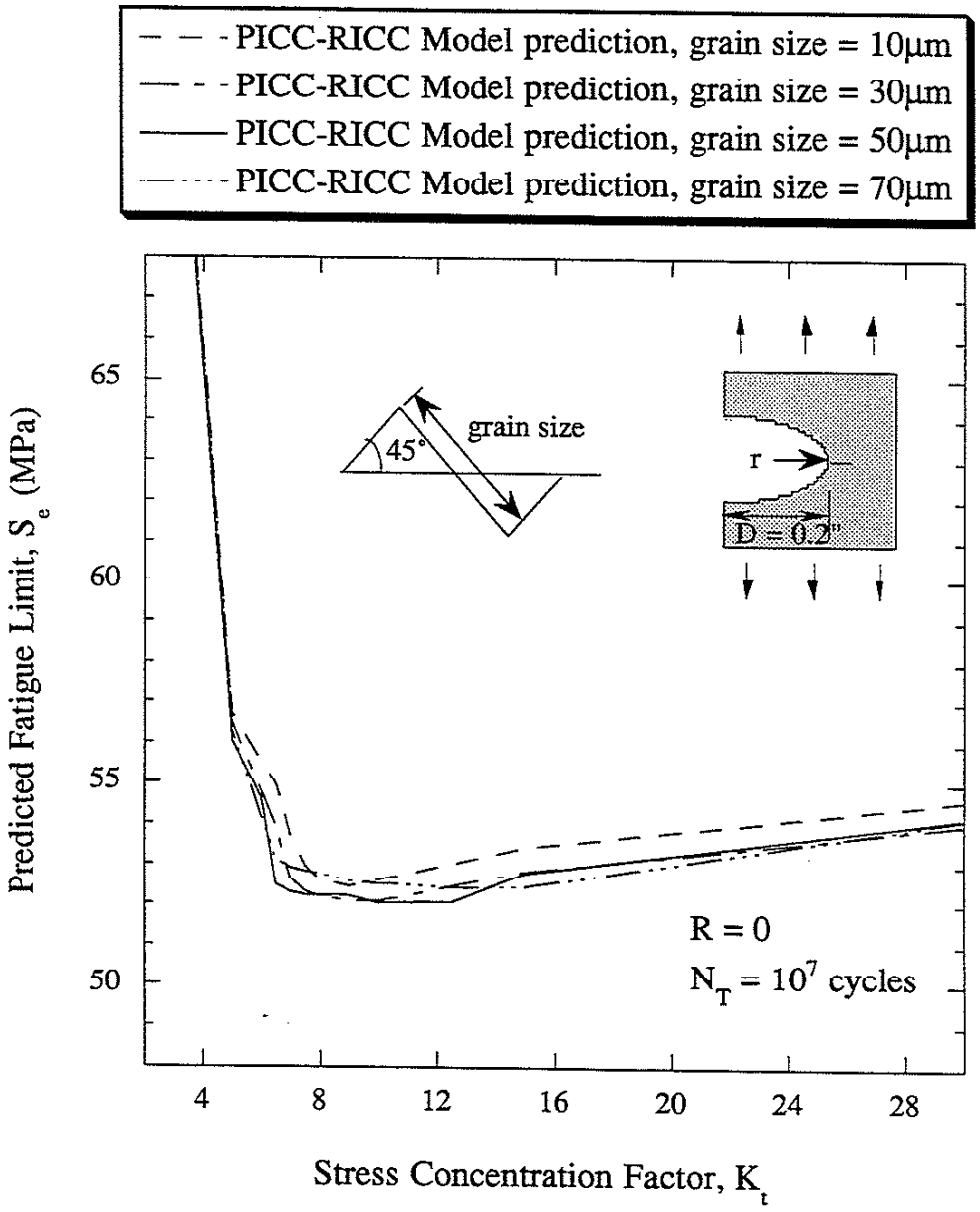


Fig. 8.7 Predicted variation of fatigue notch strength with grain size for stress ratio R=0 using the PICC-RICC Model and compared with test data.

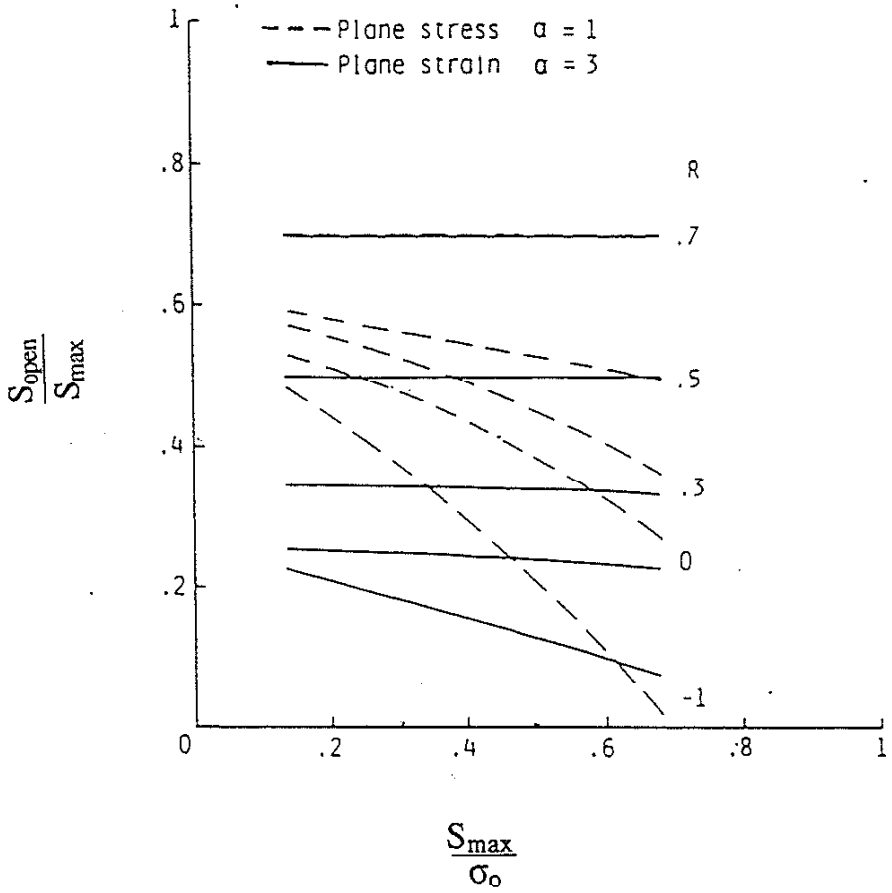


Fig. 8.8 Predicted variation of PICC with $\frac{S_{max}}{\sigma_0}$, where $\sigma_0$ is the flow stress of the material [33].

## REFERENCES


1. Elber, W., "Fatigue Crack closure Under Cyclic Tension," *Engineering Mechanics*, Vol. II, No. 1, 1970, pp. 37-45.

2. Elber, W., "The Significance of Fatigue Crack Closure," *Damage Tolerance in Aircraft Structure, ASTM STP 486*, American Society for Testing and Materials, 1971, pp. 230-242.

3. Ritchie, R.O., Suresh, S., and Moss, C. M., "Near-threshold Fatigue Crack Growth in 2-1/4 Cr-1 Mo Pressure Vessel Steel in Air and Hydrogen," *Journal of Engineering Materials and Technology, Trans. ASME Series H*, V0l. 102, 1980, pp. 293-299.

4. Walker, N. and Beevers, C. J., "A Fatigue Crack Closure Mechanism in Titanium," *Fatigue of Engineering Materialsand Structures*, Vol. 1, 1979, pp. 135-148.

5. Ritchie, R.O., *Fatigue Thresholds*, Proceedings of 1st International Conference, Stockholm, J. Bäcklund, A. Blom, and C. J. Beevers, eds., EMAS Publ. Ltd., Warley, U.K., 1981, pp. 503-526.

6. Purushothaman, S. and Tien, J. K. , "A Fatigue Crack Growth Mechanism for ductile Materials," *Scripta Metallurgica*, Vol. 9, 1975, pp. 923-926.

7 Purushothaman, S. and Tien, J. K, *Strength of Metals and Alloys, Proceedings of ICSMA5 Conference*, Pergamon Press, New York, NY, 1979, Vol. 2, pp1267-1271.

8. Beever, C. J., *Metal Science*, Vol. 14, 1980, pp. 418.

9. Suresh, S., Zamiski, G. F., and Rotchie, R.O., "Oxide-Induced Crack Closure: an Explanation for Near-Threshold Corrosion Fatigue Crack Growth Behavior," *Metallurgical Transactions A*, Volume 12A, 1981, pp. 1435-1443.

10. Mayes, I. C. and Baker, C. J., *Fatigue and Engineering of Materials and Styructures*, Vol. 4, 1981, pp. 79-86.

11. Minakawa, K., and McEvily, A. J., "On Crack Closure in the Near-Threshold Regine," *Scripta Metallurgica*, Vol. 15, 1981, pp. 633-636.

12. Gray, III, G, T., Thompson, A. W., Williams, J. C. and Stone, D. H., *Fatigue Thresholds*, Proceedings of 1st International Conference, Stockholm, J. Bäcklund, A. Blom, and C. J. Beevers, eds., EMAS Publ. Ltd., Warley, U.K., 1981, pp. 345-361.

13 Gray, III, G. T., Williams, J. C. and Thompson, A. W., " Roughness-Induced Crack Closure: An Explanation for Microstructrally Sensitive Fatigue Crack Growth," *Metallurgical Transactions*, Vol. 14A, 1983, pp.421-433.

14. Paris, P. C., Bucci, R., J., Wessel, E. T., Clark, W. G. and Mager, T. R., "Extensive Study of Low Fatigue Crack Growth Rates in A533 and A508 Steels," *Stress Analysis and Growth of Cracks, ASTM STP 513*, American Society and Testing and Materials, 1972, pp. 141-176.

15. Stewart, A.T., "The Influence of Enviornment and Stress Ratio on Fatigue Crack Growth at Near-threshold Stress Intensities in Low Alloy Steels," *Engineering Fracture Mechanics*, Vol. 13, 1980, pp.463-478.

16 Benoit, D., Namdar-Irani, R., and Tixier, R., "Oxidation of Fatigue Fracture Surface at Low Grwoth Rates," *Materials Science and Engineering*, Vol. 45, 1980, pp. 1-7.

17. Suresh, S., Parks, D. M. and Ritchie, R. O., *Fatigue Thresholds*, Proceedings of 1st International Conference, Stockholm, J. Bäcklund, A. Blom, and C. J. Beevers, eds., EMAS Publ. Ltd., Warley, U.K., 1981, pp. 391-408.

18. Liaw, P. K., Leax, T. R., and Logsdon, W. A., *Acta Metallurgica*, Vol. 31, 1983, pp. 1581.

19. Pineau, A. G. and Pelloux, R. M. N., "Influence of Strain-induced martensitic Transformation on Fatigue Crack Growth Rates in stainless Steels," *Metallurgical Transactions*, Vol. 5A, 1974, pp. 1103-1112.

20. Hornboger, E., "Martensitic Transformation at a Propagating Crack," *Acta Metallurgica*, Vol. 26, 1978, pp. 147-152.

21. Endo, K., Okada, T. and Hariya, T., "Fatigue Crack Propagation in Bearing Metals Lining of Steel Plates in Lubricating Oil," *Bulletin of the Japanese Society of Mechanical Engineers*, Vol. 15, 1972, pp. 439-445.

22. Tzou, J.-L., Suresh, S. and Ritchie, R. O., "Fatigue Crack Propagation in Oil Enviornment: I. Crack Growth Behavior in Silicone and Paraffin Oils," *Acta Metallurgica*, Vol. 33, 1985, pp. 105-116.

23. Forrest, P. G. and Tate, A. E. L., *Journal of Institute of Metals*, Vol. 93, 1964-65, pp. 438.

24 Lankford, J., *Fatigue of Engineering Materials and Structures*, Vol. 5, 1982, pp. 233.

25. Morris, W. L. and James, M. R., *Fatigue Mechanism: Advances in Quantitative Measurement of Physical Damage, ASTM STP 811*, American Society for Testing and Materials, 1983, pp. 46-70.

26. Paris, P. C., Gomez, M. P. and Anderson, W. P., "A Rational Analytic Theory of Fatigue," *The Trend in Engineering*, Vol. 13, 1961, pp. 9-14.

27. Budiansky, B. and Hutchinson, J. W., "Analysis of Closure in Crack Growth," *Journal of Applied Mechanics*, Vol. 45, 1978, pp. 267-275.

28. Dugdale, D. S., "Yielding of Steel Sheets Containing Slits," *Journal of the Mechanics and Physics of Solids*, Vol. 8, 1960, pp. 100-108.

29. Führing, H. and Seeger, T., "Dugdale Crack Closure Analysis of Fatigue Crack Under Constant Amplitude Loading," *Engineering Fracture Mechanics*, Vol. 11, 1979, pp. 99-122.

30. Führing, H. and Seeger, T., "Structural Memory of Cracked Components Under Irregular Loading," *Fracture Mechanics, ASTM STP 677*, American Society and Testing and Materials, 1979, pp. 144-167.

30. Dill, H. D. and Saff, C. R., "Spectrum Crack Growth Prediction Method Based On Crack Surface Displacement And Contact Analyses," *Fatigue Crack Growth under Spectrum Loads. ASTM STP 595*, American Society and Testing and Materials, 1976, pp. 306-319.

31. Ohji, K., Ogura, K. and Yoshiji, O., "Cyclic Analysis Of A Propagating Crack And Its Correlation With Fatigue Crack Growth," *Engineering Fracture Mechanics*, Vol.7, 1975, pp. 457-464.

32. Newman, J. C., Jr., "A Finite-Element Analysis of Fatigue Crack Closure," *Mechanics of Crack Growth, ASTM STP 590*, American Society for Testing and Materials, 1976, pp. 281-301.

33. Newman, J.C., Jr., "A Crack-Closure Model for Prediction Fatigue Crack Growth Under Aircraft Spectrum Loading," *Methods and Models for Predicting Fatigue Crack Growth Under Random Loading, ASTM STP 748*, American Society for Testing and Materials, 1981, pp. 53-84.

34. Blom, A.F. and Holm, D.K., "An Experimental and Numerical Study of Crack Closure," *Engineering Fracture Mechanics*, Vol.22, No.6, 1985, pp. 997-1011.

35. Fleck, N. A., "Finite Element Analysis of Plasticity -Induced CRack Closure Under Plane Strain Condition," *Engineering Fracture Mechanics*, Vol. 25, 1986, pp. 441-449.

36 McClung, R. C., "Fatigue Crack closure and Crack Growth Outside the Small Scalew Yielding Regime," *PhD thesis*, Department of Mechanical and Indistrical Engineering, University of Illinois at Urbana-Champaign, 1987.

37. Fleck, N.A. and Newman, J. C., Jr., "Analysis of Crack Closure Under Plane Strain Conditions," *Mechanics of Fatigue Crack Closure, ASTM STP 982*, American Society for Testing and Materials, 1988, pp. 319-341.

38. McClung, R. C. and Sehitoglu, H., "On the Finite Element Analysis of Fatigue Crack Closure - 1. Basic Modeling Issues," *Engineering Fracture Mechanics*, Vol. 33, 1989, pp. 237-252.

39. McClung, R. C. and Sehitoglu, H., "On the Finite Element Analysis of Fatigue Crack Closure - 2. Numerical Results," *Engineering Fracture Mechanics*, Vol. 33, 1989, pp. 253-252.

40. Sun, W., "Finite Element Simulations of Fatigue Crack Growth and Closure," *PhD. Thesis*, Department of Mechanical Engineering, University of Illinois at Urbana-Champaign, 1991.

41. Chermahini, R.G., Shivakumar, K.N. and Newman, J.C., Jr., "Three-dimensional Finite-Element Simulation of Fatigue Crack Growth and Closure," *Mechanics of Fatigue Crack Closure, ASTM STP 982*, American Society for Testing and Materials, 1988, pp. 398-413.

42. Chermahini, R.G. and Blom, A.F., "Variation Of Crack-Opening Stress In Three-Dimensions: Finite Thickness Plate," *Theoretical and applied Fracture Mechanics*, Vol. 15, 1991, pp. 267-276.

43. Newman, J. C., Jr., "A Crack-Closure Model for Predicting Fatigue Crack Growth Under Aircraft Spectrum Loading," *Methods and Models for Predicting Fatigue Crack Growth Under Random Loading, ASTM STP 748*, American Society for Testing and Materials, 1983, pp. 53-84.

44. Newman, J. C., Jr., "A Nonlinear Fracture Mechanics Approach to the Growth of Small Cracks," *AGARD-CP-328, Behavior of Short Cracks in Airframe Components* (Meeting held in Toronto, Canada, 19-24, Sept. 1982), Loughton, England, 1983. pp. 6.1-6. 26..

45. Broek, D., *Elementary Engineering Fracture Mechanics*, Noordhoff, Leyden, 1974, pp. 105-107.

46. Irwin, G. R., "Plastic Zone Near a Crack and Fracture Toughness," *Proceedings of the 7th Sagamore Conference*, 1960, pp. IV63-IV 76.

47. Wang, G. S. and Blom, A. F., "A Strip Model for Fatigue Crack Growth Predictions Under General Load Conditions," *Engineering Fracture Mechanics*, Vol. 40, 1991, pp. 507-533.

48. Blom, A. F., Palmberg, B. and Wang, G. S., "Stress state-Related Fatigue Crack Growth Under Spectrum Loading," *Fatigue and Fracture of Engineering Materials and Structures*, Vol. 15, No. 7, 1992, pp. 695-712.

49. Newman, J. C., Jr., Bigelow, C. A. and Shivakumar, K. N., "Three-Dimensional Elastic-Plastic Finite-Element Analyses of Constraint Variations in Cracked Bodies," *NASA Technical Memorandum No. 107704*, 1993.

50. de Koning, A. U. and Liefting, G., "Analysis of Crack Opening Behavior by Application of a Discretized Strip Yield Model," *Mechanics of Crack Closure, ASTM STP 982*, American Society for Testing and Materials, 1988, pp. 437-458.

51. Ibrahim, F. K., Thompson, J. C. and Topper, T. H., "A Study of the Effect of Mechanical Variables on Fatigue Crack Closure and Propagation," *International Journal of Fatigue*, Vol. 8, 1986, pp. 135-142.

52. Frost, N. E. and Dugdale, D. S., "Fatigue Tests on Notched Mild Steel Plates with Measurements of Fatigue Cracks," *Journal of Mechanics and Physics of Solids*, Vol. 5, 1957, pp. 182-192.

53. Frost, N. E., "Notch Effect and the Critical Alternating Stress Required to Propagate a Crack in an Aluminum Alloy Subject to Fatigue Loading," *Journal of Mechanical Engineering Science*, Vol. 2, 1960, pp. 109-119.

54. Smith, R. A. and Miller, K. J., "Fatigue Cracks at Notches," *International Journal of Mechanical Science*, Vol. 19, 1977, pp. 11-22.

55. El Haddad, M. H., Dowling, N. E., Topper, T. H. and Smith, K. N., "J-Integral Applications for short Fatigue Cracks at Notches," *International Journal of Fracture*, Vol. 16, 1980, pp. 15-30.

56. Tanak, K., and Nakai, Y., "Propagation and Non-Propagation of Short Fatigue Cracks at a Sharp Notch," *Fatigue of Engineering Materials and Structures*, Vol. 6, 1983, pp. 315-327.

57. Socie, D. F., "Prediction of Fatigue Crack Growth in Notched Memebers under Variable Amplitude Loading Hstories," Engineering Fracture Mechanics, Vol. 9, 1977, pp. 849-865.

58. Dowling, N. E., "Crack Growth During Low-Cycle Fatigue of Smooth Axial Specimens," *Cyclic Stress-Strain and Plastic Deformation Aspects of Fatigue Crack Growth, ASTM STP 637*, American Society for Testing and Materials, 1977, pp. 97-121.

59. Dowling, N. E., "Fatigue at Notches and the Local Strain and Fracture Mechanics Approaches," *Fracture Mechanics, ASTM STP 677*, American Society for Testing and Materials, 1979, pp. 247-273.

60. Sehitoglu, H., "Fatigue Life Prediction of Notched Members Based on Local Strain and Elastic-Plastic Fracture Mechanics Concepts," *Engineering Fracture Mechanics*, Vol. 18, 1983, pp. 609-621.

61. Socie, D. F., Dowling, N. E. and Kurath, P., "Fatigue Life Estimation of Notched Members," *Fracture Mechanics, ASTM STP 833*, Society for Testing and Materials, 1984, pp. 284-299.

62. Leis, B. N., "Displacement Controlled Fatigue Crack Growth in Inelastic Notch Fields: Implications for Short Cracks," *Engineering Fracture Mechanics*, Vol. 22, 1985, pp. 279-293.

63 Sehitoglu, H., "Characterization of Crack Closure," *Fracture Mechanics, ASTM STP 868*, American Society for Testing and Materials, 1985, pp. 361-380.

64. Ogura, K., Miyoshi, Y. and Nishikawa, I., "Fatigue Crack Growth and Closure of Small Cracks at Notch Root," *Current Japanese Materials Research, MRS*, Society of Material Science, Japan, Vol. I, 1987, pp. 67-91.

65. Shin, C. S. and Smith, R. A., "Fatigue Crack Growth at Stress Concentrations - The Role of Notch Plasticity and Crack Closure," *Engineering Fracture Mechanics*, Vol. 29, 1988, pp. 301-315.

66. Lalor, P., Sehitoglu, H. and McClung, R. C., "Mechanical Aspects of Small Crack Growth from Notches - the Role of Crack Closure," *The behavior of Short Fatigue Crack, EGF Pub. 1*, Mechanical Engineering Publications, London, 1986, pp. 369-386.

67. Lalor, P.L. and Sehitoglu, H., "Fatigue Crack Closure Outside a Small Scale Yielding Regime," *Mechanics of Fatigue Crack Closure, ASTM STP 982*, American Society for Testing and Materials, 1988, pp. 342-360.

68. McClung, R. C and Sehitoglu, "Fatigue Crack Growth From Notches," Journal of Engineering Materials, 1991.

69. Ting, J. C., "A Model for the Long-Life Fatigue Behavior of Small Notches," *Ph.D. Thesis*, Department of Metallurgical Engineering, University of Illinois at Urbana-Champaign.

70. Ting, J. C. and Lawrence, F. V., "Modeling the Long-Life Fatigue Behavior of a Cast Aluminum Alloy," *Fatigue Fract. Engng. Mater. Struct.*, Vol. 16, 1993, pp. 631-647.

71. Ting, J. C. and Lawrence, F. V., "A Crack Closure Model for Predicting the Threshold Stresses of Notches," *Fatigue Fract. Engng. Mater. Struct.*, Vol. 16, 1993, pp. 93-114.

72. Tanaka, K., Nakai, Y. and Yamashita, M., "Fatigue Growth Threshold of Small Cracks," *International Journal of Fracture*, Vol. 17, 1981, pp. 519-533.

73. Hou, C. Y. and Lawrence, F. V., "A Model for Weldment Fatigue Based on Crack-Closure Concepts (CCN Model)," *Proceeding of the 12th International Conference on Offshore Mechanics and Arctic Engineering*, 1993, pp. 513-528.

74. Newman, J. C. Jr., Swain, M. H. and Phillips, E. P., "An Assesment of the Small-Crack Efect for 2024-T3 Aluminum Alloy," *Small Fatigue Cracks, Proceedings of the Second Engineering Foundation International Conference/Workshop*, Santa Barbara, California, January 5-10, 1986, pp. 427-452.

75. Newman, J. C. Jr., Phillips, E. P. and Swain, M. H., "Predicting the Growth of Small and Large Cracks Using a Crack-closure Model," *Mechanical Behavior of Materials - V, Prodceeding of the fifth International Conference*, Beijing, China, pp. 51-60.

76. Hou, C.Y., "A Crack Closure Model for the Fatigue Behavior of Notched Components And Welded Joint," *Ph.D. Thesis*, Department of Civil Engineering, University of Illinois at Urbana-Champaign.

77. Hou, C. Y. and Lawrence, F. V., "A Crack-closure Model for the Fatigue Behavior of Notched Components," *Advances in Fatigue Lifetime Predictive Techniques, ASTM STP 1292*, American Society for Testing and Materials, 1996, pp. 116-135.

78. Hou, C. Y. and Lawrence, F. V., "Crack-closure in Weldments," *Fatigue and Fracture of Engineering Materials and Structures*, Vol.19, No. 6, pp. 683-693, 1996.

79. Verreman, Y., Ballon, J.-P., Masounave, J., "Closure and Propagation Behavior of Short Fatigue Cracks" at Different R-Ratios," *Fatigue 87*, 1987, pp. 371-380.

80. Cooke, R. J. and Beevers, C. J., *Materials Science and Engineering*, Vol. 13, 1974, pp. 201-210.

81. Lindley, T. C., and Richards, C.E., "The Relevence of Crack Closure to Fatigue Crack Propagation," *Materials Science and Engineering*, Vol. 14, 1974, pp. 281-293.

82. Ritchie, R.O., *Fatigue Thresholds*, J.Backlund, A. Blom, and C. J. Beevers, Eds., EMAS Publ. Ltd., Warley, U.K., 1981, pp. 503-526.

83. Ritchie, R. O., Suresh, S., "Communications: Some Considerations on Fatigue Crack Closure at Near-Threshold stress Intensities Due to Fracture Surface Morphology," *Metallurgical Transactions A*, Volume 13A, 1982, pp. 937-940.

84. Suresh, S., "Crack Defelction: Implications for the Growth of Long and Short Fatigue Cracks," *Metallurgical Transactions A*, Vol. 14A, 1983, pp. 2375-85.

85 Ritchie, R. O. and Yu, W., "Short Crack Effects in Fatigue: a Sequence of Crack Tip shielding," *Small Fatigue Cracks, Proceedings of the Second Engineering Foundation International conference/workshop*, Santa Barbara, California, January 5-10, 1986. Ritchie, R. O. and Lankford, J., Eds., 1986, pp. 167-189.

86. Ritchie, R. O. and Lankford, J., "Small Fatigue Cracks: A Statement of the Problem and Potential solutions," *Materials Science and Engineering*, 84, 1986, pp. 11-16.

87. Ritchie, R.O., Yu, W., Blom, A. F. and Holm, D. K., "An Analysis of Crack Tip Shielding in Aluminum Alloy 2124: A Comparison of Large, Small, through-thickness and Surface Fatigue Cracks," *Fatigue Fract. Engng Mater. Struct.*, Vol. 10, No. 5, 1987, pp. 343-362.

88. Shang, J. K. and Ritchie, R. O., "On the Particle-size Dependence of Fatigue-Crack Propagation Thresholds In SiC-Particulate-Reinforced Aluminum-Alloy Composites: Role of Crack closure and Crack Trapping," *Acta Metall.*, Vol. 37, No. 8, 1989, pp. 2267-2278.

89. Tokaji, K., Ando, Z. and Nagae, K., "The Effect of Sheet thickness on Near-threshold Fatigue Crack Propagation and Oxide and Roughness-Induced Crack Closure," *ASME Transaction*, Vol. 109, 1987, pp. 89-91.

90. Venkateswara Rao, K. T., Yu, W. and Ritchie, R. O., "On the Role of Crack Tip Shielding In Influencing the Behavior of Long and Small Fatigue Cracks in Aluminum-Lithium Alloy 2090," Fatigue 87, Ritchie, R. O. and Starke, E. A. Jr., Eds., EMAS Publ. Ltd., Warley, U.K., 1987, pp. 291-301.

91. Forsyth, P. J. E., *Crack Propagation, Proceeding Symp.*, Crandield, College of Aeronautics, Cranfield Press, Cranfield, U. K., 1962, pp. 76.

92. Minakawa, K., and McEvily, A. J., *Fatigue Thresholds*, Proceedings of 1st International Conference, Stockholm, J. Bäcklund, A. Blom, and C. J. Beevers, Eds., EMAS Publ. Ltd., Warley, U.K., Vol. 1, 1982, pp. 373.

93. Schijve, J., *Fatigue Thresholds*, Proceedings of 1st International Conference, Stockholm, J. Bäcklund, A. Blom, and C. J. Beevers, Eds., EMAS Publ. Ltd., Warley, U.K., Vol. 2, 1982, pp. 881.

94. Ogawa, Takeshi and Tokaji, Keiro, and Ohya, Kohji, "The Effect of Microstructural and Fracture surface Roughness on Fatigue Crack Propagation in a Ti-6Al-4V Alloy," Fatigue and Fracture of the Engineering Materials and Structures, Vol. 16, No. 9, 1993, pp. 973-982.

95. Davison, D. L., *Fat. Eng. Mat. Tech.*, 1981, Vol. 3, pp. 229.

96. Davison, D. L. and Lankford, J., *Fatigue of engineering Materials and Structures*, Vol. 15, 1979, pp. 439.

97. Asaro, R. J., Hermann, L. and Baik, J. M., *Metall. Trans. A*, 1981, Vol. 12A, pp. 1135.

98. Ritchie, R. O., "Near-threshold Fatigue-crack Propagation in Steels," *International Metal Reviews*, Vol. 20, 1979, pp. 205-230.

99. Thompson, A. W. and Bucci, R. J., *Metall Trans*, Vol. 4, 1973, pp. 1173.

100. Suresh, S., and R. O. Ritchie, "Geometrical Model for Fatigue Crack Closure Induced by Surface Roughness," *Metallurgical Transactions A*, Volume 13A, 1982, pp. 1627-31.

101. Suresh, S., "Fatigue Crack Deflection and Fracture Surface Contact: Micromechanical Models," *Metallurgical Transaction A*, Vol. 16A, 1985, pp. 249-260.

102. Suresh, S., "Micromechanism of Fatigue Crack Growth Retardation Folowing Overloads," *Engin. Frac. Mechanics*, Vol. 18, No. 3, 1983, pp. 577-93.

103. Ravichandran, K. S., "A theoretical Model for roughness Induced Crack Closure," *International Journal of Fracture*, Vol. 44, 1990, pp. 97-110.

104. LLorca, J., "Roughness-Induced Fatigue Crack Closure: A Numerical Study," *Fatigue Fract. Engng. Struct.*, Vol. 15, No. 7, 1992, pp. 655-669.

105. Williams, M. L., *Journal of Applied Mechanics*, Vol. 24, 1957, 109-114.

106. Lawrence, F. V., Jr., Mattos, R. J., Higashida, Y. and Burk, J. D., "Estimating the Fatigue Crack Initiation Life of Welds," *Fatigue Testing of Weldments, ASTM STP 648,* American Society for Testing and Materials, 1978, pp. 134-158.

107. Ho, N. J. and Lawrence, F. V., Jr., "Constant Amplitude and Variable Load History Fatigue Testing Results and Predictions for Cruciform and Lap Welds," *Theoretical and Applied Fracture Mechanics*, Vol. 1, No. 1, 1984, pp. 3-21.

108. Yung, J.-Y. and Lawrence, F. V., Jr., "Analytical and Graphical Aids for the Fatigue Design of Weldments," *Fatigue Frac. Engng. Mater. Struct.*, Vol. 8, No. 3, 1985, pp. 223-241.

109. Tanaka, K. and Mura, T., "A Disclocation Model for Fatigue Crack Initiation," *Journal of Applied Mechanics,* Vol.48, March 1981, pp.97-103.

110. Hoshide, T. and Socie, D. F., "Crack Nucleation and Growth Modeling in Biaxial Fatigue," *Engineerng Fracture Mechanics*, Vol. 29, No. 3, pp. 287-299, 1988.

111. Socie, D. F. and Furman, S., "Fatigue Damage Simulation Models for Multiaxial Loading," *Fatigue '96, Proceedings of the Sixth International Fatigue Congres,* Berlin, Germany, Lutjering, G. and Nowack H., Eds., Pergamon Press, New York, NY, 1996, pp. 967-976.

112. Frost, N. E., "A Relation Between the Critical Alternating Propagation Stress and Crack Length for Mild Steel," *Proceeings Institutions of Mechanical Engineers*, Vol. 173, No. 35, 1959, pp. 811-836.

113. Lawrence, F. V., Burk, J. D. and Yung, J.-Y., "Influence of Residual Stress on the Predicted Fatigue Life of Weldments," *Residual Stress Effects in Fatigue, ASTM STP 776*, American Society for Testing and Materials, 1982, pp. 33-43.

114. Lawrence, F. V. and Dimitrakis, S. D. and Chen, N., "The Fatigue Resistance of Automatic Weldments," Submitted to the *International Institute of Welding on Performance of Dynamically Loaded Structures*, !997.

115. McMahon, J. C. and Lawrence, F. V., "Predicting Fatigue Properties Through Hardness Measurements," *Report No. 105*, UILU-ENG 84-3605, 1984.

116. Petroski, H. J. and Achenbach, J. D., "Computation of the Weight Function from a Stress Intensity Factor," *Engineering Fracture Mechanics*, Vol. 10, 1978, pp. 257-266.

117. Görner, F., Mattheck, C., Morawietz, P. and Munz, D., "Limitations of the Petroski-Achenbach Crack Opening Displacement Approximation for the Calculation of Weight Functions," *Engineering Fracture Mechanics*, Vol. 22, 1985, pp. 269-277.

118. Bueckner, H. F., "Field Singularities and Related Integral Representations," *Mechanics of Fracture 1 - Methods of Analysis and Solution of Cracks Handbook*, Del. Research Corporation, 1973.

119. Wu, X. R., *Engineering Fracture Mechanics*, Vol. 20, No. 1, 1984, pp. 35-49.

120. Cotterell, B. and Rice, J. R., "Slightly Curved Or Kinked Cracks," *International Journal of Fracture*, Vol. 16, No. 2, 1980, pp. 155-169.

121. Liaw, P. K., "Overview of Crack Closure at Near-threshold Fatigue Crack Growth Levels," *Mechanics of Fatigue Crack Closure, ASTM STP 982*, American Society for Testing and Materials, 1988, pp. 62-92.

122. Mossonnet, C., *Proceedings of American Society of Testing and Materials*, Vol. 56, 1956. pp.954.

123. Fleck, N.A., " Influence of Stress State on Crack Growth Retardation," *Basic Questions in Fatigue: Volume 1, ASTM STP 924*, American Society for Testing and Materials, 1988, pp.157-183.

124. Juvinall, R. C., *Engineering Consideration of Stress, Strain and Strength*, McGraw-Hill, New York, 1967.

# APPENDIX A WEIGHT FUNCTIONS FOR SINGLE-EDGED AND CENTER-CRACKED SPECIMENS

Using the weight function method [116-117], the stress intensity factor K(a) of a crack in a specimen with arbitrary geometry under symmetrical loading can be estimated as:

$$K(a) = \int_0^a \sigma(x)\, g(x, a)\, dx \tag{A.1}$$

The near-tip crack face displacement u(x, a) can also be estimated using the weight function method as:

$$u(x, a) = \frac{1}{E'} \int_0^a \int_{a_1}^a \sigma(x_2)\, g(x, x_1)\, g(x_2, x_1)\, dx_1 dx_2 \tag{A.2}$$

In Eq. (A.1) and Eq. (A.2):

| | |
|---|---|
| a | crack length |
| g(x, a) | weight function |
| $\sigma(x)$ | stress distribution of the corresponding uncracked specimen along the crack line |
| $a_1$ | max[x, $x_2$] |
| E' | $\begin{cases} E, & \text{for plane stress} \\ \frac{E}{1-\nu^2}, & \text{for plane strain} \end{cases}$ |
| E | Young's modules |
| $\nu$ | Poison's ratio |

The weight function g(x, a) for single-edged specimen is [118]:

$$g(x, a) = \sqrt{\frac{2}{\pi(a - x)}} \left( 1 + m_1(1 - \frac{x}{a}) + m_2(1 - \frac{x}{a})^2 \right) \quad \text{(A.3-1)}$$

where

$$m_1 = 0.6147 + 17.1844 (\frac{a}{w})^2 + 8.7822 (\frac{a}{w})^6$$
$$m_2 = 0.2502 + 3.2889 (\frac{a}{w})^2 + 70.0444 (\frac{a}{w})^6 \quad \text{(A.3-2)}$$

The weight function g(x, a) for center-cracked specimen is [119]:

$$g(x, a) = 2\sqrt{\frac{a}{\pi(a^2 - x^2)}} + \frac{1}{w}\sqrt{\frac{\pi(a^2 - x^2)}{a}} \tan(\frac{\pi a}{w}) \quad \text{(A.4)}$$

In Eq. (A.3.-1), Eq. (A.3.-2) and Eq. (A.4), w is the width of the specimen.

# APPENDIX B A DOUBLE PILE-UP DISLOCATION MODEL FOR CRACK NUCLEATION

The dislocation model of a double pileup was first proposed by Tanaka and Mura [109]. The model was later applied multi-axial fatigue by Socie, et al. [110-111]. The basic idea of the model is described below:

As shown in Fig. B.1, the cyclic shear stress $\tau$ causes dislocation of positive and negative signs to pileup on adjacent planes within a grain; as the result, a slip band is formed. A shear crack will be developed along the shear band based on the following energy criterion: when the stored strain energy due to the dislocation accumulated after $N_N$ cycles exceeds fracture surface energy, the layers of dislocation dipoles can be transformed into a free surface.

The stored strain energy after $N_N$ cycles can be estimated as:

$$U_{\text{strain energy}} = N_N \Delta\gamma_\psi (\Delta\tau_\psi - 2\tau_c) \tag{B.1}$$

where

$$\Delta\gamma = \frac{\pi(1 - \nu)(\Delta\tau_\psi - 2\tau_c) d^2}{G} \tag{B.2}$$

The fracture energy can be calculated as

$$U_{\text{fracture surface}} = 4dw_c \tag{B.3}$$

In Eqs.(B1-B3),

| | |
|---|---|
| $\Delta\tau_\psi$ | range of the resolved shear stress on $\psi$ plane |
| $\Delta\gamma_\psi$ | range of shear strain |
| $w_c$ | specific fracture energy for a unit area |
| $\tau_c$ | critical stress to initiate slip |
| d | grain size of the material |
| $\psi$ | inclination angle of the slip plane |
| G | shear modules of the material |
| $\nu$ | Poisson's ratio |

After substituting Eq.(B.2) into Eq.(B.1) and setting $U_{\text{strain energy}} = U_{\text{fracture surface}}$, one gets the following equation for $N_N$:

$$N_N = \frac{4Gw_c}{\pi(1-\nu)\,(\Delta\tau_\psi - 2\tau_c)^2 d} \tag{B.4}$$

The specific fracture energy $w_c$ is estimated to be $2 \times 10^3$ J/m$^2$ based on the knowledge that $w_c$ is about $10^3$ times the value of surface energy (which is about 2 J/m$^2$ for ordinary metals).

The critical stress to initiate slip, $\tau_c$, can be determined from the fatigue limit of the material (at total fatigue life $N_T$. In long life, it is assumed that $N_T = N_N$) along the plane of the critically resolved shear stress, $\tau_\psi^{N_T}$, as:

$$\tau_c = \tau_\psi^{N_T} - \sqrt{\frac{G\,w_c}{\pi\,(1-\nu)\,d\,N_T}} \tag{B.5}$$

For the ASTM A36 steel considered in Section 7.3.1, d = 30um, G = 78.8GPa, $\nu = 0.3$. The tensile fatigue limit $S_e$ at $N_T = 10^7$ is 214.45MPa [112]. The crack is assumed to nucleate along maximum shear stress direction of $\psi = 45°$. Therefore $\tau_\psi^{N_T} = 0.5S_e$. The value of $\tau_c$ can be estimated from Eq. (B.5) to be 105MPa.

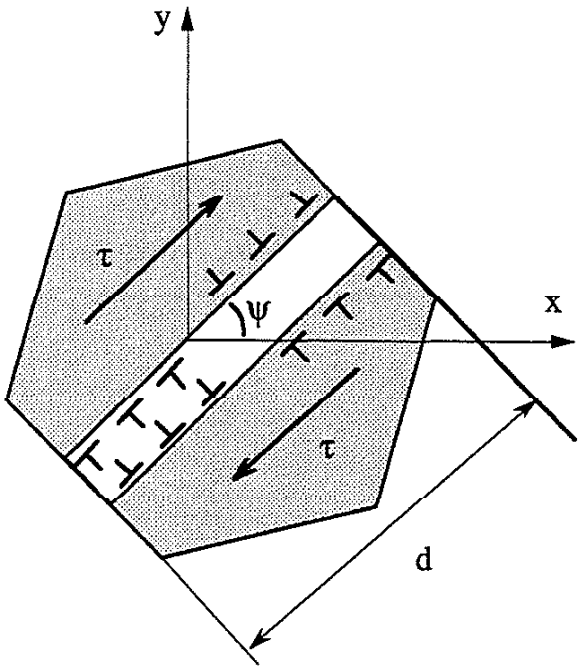


Fig. B.1 Illustration of a dislocation double pile-up model for the calculation of fatigue crack nucleation life [111].

# VITA

Nong Chen was born in 1968 in Fujian, China, daughter of Mr. Q.-Y. Chen and Mrs. G.-H. Liu. She graduated in 1985 from the First High School of Central-China Normal College in Wuhan, China. She received her B.S. degree in Engineering Mechanics in 1989 from the Southwest Jiaotong University, China. She was a graduate student in the Applied Mechanics Institute of Southwest Jiaotong University for one year before entering the University of Illinois at Urbana-Champaign in 1990. There she received her M.S. degree in the Theoretical and Applied Mechanics Department in 1992 with Teaching and Research Assistantships. She started pursuing her Ph.D. degree as a Research Assistant in the Civil Engineering Department of the University of Illinois at Urbana-Champaign in May, 1993.

Nong is the wife of Dr. Ji-min Duan.